

**Synthesis and Evaluation of Guanidino
Phthalocyanines
for G-quadruplex Binding**

Diplom-Arbeit

Durchgeführt am
Organisch-Chemischen Institut
der Universität Zürich

von

Phillipe Juan Carlos Roth

aus Kesswil Thurgau

Unter der Leitung von
Prof. Dr. Nathan W. Luedtke
und
Dr. Jawad Alzeer

Zürich 2008

Para la gente importante en mi vida...

Table of Contents

1. Introduction	1
1.1 DNA	1
1.1.1 The well known DNA structures: B-, A- and Z-DNA	1
1.1.2 Non-duplex DNA structures: triplex, i-motif and G-quadruplex	3
1.2 G-quadruplex DNA	5
1.2.1 General features of Quadruplex topology and structure	5
1.2.2 Vertebrate telomeric quadruplex	8
1.2.3 Non-telomeric quadruplexes	11
1.2.4 G-Quadruplex: a potential target for anti-cancer drug design	13
1.3 Known G-quadruplex Ligands	13
1.4 Summary of our approach	16
2. Phthalocyanines	19
2.1 Synthesis of Phthalocyanines	19
2.2 Our approach for synthesising C ₄ symmetric phthalocyanines	23
3. Synthesis of Guanidino Phthalocyanines	26
3.1 Guanidinylation reactions	26
3.2 Our approach	27
3.2.1 Yields	28
3.2.2 Purification	28
3.2.3 NMR spectrums	29
3.2.4 Mass spectroscopy	33
4. Fluorescence assays	35
4.1 General features	35
4.2 UV-vis spectroscopy	36
4.3 Fluorescence assays: Comparison of all compounds	37
4.3.1 Fluorescence enhancement assays	37
4.3.2 Fluorescence quenching assay	42
5. Experimental Part	47
5.1 General Remarks	47
5.1.1 Reaction conditions, solvents, chemicals	47
5.1.2 Chromatography, and recording of spectrums	47
5.1.3 Other machines used	48
5.2 Synthesis of Phthalocyanines	48
5.2.1 Synthesis of 3,3',3'',3'''-tetranitro zinc phthalocyanine (3)	48
5.2.2 Synthesis of 3,3',3'',3'''-tetraamino zinc phthalocyanine (4)	48
5.2.3 Synthesis of 4,4',4'',4'''-nitrotetrad zinc phthalocyanine (1)	49
5.2.4 Synthesis of 4,4',4'',4'''-tetraamino zinc phthalocyanine (2)	49
5.2.5 Synthesis of 4,4',4'',4'''-tetraamino phthalocyanine (11)	50
5.3 Synthesis of Guanidino Phthalocyanines	51
5.3.1 Synthesis of tetra-guanidine phthalocyanine (5)	51
5.3.2 Synthesis of tetra-guanidine zinc phthalocyanine (8)	52
5.3.3 Synthesis of tetra-(diisopropylguanidine) phthalocyanine (6)	53
5.3.4 Synthesis of tetra-(diisopropylguanidine) zinc phthalocyanine (9)	54
5.3.4 Synthesis of tetra-(diclohexylguanidine) phthalocyanine (7)	55
5.3.6 Synthesis of tetra-(diclohexylguanidine) zinc phthalocyanine (10)	56
5.3.7 Synthesis of tetra-(diisopropylguanidine) phthalocyanine (6) from tetra-(diisopropylguanidine) zinc phthalocyanine (9)	58
5.4 Fluorescence experiments	59
5.4.1 Methods	59
5.4.2 Titrations	59
5.4.3 Job Plot	61

Table of Contents

6. Summary	62
7. Appendix	63
7.1 NMR spectra of 2 (A) and 4 (B)	63
7.2 NMR spectra of 5	64
7.2.1 ¹ H-NMR spectrum.....	64
7.3 NMR spectra of 6	65
7.3.1 ¹ H-NMR spectrum.....	65
7.3.2 2D-NMR spectrum: DQF-COSY	66
7.4 NMR spectra of 7	67
7.4.1 ¹ H-NMR spectrum.....	67
7.5 NMR spectra of 8	68
7.5.1 ¹ H-NMR spectrum.....	68
7.5.2 2D-NMR spectrum: DQF-COSY	69
7.6 NMR spectra of 9	70
7.6.1 ¹ H-NMR spectrum.....	70
7.7 NMR spectra of 10	71
7.7.1 ¹ H-NMR spectrum.....	71
7.8 Fluorescence Quenching results of 9	72
7.9 Fluorescence enhancement results	72
8. Abbreviations	73
9. References	74
10. Acknowledgements	76

1. Introduction

1.1 DNA

In every known organism, the ultimate source of biological information is nucleic acid. The shapes and activities of individual cells are, to a large extent, determined by genetic instructions contained in DNA.

1.1.1 The well known DNA structures: B-, A- and Z-DNA

The most studied form of DNA is the B-form, which structural features were first described by James Watson and Francis Crick. ^[1] Double-helical DNA can assume several distinct structures depending on the solvent composition and base sequence. The major structural variants of DNA are A-DNA and Z-DNA. Under dehydrating conditions, B-DNA undergoes a reversible conformational change to A-DNA, which forms a wider and flatter right-handed helix than does B-DNA. Over 25 years after the discovery of the Watson-Crick DNA structures, the crystal structure determination of d(CGCGCG) by Andrew Wang and Alexander Rich revealed, quite surprisingly, a left-handed double helix, the Z-form of DNA (Fig. 1). ^[2]

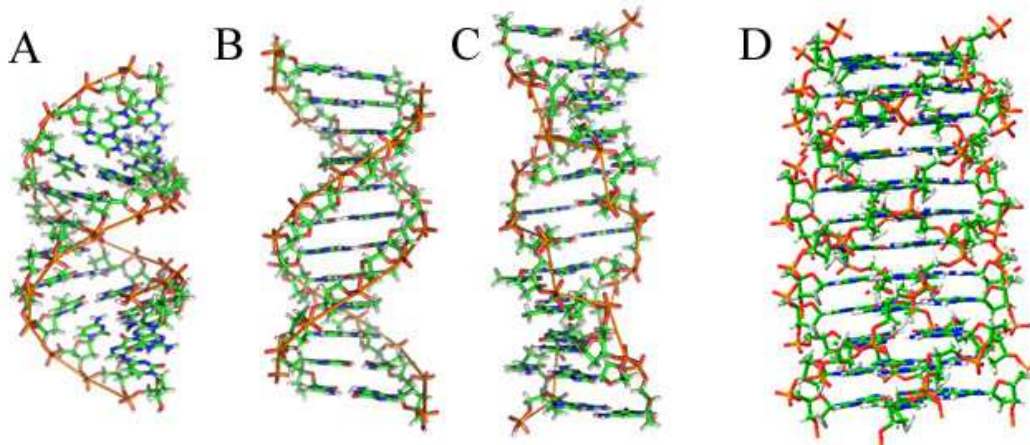


Fig. 1 A) A-DNA; B) B-DNA; C) Z-DNA; D) 4-Stranded G-quadruplex constructed from PDB (entry 139D)

DNA molecules, which are 20 Å thick and many times as long, are not perfectly rigid rods. In fact, it is imperative that these molecules be somewhat flexible so that they can be packaged in cells and made available as the single-stranded template for RNA and DNA polymerases. DNA helices can adopt different degrees of curvature ranging from gentle arcs to sharp bends. The more severe distortions from linearity, generally occur in response to the binding of specific proteins and mechanical/torsional strains such as negative supercoiling. ^[3]

In B-DNA, the two antiparallel polynucleotide stands wind in a right-handed manner around a common axis to produce an $\sim 20\text{-\AA}$ -diameter double helix. The planes of the nucleotide bases, which form hydrogen-bonded pairs, are nearly perpendicular to the helix axis. The bases occupy the core of the helix while the sugar-phosphate backbones wind around the outside, forming the major and minor grooves. Only the edges of the base pairs are exposed to solvent. Each base pair has approximately the same width, which accounts for the near-perfect symmetry of the DNA molecule, regardless of base composition. The ideal B-DNA helix has 10 base pairs per turn (a helical twist of 36° per bp) and, since the aromatic bases have van der Waals thicknesses of 3.4 \AA and are partially stacked on each other, the helix has a pitch (rise per turn) of 34 \AA . A-DNA has 11 bp per turn and pitch of 28 \AA , which gives it an axial hole. A-DNA's most striking feature, however, is that the planes of its base pairs are tilted 20° with respect to the helix axis. Since the axis does not pass through its base pairs, A-DNA has a deep major groove and a very shallow minor groove; it can be described as a flat ribbon wound around a 6-\AA -diameter cylindrical hole. ^[4]

Z-DNA, has 12 base pairs per turn, a pitch of 45 \AA , a deep minor groove, and no discernible major groove. Z-DNA therefore resembles a left-handed drill bit in appearance. Fiber diffraction and NMR studies have show that complementary polynucleotides with alternating purines and pyrimidines, such as poly d(GC)-poly d(GC) or poly d(AC)-poly d(GT), assume the Z conformation at high salt concentrations. The salt stabilizes Z-DNA relative to B-DNA by reducing the electrostatic repulsions between closest approaching phosphate groups on opposite strands (which are 8 \AA apart in Z-DNA and 12 \AA apart in B-DNA).

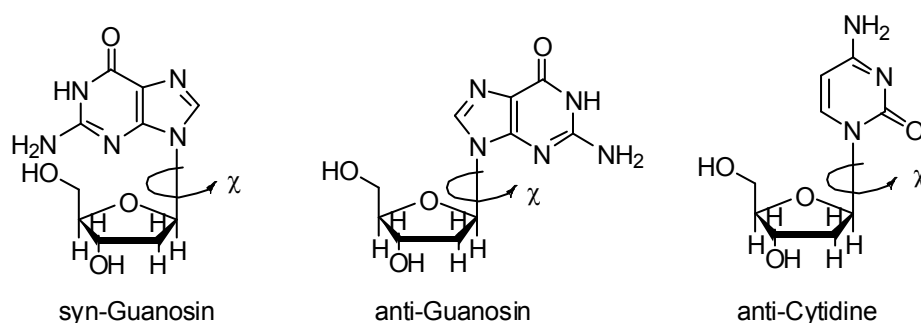


Fig. 2 The sterically allowed orientations of purine and pyrimidine bases with respect to their attached ribose units.

The conformations of nucleotide units are specified by the six torsion angles of the sugar-phosphate backbone and the torsion angle describing the orientation of the base around the glycosidic bond. Torsions angles are subject to a variety of internal constraints that greatly restrict their rotational freedom. The rotation of a base around its glycosidic bond is greatly

Homopurine-homopyrimidine mirror repeats are often found in non-protein coding sequences. They frequently occur in promoter regions and around recombination hot spots, strongly suggesting a regulatory role *in vivo*. *In vitro* studies have already shown that these repeats can fold into triple helix-containing structures called H-DNA. Upon H-DNA formation, the DNA double helix within one-half of the H-palindrome denatures into two single strands, and one of these complementary strands folds back to form a DNA triplex with the nondenatured half of the H-palindrome, whereas the other strand remains denatured. The presence of denatured regions makes this structure hypersensitive to single strand-specific endonucleases, like S1, which are commonly used for detection of H-DNA (Fig. 3). Because H-DNA is topologically equivalent to complete unwinding of the entire region that participates in the structure formation, it is stabilized by negative supercoiling. Within H-DNA, the triplex is stabilized by either Hoogsteen (YRY triplex) or reverse Hoogsteen (RRY triplex) interactions, depending upon whether the pyrimidine or the purine-rich strand participates in the triplex formation^[5] (Fig. 4).

In vivo studies subsequently provided experimental evidence for the occurrence of H-DNA in *Escherichia coli* and eukaryotic cells, but its precise biological role has been difficult to prove.^[6]

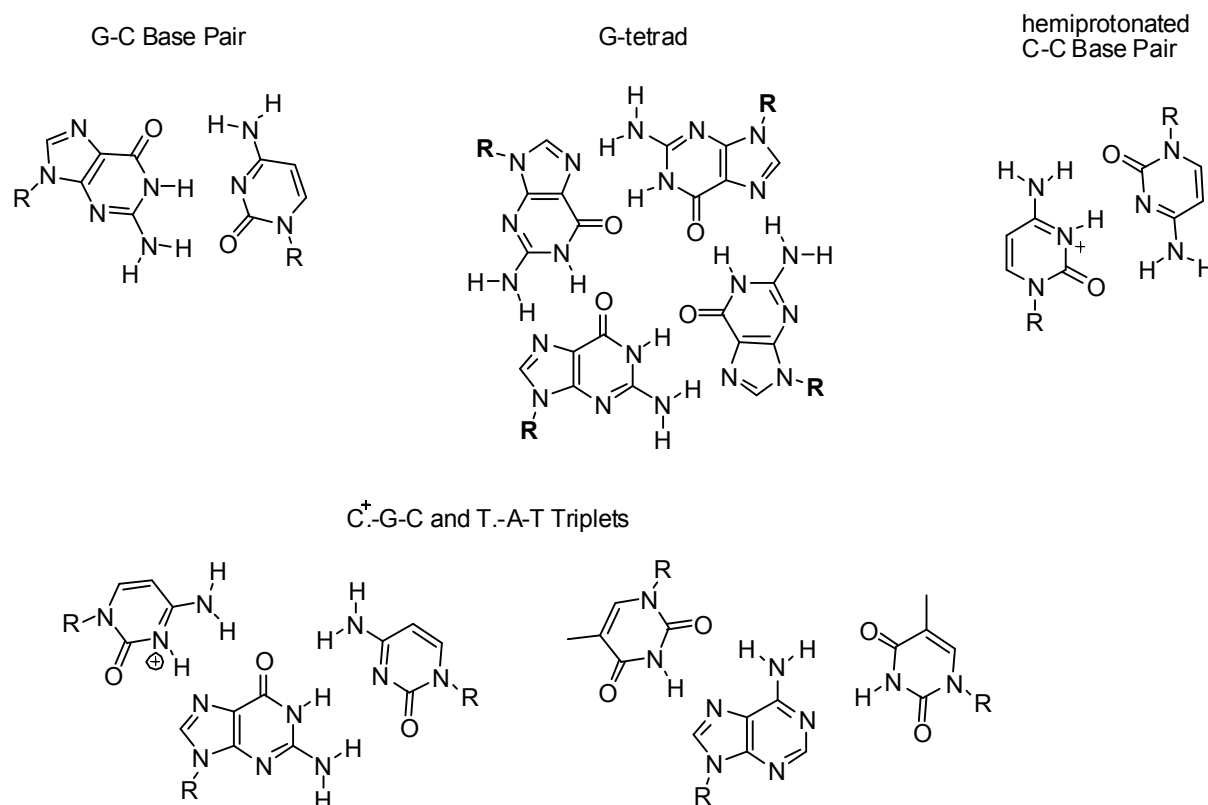


Fig. 4 Base Pairing of duplex DNA, G-quadruplex, i-motif and two possibilities of base pairing in triplex DNA.

The same homopurine-homopyrimidine mirror repeats that fold into H-motif can also dissociate into G-quadruplex and i-motif structures ^[7] (Fig. 3). The i-motif is an intercalated structure of nucleic acids formed by the association of two parallel stranded duplexes containing hemi-protonated cytidine-cytidine base pairs (one cytosine must be hemiprotonated at the N3 position, Fig. 4). The i-motif was first observed by NMR in the tetramer of d(TCCCCC). ^[8] The original report pointed out that it might also form by intramolecular folding of a single-strand DNA sequence containing four stretches of a few cytidines, such as are found in the C-rich strand of telomeres. Telomeric sequences of *Tetrahymena* and of vertebrates were indeed shown to fold into a monomeric i-motif which persisted even at pH 7 despite the requirement for cytidine hemi-protonation, pointing to the possibility of intracellular occurrence. ^[9, 10] The G-rich complementary strand, by requirement, must contain four or more closely localized guanine blocks that have three or more guanines each, this strand can fold into another unusual DNA structure, a DNA quadruplex stabilized by G-quartets. ^[5]

1.2 G-quadruplex DNA.

G-quadruplexes can form at the ends of chromosomes in the telomeric regions and possibly in the transcriptional regulatory regions of several important oncogenes. Both regions may be important targets for drug design.

1.2.1 General features of Quadruplex topology and structure

G-quadruplexes are higher-order DNA and RNA structures formed from G-rich sequences that are built from two or more stacked tetrads of hydrogen-bonded guanine bases. Potential quadruplex sequences have been identified in G-rich eukaryotic telomeres, and more recently in non-telomeric genomic DNA, e.g. in nuclease-hypersensitive promoter regions. The synthetic polynucleotides poly(dG) and poly(G) were determined in different studies to form four-stranded intermolecular helical structures with the G-tetrads stacked on one another (Figure 1D). Formation of intramolecular quadruplex structures at telomere ends is possible since the 3' terminal nucleotides of all telomeric DNAs are single-stranded, albeit in association with single-strand-binding proteins, such as hPOT1 in *Homo sapiens*, where the single-strand overhang is ca. 100–200 nt long. ^[11]

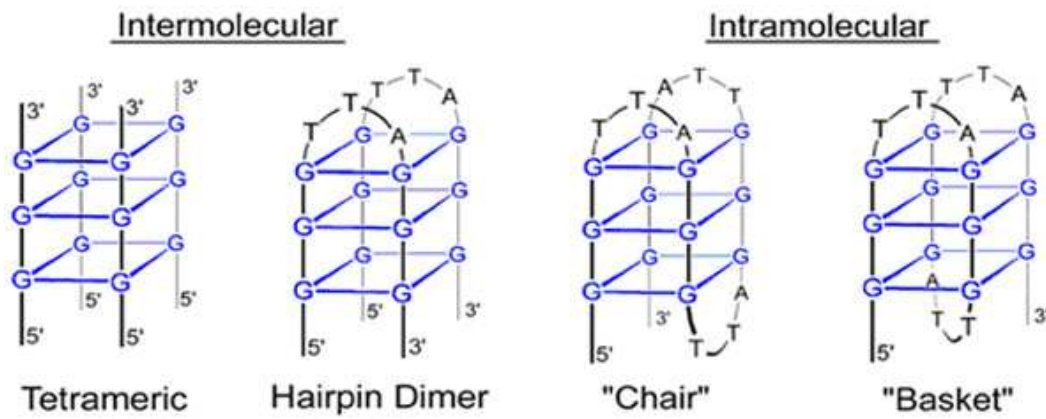


Fig. 5 G-quadruplex structures

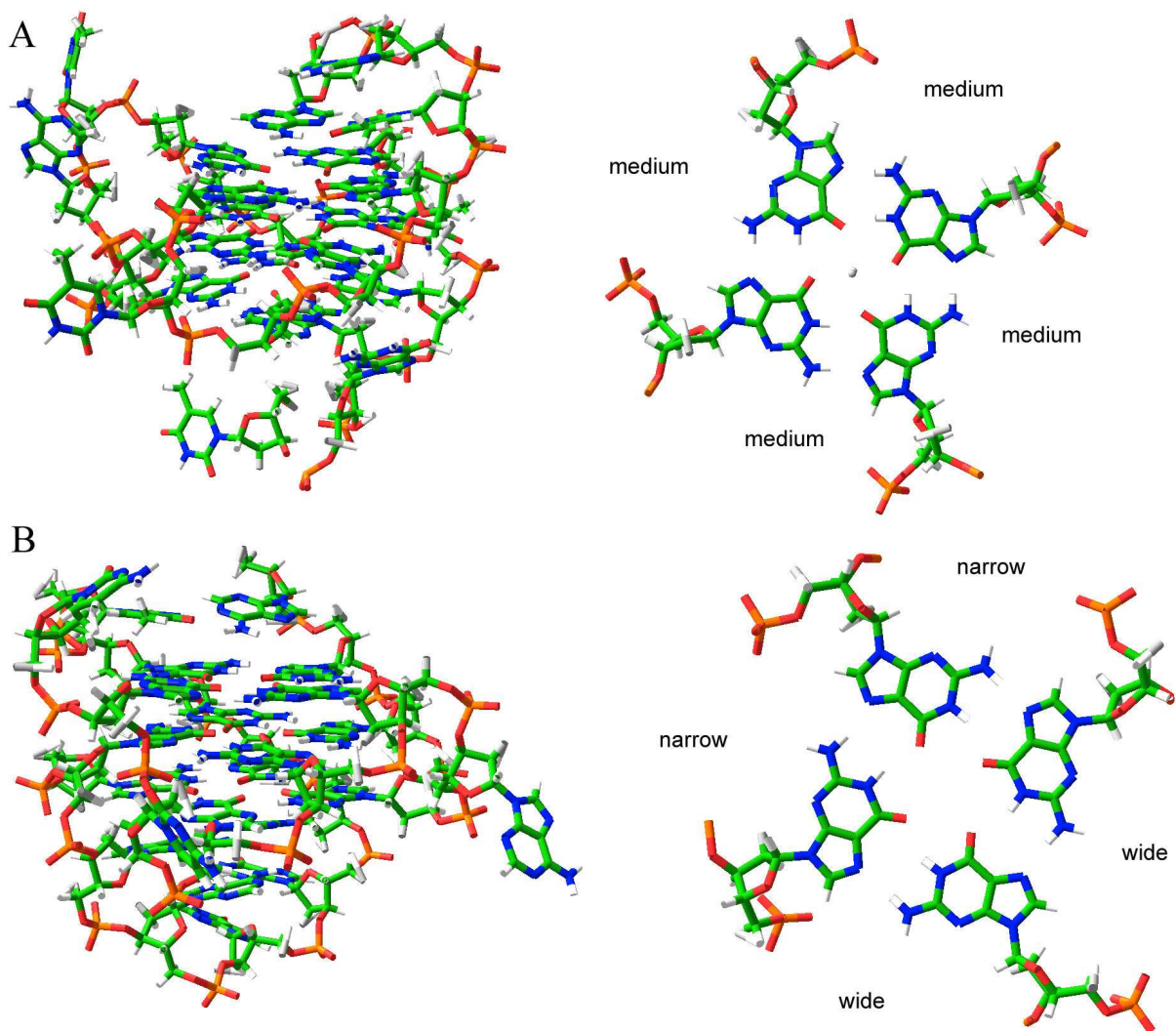


Fig. 6 NMR-derived topology and one of deposited structures of the c-myc quadruplex (A) (PDB 1XAV) and c-kit quadruplex (B) (PDB 2O3M)

An other category of quadruplexes involve oligonucleotide aptamers comprising quadruplex forming sequences, which have the ability to selectively act as inhibitors of signal

transduction or transcription via binding to particular targets, such as Stat3 or nucleolin in cancer cells. Few 3D structures of quadruplexes formed from aptamer sequences have been fully characterized; that of the thrombin-binding sequence d(GGTTGGTGTGGTTGG) is a notable exception. The third category comprises potential quadruplexes that may be formed from appropriate G-rich sequences that are present within a wide range of genes (and very extensively in non-coding regions of many genomes).

Quadruplexes can be formed from one, two or four separate strands of DNA (or RNA) and can form a wide variety of topologies. Potential unimolecular (i.e. intramolecular) G-quadruplex forming sequences can be described as follows: $G_m X_n G_m X_o G_m X_p G_m$, where m is the number of G residues in each short G-tract, which are usually directly involved in G-tetrad interactions. X_n , X_o and X_p can be any combination of residues, including G, forming the loops. The assumption that all G tracts within a quadruplex sequence are identical is true for vertebrate telomeric sequences, but is not always the case for non-telomeric genomic sequences. Quadruplex structures may be classified according to their strand polarities and the location of the loops that link the guanine strand(s) for quadruplexes formed either from a single-strand or from two strands. Quadruplexes are designated as parallel and anti-parallel. The anti-parallel topology is found in the majority of bimolecular and in many unimolecular quadruplex structures determined. The formation of propeller type loops is observed in the parallel strands. Adjacent G-strands join creating lateral loops while opposite G-strands join forming diagonal loops. ^[11]

All parallel quadruplexes have all guanine glycosidic angles in an anti conformation (Fig. 2). Anti-parallel quadruplexes have both syn and anti guanines, arranged in a way that is particular for a given topology and set of strand orientations, since different topologies have the four strands in differing positions relative to each other. All quadruplex structures have four grooves, defined as the cavities bounded by the phosphodiester backbones. Groove dimensions are variable, and depend on overall topology and the nature of the loops. Grooves in quadruplexes with only lateral or diagonal loops are structurally simple, and the walls of these grooves are bounded by monotonic sugar phosphodiester groups. Grooves that incorporate propeller loops have more complex structural features that reflect the insertion of the variable-sequence loops into the grooves (Fig. 6).

G4 DNAs have several distinct structural features compared with duplex DNA, notably the possession of four quasiequivalent grooves and a pronounced channel of negative electrostatic potential running through the center of the planes of G quartets, allowing metal ions to be coordinated between the planes in a bipyramidal antiprismatic manner. The stability

and formation of G-quadruplexes is cation dependent. The precise location of the cations between the tetrads is dependent on the nature of the ion, with Na⁺ ions within the channel being observed in a range of geometries; in some structures, a Na⁺ ion is in plane with a G-tetrad whereas in others it is between two successive G-tetrads. K⁺ ions are always equidistant between each tetrad plane, and form the eight oxygen atoms in a symmetric tetragonal bipyramidal configuration. There are a number of well-established examples where the change from Na⁺ to K⁺ induces profound structural alteration, implying high conformational flexibility for these particular quadruplexes. ^[11]

Bimolecular quadruplexes are an association of two strands which increases the topological variation (Hairpin Dimer in Fig. 5). It is noteworthy that even conservative changes in the sequence have major topological consequences. In solution it is apparent that multiple structures sometimes exist in equilibrium. It is not possible at present to define a comprehensive set of rules that specifies the folding of bimolecular G-quadruplexes based upon their sequences. However, several significant contributing factors are apparent including loop length and sequence, and G-tract length. ^[11]

1.2.2 Vertebrate telomeric quadruplex

The ends of linear chromosomes present a problem for the replication machinery. Specifically, DNA polymerase cannot synthesize the extreme 5' end of the lagging strand. Even if an RNA primer were paired with the 3' end of the DNA template, it could not be replaced with DNA. Consequently, in the absence of a mechanism for completing the lagging strand, DNA molecules would be shortened at both ends by the length of an RNA primer with each round of replication. This would eventually lead to the loss of essential genetic information at the ends of the chromosomes.

The ends of eukaryotic chromosomes, the telomeres (Greek: telos, end) have a repetitive sequence (Fig. 7). Telomeric DNA consists of 1000 or more tandem repeats of a short G-rich sequence (TTGGGG in the protozoan *Tetrahymena* and TTAGGG in humans) on the 3'-ending strand of each chromosome end. Moreover, this strand has a 12- to 100-nt single-strand overhang. This 3' extension can serve as a template for the primer that initiates the final Okazaki fragment of the lagging strand.

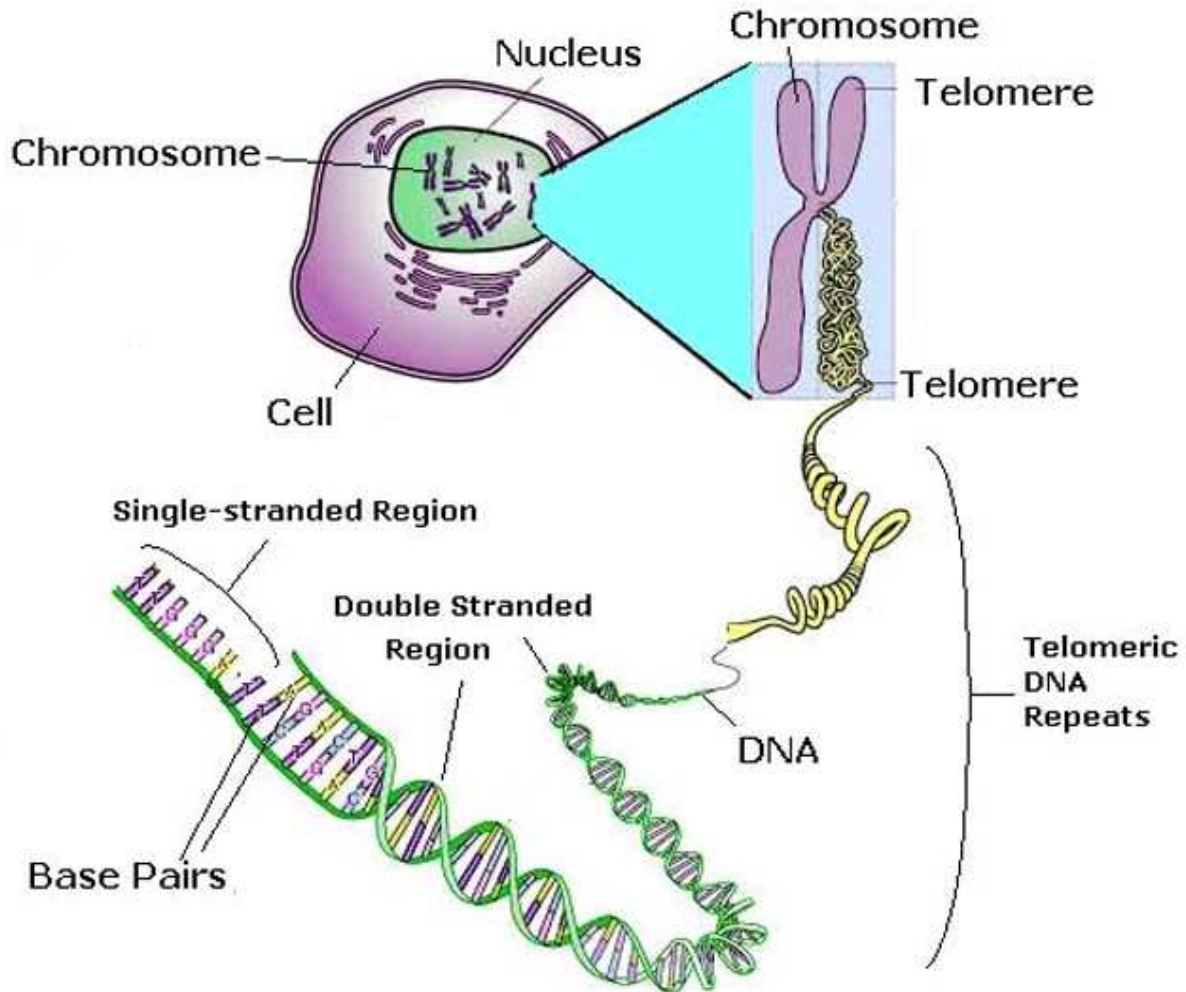


Fig. 7 Telomeric DNA, the end of eukaryotic chromosomes.

Elizabeth Blackburn (1984) has shown that telomeric DNA is synthesized and maintained by an enzyme named telomerase. Tetrahymena telomerase, for example, adds tandem repeats of the telomeric sequence TTGGGG to the 3' end of any G-rich telomeric oligonucleotide independently of any exogenously added template. A clue as to how this occurs came from the discovery that telomerases are ribonucleoproteins whose RNA components contain a segment that is complementary to the repeating telomeric sequence. This RNA apparently acts as a template for a reaction in which nucleotides are added to the 3' end of the DNA. Telomerase thus functions similarly to reverse transcriptase; in fact, its protein component is homologous to reverse transcriptase. Telomerase repeatedly translocates to the new 3' end of the DNA strand, thereby adding multiple telomeric sequences to the DNA. The DNA strand complementary to the telomeric G-rich strand is apparently synthesized by the normal cellular machinery for lagging strand synthesis, which necessarily leaves a 3' overhang on the G-rich strand.^[4]

Several recent studies have suggested that the structure of the ends of telomerase may be more complex than originally thought. Griffith, de Lange and co-workers have found that telomers do not end in a linear manner. ^[12] They demonstrated, using electronic microscopy, that the human telomeric binding protein TRF2 can remodel telomeric DNA into a large duplex loop (t-loop) in vitro (Fig. 8). In their model of the formation of the t-loop structure, the single stranded overhang folds back and invades the duplex region to form a displacement loop (D-loop) at the loop-tail junction in which the G-rich strand that originally forms the duplex is displaced and becomes single stranded. ^[13]

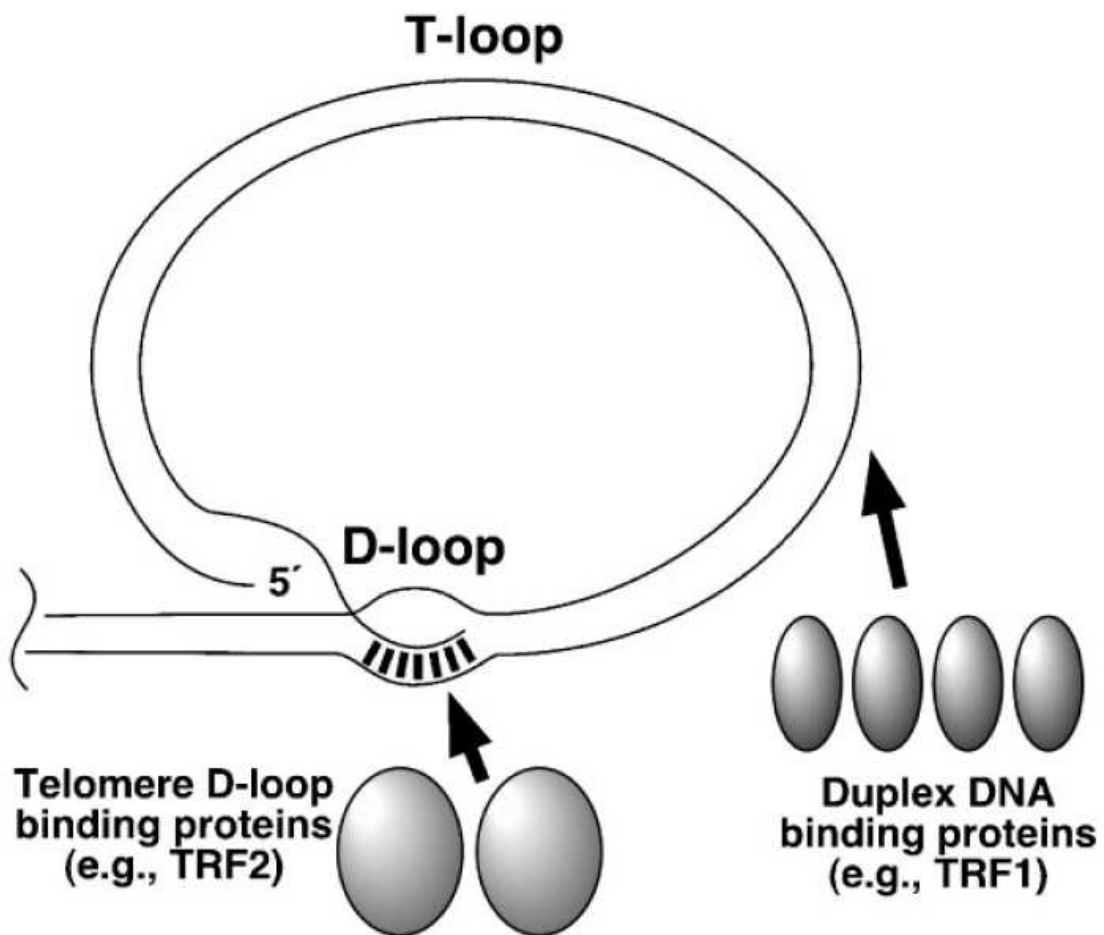


Fig. 8 Cartoon showing the T-loop and D-loop and associated telomere binding proteins. ^[14]

Telomere ends are capable of binding a number of telomeric proteins, including TRF-1 and TRF-2. These proteins bind in a sequence-specific manner to telomeric DNA and protect chromosome ends from end-to-end fusion. The protection of the telomere ends is important to cell survival because loss of normal telomere capping leads to cell death by apoptosis. ^[14]

The four-repeat quadruplex formed by the human telomeric sequence d(TTAGGG)₄ (and variants on it, notably d[AGGG(TTAGGG)₃]), can adopt different topologies in Na⁺ versus K⁺ solution.

One key feature of the crystal structure's parallel fold is that the open nature of the G-tetrad surfaces of individual quadruplexes, due to the absence of lateral or diagonal loops, facilitates their stacking together into a very compact and stereochemically acceptable arrangement. This feature would also enable the assembly of successive quadruplexes, as would occur in biological telomeric DNA, and the binding of appropriate small-molecule drugs. Formation of the telomeric quadruplex, may regulate telomerase activity.

1.2.3 Non-telomeric quadruplexes

The equilibrium for vertebrate telomeric DNA, in the absence of proteins or small molecules, has been found to favor duplex over dissociation into quadruplex and i-form motifs. However, at lower pH values or higher temperatures, the G-quadruplex and/or the i-motif were dominant. ^[7] The formation of G-quadruplex versus duplex is sequence dependent. There are several of examples of sequences in the literature where G-quadruplex is preferentially formed over the duplex, as in the relevant G-quadruplex element in the human c-MYC promoter ^[15] or in the platelet-derived growth factor-A (PDGF-A) gene through the NHE region. This region is structurally dynamic and capable of adopting non-B-DNA conformations. ^[16] In figure 3 we summarise some of the factors which influence the equilibrium. Ligand binding my strongly influence this equilibrium.

G-quadruplex-forming sequences can occur in double-stranded non-telomeric regions of the human genome, e.g. in promoter and immunoglobulin switch regions and in recombination hot spots. ^[17]

The majority of potential quadruplex sequences of the complete human genome sequence appear to be involved in more than one possible quadruplex, either as a result of being in a sequence with more than four consecutive runs of guanine or because a lack of parity in the lengths of the loop sequence means that some of the guanines in the G-runs have to be part of at least one of the loop sequences.

The findings that quadruplex sequences can occur in the promoter regions of several cancer genes have stimulated a number of structural studies (Fig. 9).

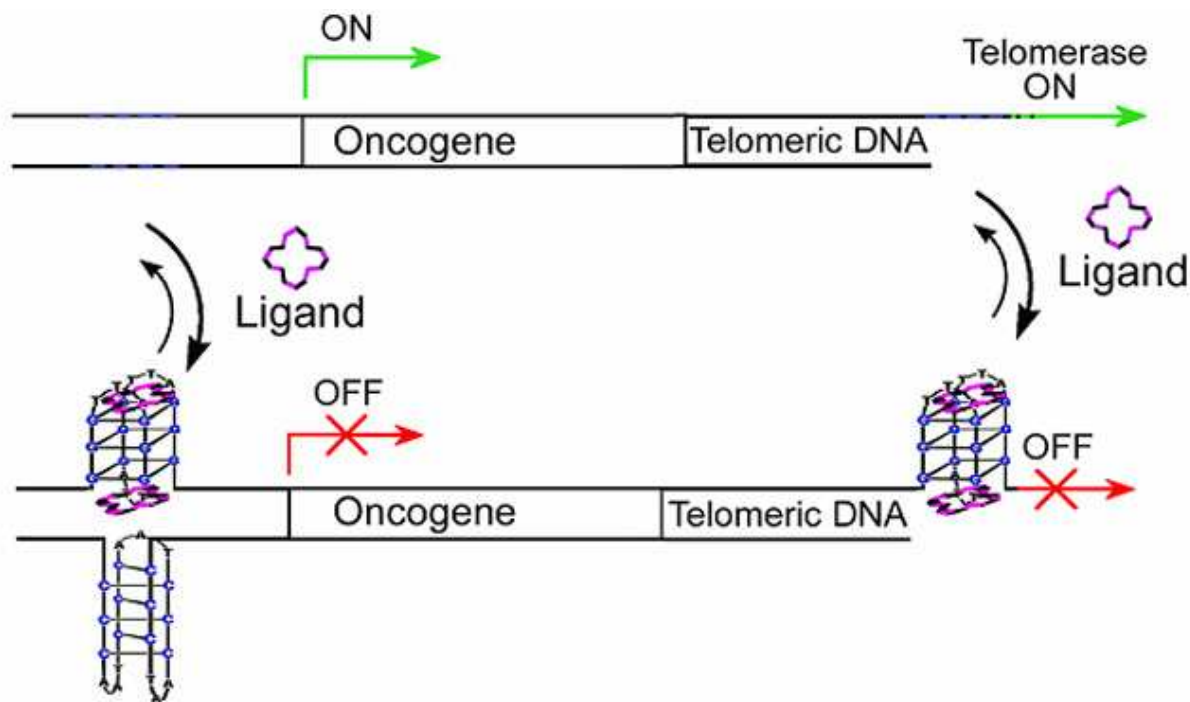


Fig. 9 Telomere and promoter inhibition by the binding of a synthetic ligand to G-quadruplex DNA.

There is a significant correlation between quadruplex sequence occurrence and classes of gene, with proto-oncogenes having a high quadruplex forming potential compared with a low potential for tumour-suppressor genes.^[18] Potential quadruplex forming sequences also occur within regions of chromosomal translocations. Much of the interest in non-telomeric quadruplex sequences and their possible structures are due to their occurrence in genes associated with proliferation, especially in *c-myc* and a number of oncogenes. They may be involved in the regulation of gene expression, and that this might be amenable to exploitation by small-molecule therapy.^[11]

C-myc is a protooncogene, which is overexpressed in a wide range of human cancers (Fig. 6). When it is specifically-mutated, or overexpressed, it increases cell proliferation and functions as an oncogene. The NHE III1 G-rich sequence in the promoter region of the *c-myc* oncogene, which is responsible for 80–90% of its transcriptional activity, has been studied in detail.

Adam Siddiqui-Jain et al. have demonstrated that the purine-rich strand of the *c-MYC* promoter can form two different intramolecular G-quadruplex structures. The biologically relevant structure is the kinetically favored chairform G-quadruplex, which is destabilized when mutated with a single G3A mutation, resulting in a 3-fold increase in basal transcriptional activity of the *c-MYC* promoter.^[19] The G-quadruplex may therefore act as a

transcriptional repressor element. In other words: it could be possible to control the transcription of c-myc by G-quadruplex stabilization.

1.2.4 G-Quadruplex: a potential target for anti-cancer drug design.

There are two potential mechanisms: Most cancer cells express high levels of telomerase, which maintain telomere length. As most cancer cells have higher telomerase-activity rates than normal cells, both telomerase and the telomeres can be used as important targets for cancer chemotherapy. Formation of intramolecular G-quadruplex structures can block the action of telomerase. Since the substrate of telomerase is the 3' single-stranded overhang of telomeric DNA, stabilization of these quadruplex structures by small molecules can lead to the inhibition of telomerase, which is the 1st potential mechanism (Fig. 9). The 2nd potential mechanism is to target the promoter of an oncogen (Fig. 9). Indeed, a number of organic molecules have been found to be G-quadruplex stabilizers and potential antitumor agents.

1.3 Known G-quadruplex Ligands

General features of molecules that bind to G4 tetraplexes include a large flat aromatic surface and cationic charges. The molecular size, a planar chromophore and hydrophobicity are also favorable for stacking with the guanine tetrads. These compounds are generally similar to intercalators or are derivatives of well-known intercalators and can stack with the terminal G quartets and form electrostatic interactions. This binding mode was initially inferred from steric and geometric considerations and has been supported by NMR and modelling studies (Fig. 10).

The cationic porphyrin compound 5,10,15,20-tetra-(*N*-methyl-4-pyridyl)porphine (TMPyP4; Fig. 10) doesn't possess the appropriate molecular dimensions to be a highly selective G-quadruplex ligand. TMPyP4 binds to the intramolecular quadruplex DNA formed by human telomere DNA repeats (GGGTTA)₄ by stacking externally with the guanine tetrad but exhibits almost no selectivity for quadruplex DNA over duplex DNA. [20] TMPyP4 is commercially available and serves as an important comparison for new molecules. TMPyP4, as well as many compounds studied so far, suffer from poor or insufficient preference for quadruplexes over duplexes. TMPyP4 has a K_d of 50-300 nM for the G-quadruplex as well as for the duplex. This indicates that the TMPyP4 has no specificity for the G-quadruplex over other nucleic acids which would make side effects in a possible anti-cancer therapy more probable. A good G-quadruplex ligand should possess a good affinity as well as a high specificity for a single G-quadruplex DNA.

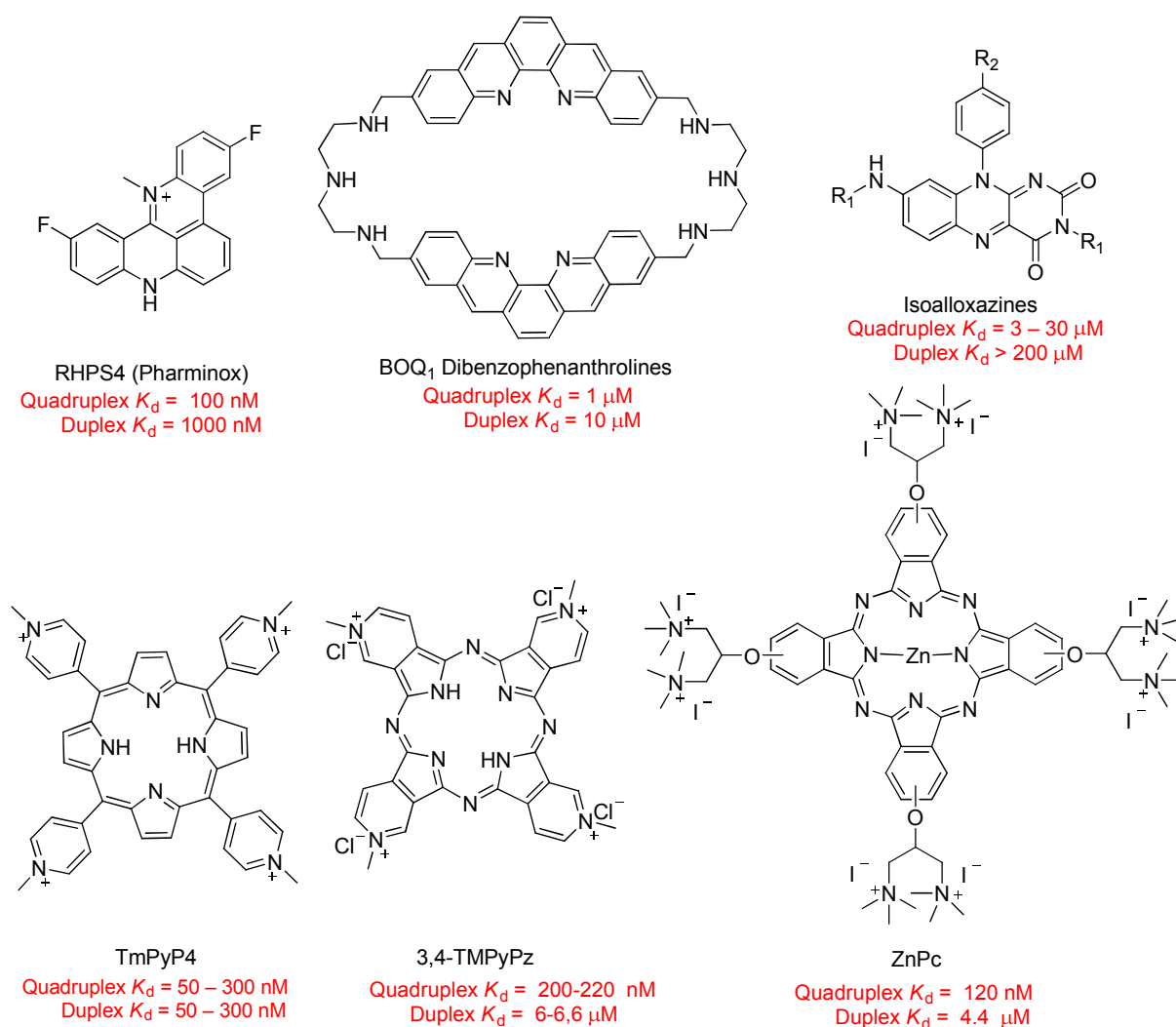


Fig. 10 G-quadruplex Ligands and the reported K_d values.

BOQ1 (a Dibenzenophenanthroline, Fig. 10), which combines large units that are able to stack on a G quartet and a macrocyclic scaffold likely to have favorable groove/loop interactions, appeared to be a potential candidate for binding to G-quadruplexes has a K_d of $1\mu\text{M}$ with low specificity for quadruplex over duplex. ^[21]

With the Isoalloxazines (Fig. 10) side chains were introduced to provide potential for interactions with quadruplex loops and grooves and the negatively charged sugar-phosphate backbone. These compounds didn't show any significant binding to the control duplex and bound to the various G-quadruplex DNA targets with modest affinity. ^[22]

RHPS4 exhibits large difference between concentrations needed for telomerase inhibition and acute cellular toxicity (Fig. 10). RHPS4 causes a marked cessation of cell growth with 21NT breast cancer cell lines, and other cell lines possessing relatively short telomeres. The drug forms complex stabilising interactions by stacking on the ends of the G-quadruplex. ^[23]

In 2006 a new class of G-quadruplex inducing and stabilising ligands were presented by Gonçalves et al: 3,4-Tetramethylpyridiniumporphyrazines. These ligands binds with modest strength and selectivity to human telomeric G-quadruplex DNA, inducing the formation of an antiparallel quadruplex in a process that mimics molecular chaperones.

Cationic porphyrins, in particular tetramethylpyridiniumporphyrin (TMPyP4), are well known for their ability to bind to different types of G-quadruplexes and, in some cases, to facilitate G-quadruplex formation (Fig. 10). Tetramethylpyridimniumporphyrazines (TMPyPz) bind with a K_d of 200 nM to quadruplexes, selectively inducing the antiparallel conformer. Using similar experimental conditions, the TMPyP4 porphyrin shows a K_d which is almost two orders of magnitude weaker than the observed binding for the porphyrazines. The porphyrazines do not show any significant binding affinities against duplex DNA at a concentration up to 5 μ M, which represents a lower limit of 30 for the binding specificity for quadruplex over duplex. This is a very important improvement in relation to TMPyP4, which does not present any quadruplex/duplex selectivity. ^[24]

A water-soluble, octacationic zinc phthalocyanine (ZnPc, Fig. 10) was found to be a very good G-quadruplex DNA stabilizer by Ren et al. This molecule could induce G-quadruplex structural transitions from the antiparallel to the parallel. More importantly, ZnPc was found to induce parallel structure formation in cation-deficient conditions. ^[25] Structural transition between antiparallel and parallel forms of G quadruplexes in telomeric DNA plays an important role in telomere formation. ^[26]

All the presented molecules have either a low affinity to the G-quadruplex and/or have a low specificity. Especially the low specificity presents a problem as it indicates that the molecules bind to many other nucleic acids, opening new alternative mechanisms for their reported biological effects. The hypothesis that telomerase inhibition occurs via a quadruplex-mediated mechanism would be strongly supported by a molecule that shows G4 selectivity over duplex DNA affinity, and increased potency for telomerase inhibition, together with a low level of acute cytotoxic activity.

1.4 Summary of our approach.

We focused on preparing small-molecules with high affinity for G-quadruplex DNA ($K_d < 10$ nM) combined with a high specificity (100 fold lower or less affinity for non-G-quadruplex structures).

Our molecules have a phthalocyanine skeletal structure which has the same shape as G-tetrad DNA. [24, 25] We were interested in making phthalocyanines with C_{4h} symmetry to match the symmetry of G-tetrad DNA (Fig. 11). The typical paths to synthesize Pcs give a statical mixture of C_{4h} , C_{2v} , C_s and D_{2h} regioisomers. Our synthesis of C_{4h} symmetric Pcs starts from 4-nitro-phthalic anhydride and urea with ammoniummolybdate as a catalyst (Fig. 12). Reduction of NO_2 gives the corresponding tetraamino zinc phthalocyanine.

We concentrated our efforts towards the synthesis of guanidine-containing phthalocyanines (GPCs) (Fig. 12), because oligo- and poly-guanidinium peptides have shown the ability to mediate efficient cellular uptake and the translocation of large molecules across plasma membranes. [27] In addition, guanidinium-containing small molecules can also exhibit improved cellular uptake and enhanced RNA binding as compared to analogous molecules containing ammonium groups. [28, 29] In contrast to ammonium groups, guanidinium groups are highly basic, planar and exhibit directionality in their H-bonding interactions. Guanidine side chains were also introduced to facilitate the interactions with quadruplex loops and grooves (Fig. 11) and the negatively charged sugar-phosphate backbone. Depending on the substituents in the guanidine groups, and the presence or absence of zinc metal; the properties like solubility, structure-selective DNA binding, fluorescence, cellular uptake and photo-cytotoxicity can be tuned.

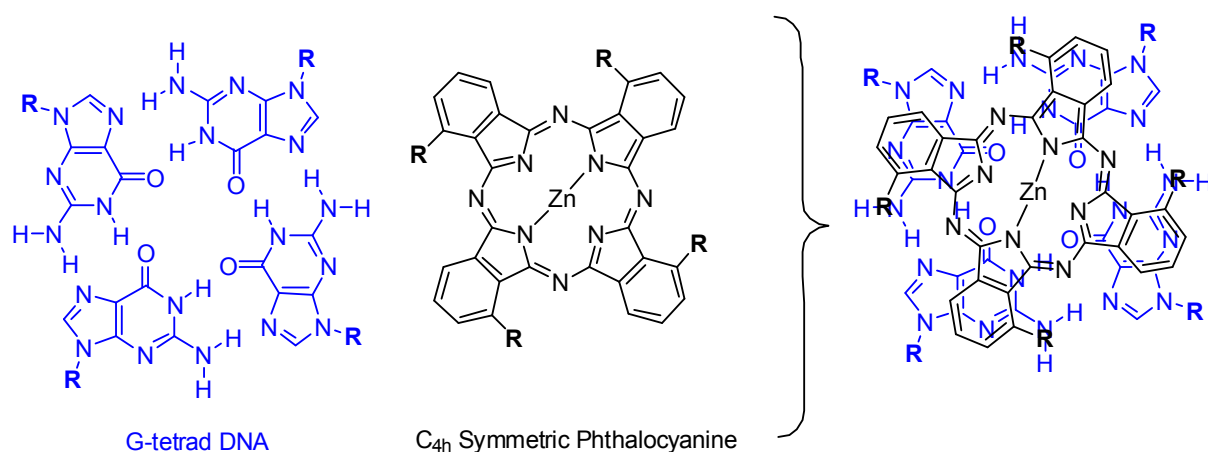


Fig. 11 The C_{4h} Symmetric Phthalocyanine stacking on top of a G-tetrad.

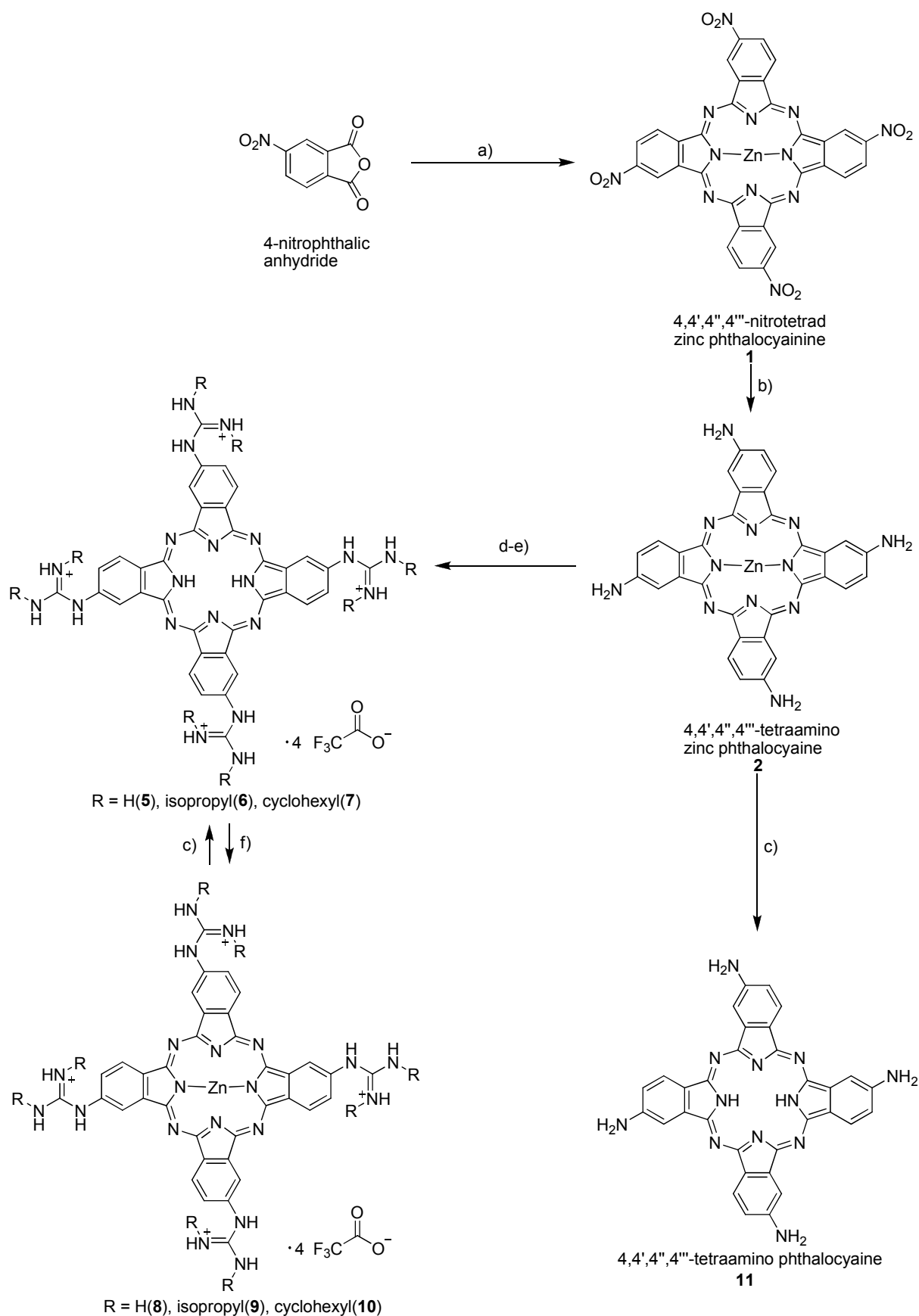


Fig. 12 Synthesis of tetraguanidino phthalocyanines **5-7**, tetraguanidino zinc phthalocyanines **8-10** and 4,4',4'',4'''-tetraamino phthalocyanine **11**. **a)** zinc chloride, urea, ammonium molybdate, nitrobenzene, 185°C, 4h; **b)** sodium sulphide, DMF, 60°C, 1.5h; **c)** pyridine-HCl, 120°C; **d)** R-N=C=N-R, pyridine-HCl, 120°C; **e)** H₂O/TFA; **f)** acetic acid, Zn Cl₂, 120°C.

From the known C_{4h} symmetric 4,4',4'',4'''-tetraamino phthalocyanine **2** [30, 31] we synthesized guanidino phthalocyanines (GPcs). We reacted **2** with various carbodiimides in the presence of pyridine-HCl at 120°C. Surprisingly, under these conditions the zinc atom was removed to furnish the metal-free GPcs **5 – 7**. It was also possible to remove the zinc from the starting material (**2**) using the same conditions (reaction **c** in Fig. 12). This opened a new tuning option for the physical and biological properties of GPcs. In a combinatorial fashion variable metal ions can be re-inserted into the metal-free GPcs. The removal of a metal has never previously been reported and only was possible by destroying the macrocycle. The synthesised compounds **5 – 10** were characterized by MALDI TOF MS, high resolution ESI MS and NMR. With UV-VIS the extinction coefficients were determined for each of the compounds.

Fluorescence is a very important feature of these compounds. By addition of DNA the fluorescence of the diisopropyl derivatives (**6** and **9**) dramatically increased and could be detected down to concentrations in the nM range allowing fluorescence enhancement assays to determine the binding affinity (K_d value). We compared the binding affinity of diisopropyl substituents with other GPcs in the presence or absence of zinc metal. The K_d values which were obtained were < 2 – 90 nM. Especially the diisopropyl derivatives (**6** and **9**) had K_d values in the low nM range which surpassed all the K_d values published until this moment. In addition to high affinity diisopropyl compounds showed a high specificity for the G-quadruplex. The specificity was checked by addition of calf thymus DNA (CT DNA) or addition of a mixture of yeast tRNA (tRNA).

The additional advantage of fluorescence enhancement method was that Balayeshwanth R. Vummidi could detect the compounds in living cells, which normally requires a fluorescence tag. The diisopropyl derivatives (**6** and **9**) pass through cell membrane into the cell. These compounds also exhibit relatively low cytotoxicity, and anti-cancer activity in vivo.

2. Phthalocyanines

Phthalocyanines (Pcs) have an immense potential in diverse fields, making them one of the most highly studied macrocyclic and coordination compounds. Pcs were discovered as an impurity in an industrial preparation of phthalimide in 1907. Long after its unglamorous discovery it was often considered as the unsophisticated relative of the porphyrin family.

Phthalocyanines got their name by a combination of the prefix phthal, originally from naphtha (rock oil), to underline the association with its various phthalic acid derived precursors, and cyanine (blue). Linstead, who conceived the name of this molecule, was also the first to recognize the capacity of the Pcs in academic science. Linstead obtained Pcs from the Imperial Chemical Industries (ICI), a pigment company eager to understand the structure of the coloured substance. This material was the result of a serendipitous accident in 1928 during the industrial preparation of phthalimide from phthalic anhydride: the glass-lined reaction vessel cracked, exposing the outer steel casing to the reaction, resulting in the formation of a blue-green material. The result of the collaboration between Linstead and ICI was a series of six papers describing the structure of Pcs and the synthesis of some of its metal derivatives.

Their high degree of aromaticity, their singular chemical structure, the flexibility involved in the synthesis of phthalocyanines, and their unique electronic spectra have made Pcs useful in a wide range of applications as in synthetic catalysts, photovoltaic devices, chemical sensors and data storage devices.^[32-35] Pcs also have interesting applications in vivo like tattoo inks and in sensitizers for photodynamic therapy.^[36] Only to satisfy the demand for blue-green colours many thousands of tons of phthalocyanines are produced world-wide, per annum. Phthalocyanines are a remarkably robust and versatile family of compounds of central importance for the industrial manufacture of blue and green pigments. In light of their diverse repertoire of coordination chemistry, electronic properties, and stable core that is amenable to modification, Pcs can also be considered as useful building blocks for the construction of functional supramolecular assemblies. Along these lines, Pcs bearing peripheral lipophilic substituents displaying liquid-crystalline behaviour have been prepared.^[37] Pc derivatives with extended aromatic systems are showing potential as photosensitisers for the photodynamic therapy of cancer.^[38]

2.1 Synthesis of Phthalocyanines

Pcs can be synthesized from aromatic *ortho*-dicarboxylic acid derivatives such as phthalic acid, phthalonitriles, phthalic anhydrides, phthalimides, diiminoisoindolines, *o*-cyanobenzene-

amides (Fig. 13). *Ortho*-substitution in the precursor is a definite requirement. Phthalonitriles in particular can lead to reactions of high yields and high purity for the synthesis of PcMs. The reactions often involve simply heating the phthalonitriles in the presence of a metal ion source as either a melt of reagents or in a high boiling solvent like *n*-pentanol. Phthalic anhydrides and phthalimines which, on the other hand, require the presence of a nitrogen source such as urea and a catalyst such as ammonium molybdate or boric acid in order to get macrocycle formation. Phthalimides and some of the other phthalic acids derivatives tend to give irregular results and more by-products are often obtained. Due to the inexpensive cost of phthalic anhydrides these precursors are used extensively for the large scale production of Pcs in industry.

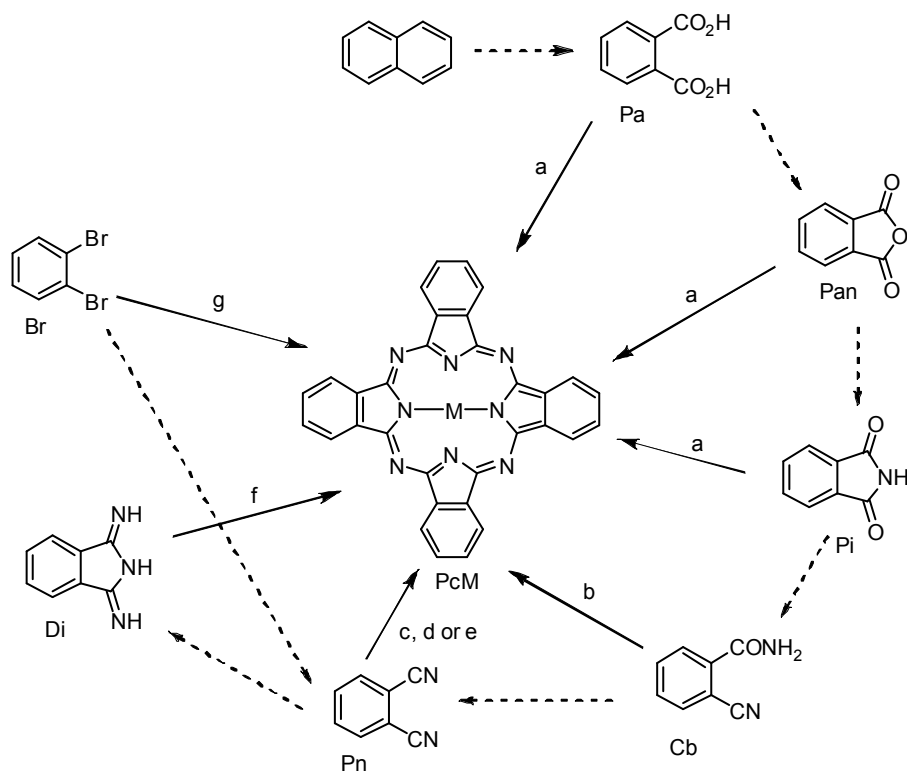


Fig. 13 The synthesis of metal-containing phthalocyanines (PcM). The letters indicate the synthetic method and the dotted arrows the synthetic connectivity between precursors. **a)** urea, Δ , Metal ion (Wyler method); **b)** DMAE, Δ ; **c)** Metal or metal salt, Δ ; **d)** Metal salt, solvent, Δ ; **e)** Metal salt, base, solvent, Δ (Tomoda method); **f)** Metal salt, DMAE, Δ ; **g)** CuCN , Δ .

There are two common precursors to make the metal-free phthalocyanine (PcH_2) (Fig. 14). The 1,2-disubstituted benzene precursors for metal-free phthalocyanine are phthalonitrile and 1,3-diiminoisoidoline. In general the yields of PcH_2 synthesis are much lower than the

metal-containing Pcs. The explanation for this is the template effects during condensation reaction of the metal containing Pcs (Fig. 15).

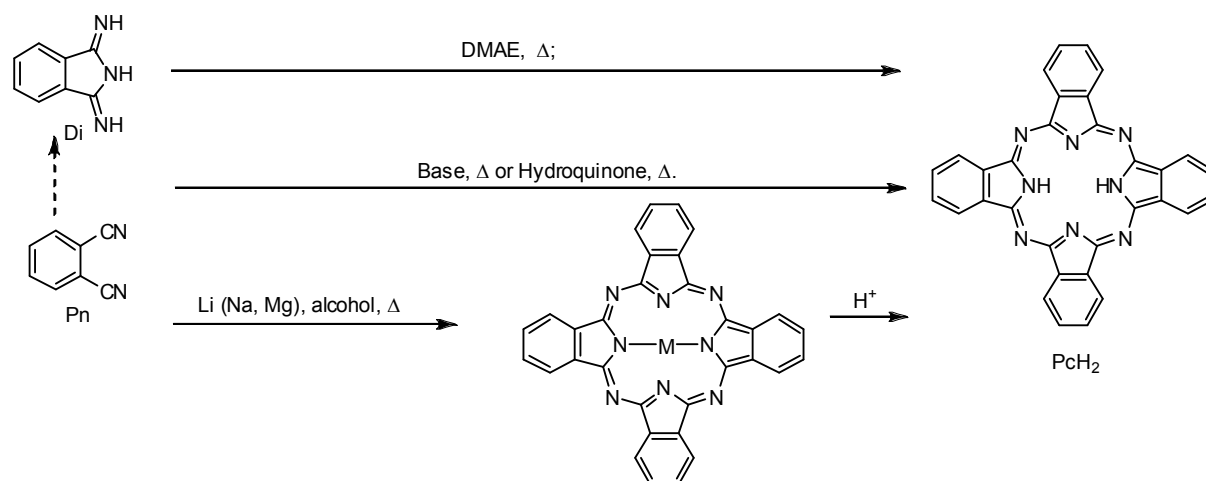


Fig. 14 The synthesis of metal free phthalocyanine (PcH₂). The dotted arrows indicate the synthetic connectivity between precursors.

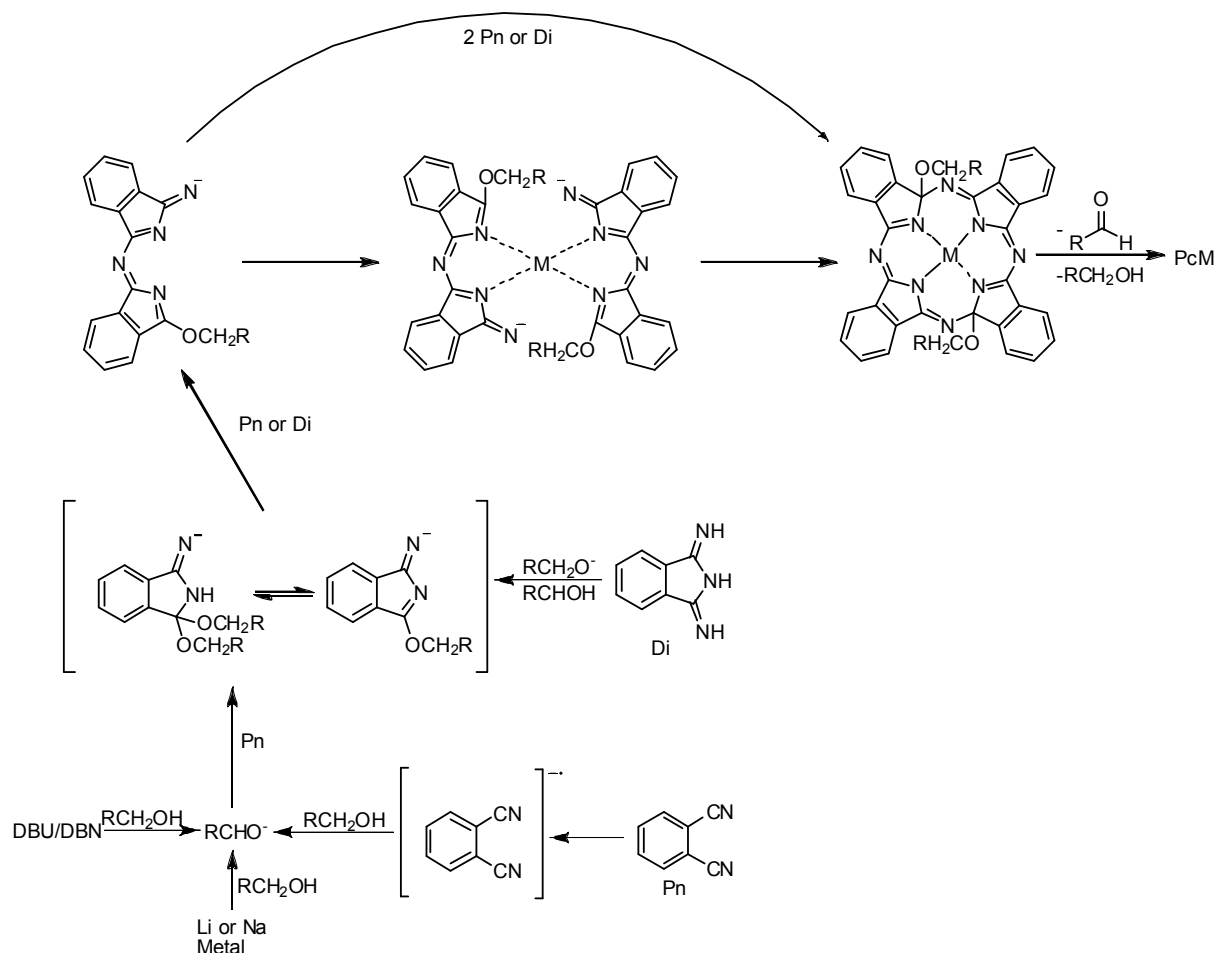


Fig. 15 Intermediates which have been isolated in mechanistic studies into phthalocyanine-forming reactions.

The mechanism of the condensation reaction has been extensively examined and most likely involves a stepwise polymerization of Pcs precursors or reactive intermediates followed

by coordination of the central metal ion and ring closure to the macrocycle. [39] Polymerization is followed by a cyclization resulting in a $16e^-$ macrocycle. A two-electron reduction is necessary to achieve the $18-\pi$ electron aromaticity (Fig. 15). This can be achieved by the elimination of an aldehyde during the aromatisation of the Pcs.

In the synthesis of the PcH_2 the metal which coordinates to the intermediate of the forming phthalocyanine is not present in the reaction. By addition of a labile metals like Mg and Li the yields can be improved somewhat (Fig. 16). The inclusion of strongly coordinating metals like Mn(II), Fe(II), Co(II), Cu(II), Zn(II) and Ni(II) can dramatically improve the yields of these reactions (Fig. 16), but their removal from metallo phthalocyanines is generally thought to be impossible without destruction of the macrocycle itself. [30, 40-43]

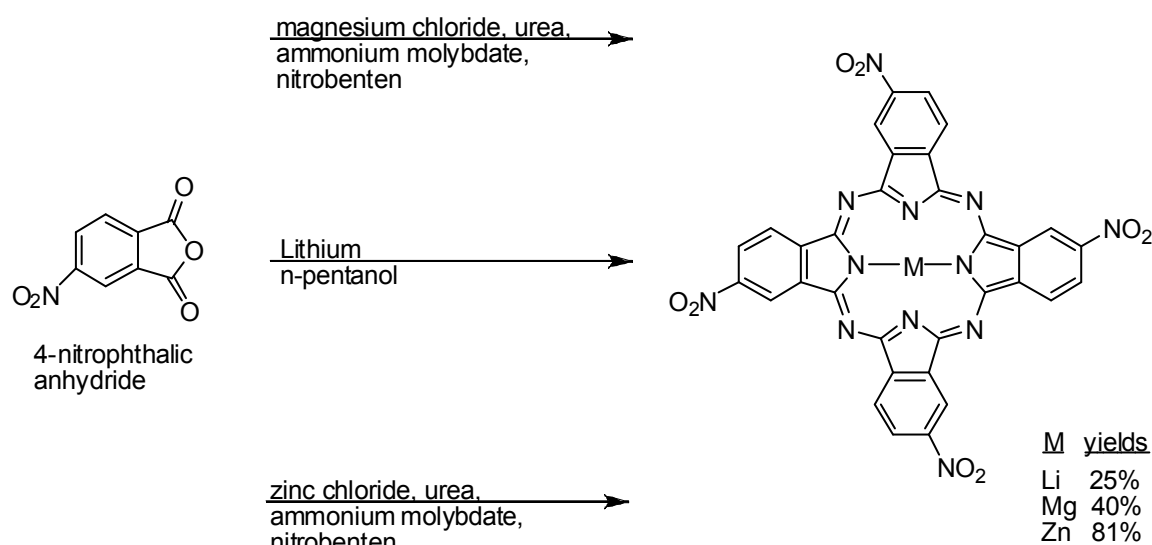


Fig. 16 Influence of the coordinating metal to the yield of Pcs formation.

It is a common practice to insert a metal-ions into the central cavity of a preformed metal-free phthalocyanine (Method a in Fig. 17) or to exchange a labile metal ion for one held more robustly (Method b in Fig. 17). But the removal of Zn(II) has never previously been reported.

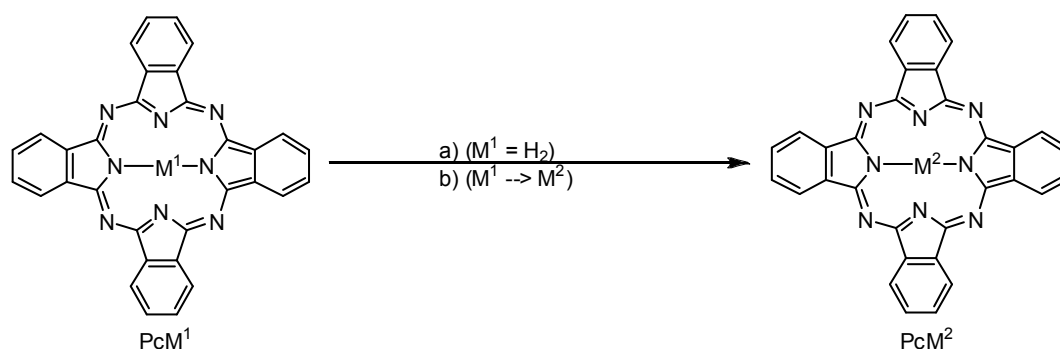


Fig. 17 Metal phthalocyanine from metal-free phthalocyanine and via metal exchange. **a)** and **b)** Metal or metal salt, Δ .

One common problem with phthalocyanines is the insolubility of their unsubstituted derivatives. This poses a significant problem for their characterization and to the development of new Pcs applications in medicine and photoelectronic devices. Through variation of substituents and functional groups the chemical, physical and electronic properties of the Pcs can be altered. Substituted phthalocyanines can be prepared by condensation of substituted precursors. For asymmetric, monosubstituted precursors this method leads to a mixture of constitutional isomers (Fig. 18). The four possible isomers can be designed by their molecular symmetry as C_{4h} , C_{2v} , C_s and D_{2h} . The 2(3)-substituted compounds often are formed in the expected statistical mixture of 12.5% C_{4h} , 25% C_{2v} , 50% C_s and 12.5% D_{2h} isomers.^[44] Due to their different geometries it should be theoretically possible to separate these isomers, but in practice is exceedingly difficult. This has motivated the design of specific Pcs precursors for the preparation of single isomers.

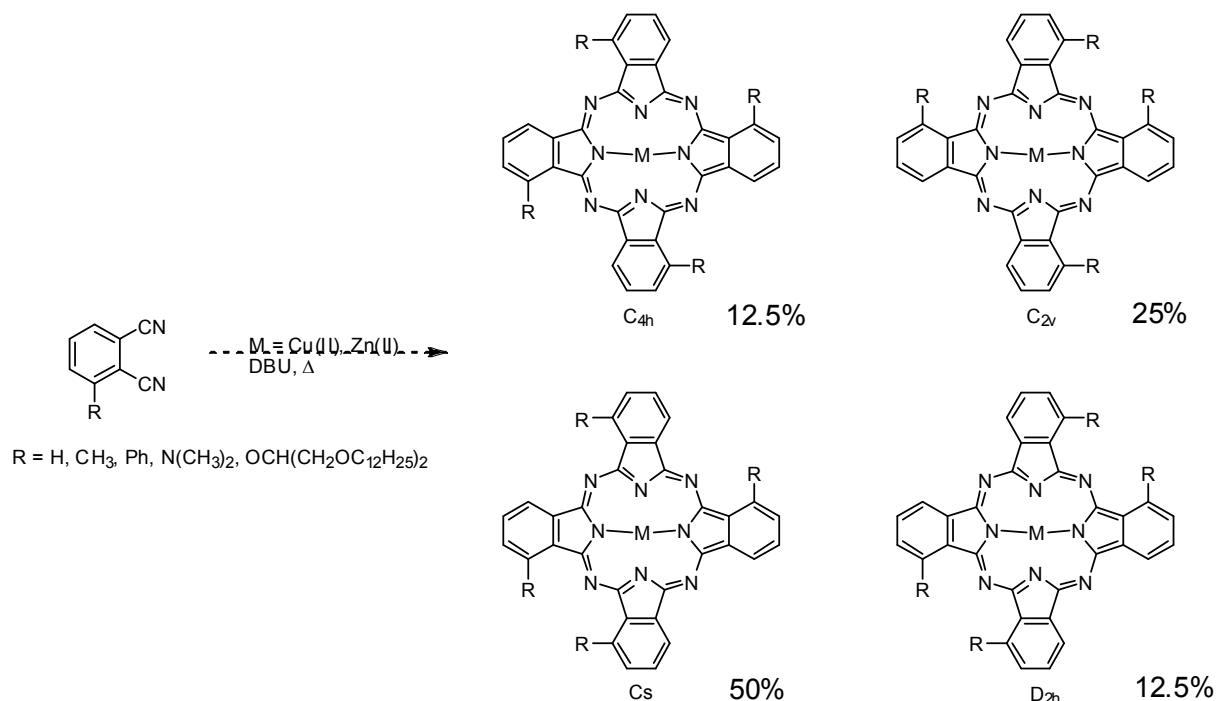


Fig. 18 Statistical mixture of constitutional isomers resulting from the condensation of an asymmetric precursor.

2.2 Our approach for synthesising C_4 symmetric phthalocyanines

Many efforts were made in getting single isomers from asymmetrically substituted precursors. The group of Chen created a facile approach to prepare peripherally substituted tetraaminometallophthalocyanines (TAMPcs) and non-peripherally substituted TAMPcs in both higher yields and purity.^[30] Using the precursors 4-nitrophthalic anhydride and 4-nitrophthalic anhydride, they synthesised the 4,4',4'',4'''-tetraamino zinc phthalocyanine (**2**) and 3,3',3'',3'''-tetraamino zinc phthalocyanine (**4**) respectively (Fig. 20). These results caught our

attention as C_{4h} symmetric isomers were reported in high yield. These materials were recognized as potential precursors for new G-quadruplex ligands containing guanidine groups (Chapter 3).

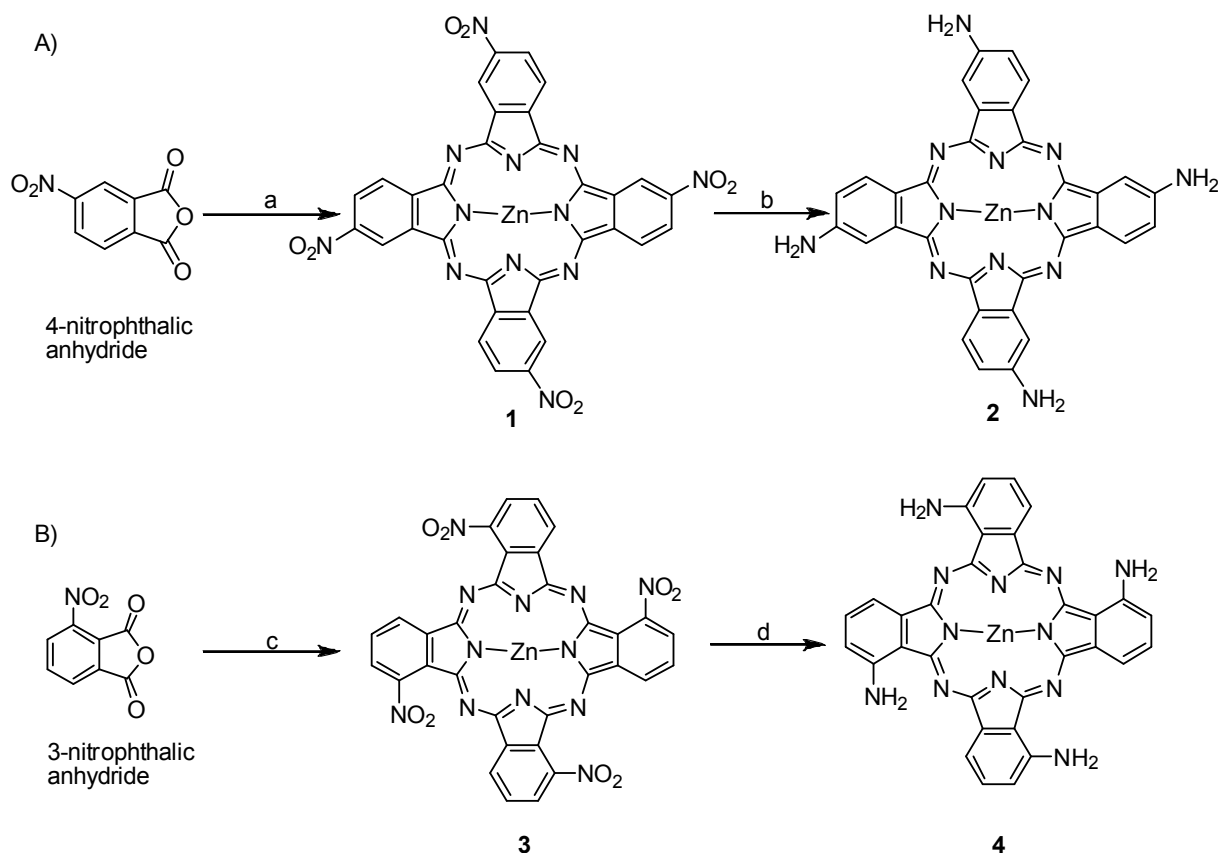


Fig. 19 Synthesis of 4,4',4'',4'''-tetraamino zinc phthalocyanine(A) and 3,3',3'',3'''-tetraamino zinc phthalocyanine(B) and our isolated yields obtained according to procedure of Cong^[30]. **a)** zinc chloride, urea, ammonium molybdate, nitrobenzene, 185°C, 4h, 65%; **b)** sodium sulphide, DMF, 60°C, 1.5h, 87.5%; **c)** zinc chloride, urea, ammonium molybdate, 150°C, 98%; **d)** sodium sulphide, DMF, 60°C, 1.5h, 43%. See appendix for NMR spectra of 2 and 4.

Given the mechanistic information available for formation of Pcs (Fig. 15), we propose a mechanism for the synthesis of the C_{4h} symmetric compound 1 (Fig. 20). The C_4 symmetry may originate from the polarization effects of the nitro group which facilitates a head-to-tail orientation of the monomers during the assembly of the macrocycle (Fig. 20).

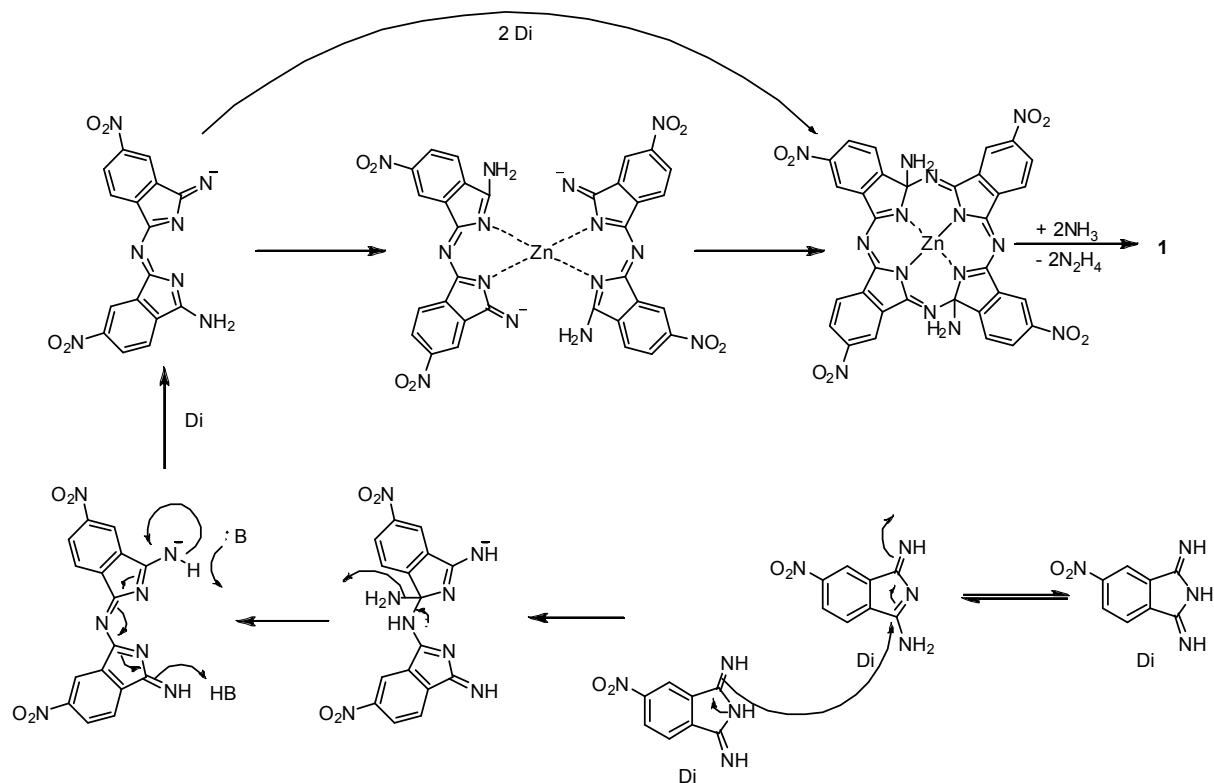


Fig. 20 Proposed mechanism of the synthesis of 4,4',4'',4'''-tetranitro zinc phthalocyanine (1).

3. Synthesis of Guanidino Phthalocyanines

3.1 Guanidinylation reactions

The guanidinium group is found in many natural products and has been extensively incorporated into various drug designs as well as artificial receptor structures. The synthesis of guanidines is complicated by their high basicity and nucleophilicity. For these reasons many methods for the synthesis of guanidines have been developed. ^[45] ^[46] Many reactions utilize reagents with easily removed protective groups.

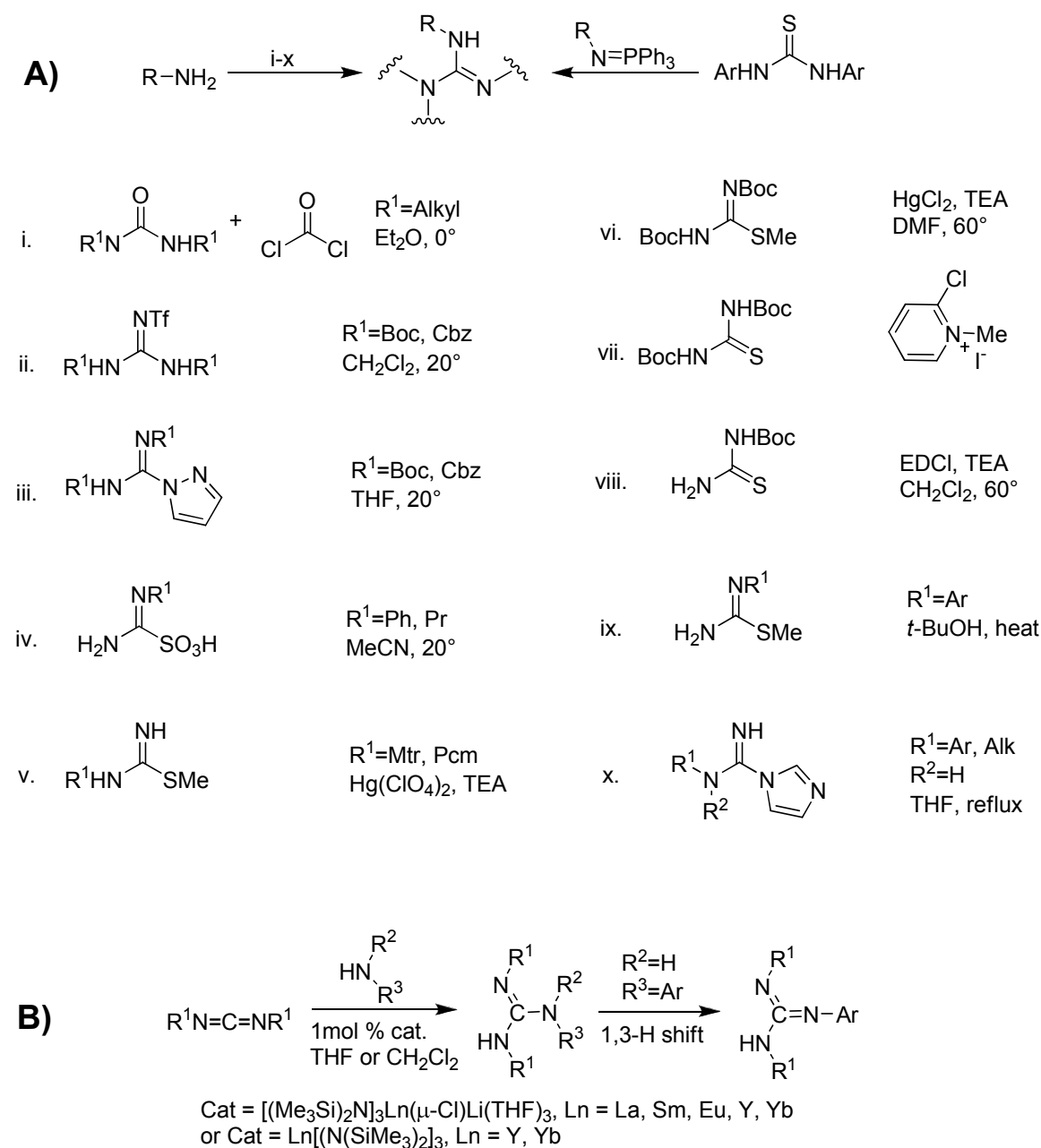


Fig. 21 Synthesis of guanidines A) attack of an amine on various activated guanidinylation reagents; B) having different substituents.

Common methods for the preparation of guanidine involve attack of an amine on various activated guanidinylation reagents (**A** in Fig. 21).^[47] Recent methods have been developed for the synthesis of guanidines having different substituents using the cyclopentadienyl-free simple lanthanide amides $[(\text{Me}_3\text{Si})_2\text{N}]_3\text{Ln}(\mu\text{-Cl})\text{Li}(\text{THF})_3$ and $\text{Ln}[(\text{N}(\text{SiMe}_3)_2)_3]$ as catalysts (**B** in Fig. 21).^[48]

3.2 Our approach

Common guanidinylation reagents like *N,N'*-diBoc-*N''*-(trifluoromethylsulfonyl)-guanidine, and *N,N'*-diBoc-1*H*-pyrazole-1-carboxamide were not sufficiently reactive to modify the electron poor amines of 4,4',4'',4'''-tetraamino zinc phthalocyanine (**2**). Carbodiimides were the first reagents for guanidinylation reported by Weith in 1873,^[49] and proved highly effective for perguanidinylation of **2**. GPCs were synthesized by reacting a C_{4h} symmetric **2**^[30, 31] with various carbodiimides in the presence of pyridine-HCl at 120°C (Fig. 22). These are the first examples, to our knowledge, using pyridine-HCl as a solvent and activator of this reaction. Surprisingly, under these conditions zinc is totally removed from the products (**5**, **6**, **7**). Zinc can be reintroduced to give **8**, **9** and **10**.

The tetraguanidine derivative **5** was synthesized by reacting the substituted aniline **2** with 100 equivalents of cyanamide. Addition of 1.2 equivalent of DMAP enhanced the guanidinylation reaction to reach completion. In the absence of DMAP a 3 substituted guanidinylation was achieved. Reinsertion of zinc was achieved by heating the metal free **5** in acetic acid and zinc chloride.

The diisopropyl derivative **6** was synthesized by reacting tetra amino **2** with 50 equivalents of the diisopropylcarbodiimide. The zinc insertion to the derivative **6** was achieved by dissolving it in acetic acid and heat it for 90 min in the presence of zinc chloride to give **9**.

The synthesis of the dicyclohexyl derivative **7** did not present any problems and reached a 4 substituted guanidinylation with 20 equivalents of *N,N'*-Dicyclohexylcarbodiimide (DCC). Zinc insertion into the dicyclohexyl derivative (**7** → **10**) was achieved using the same conditions used for the diisopropyl derivative (ZnCl_2 , Δ , acetic acid, 90°C).

The zinc removal and reinsertion can be easily followed by analytical HPLC (Fig. 23).

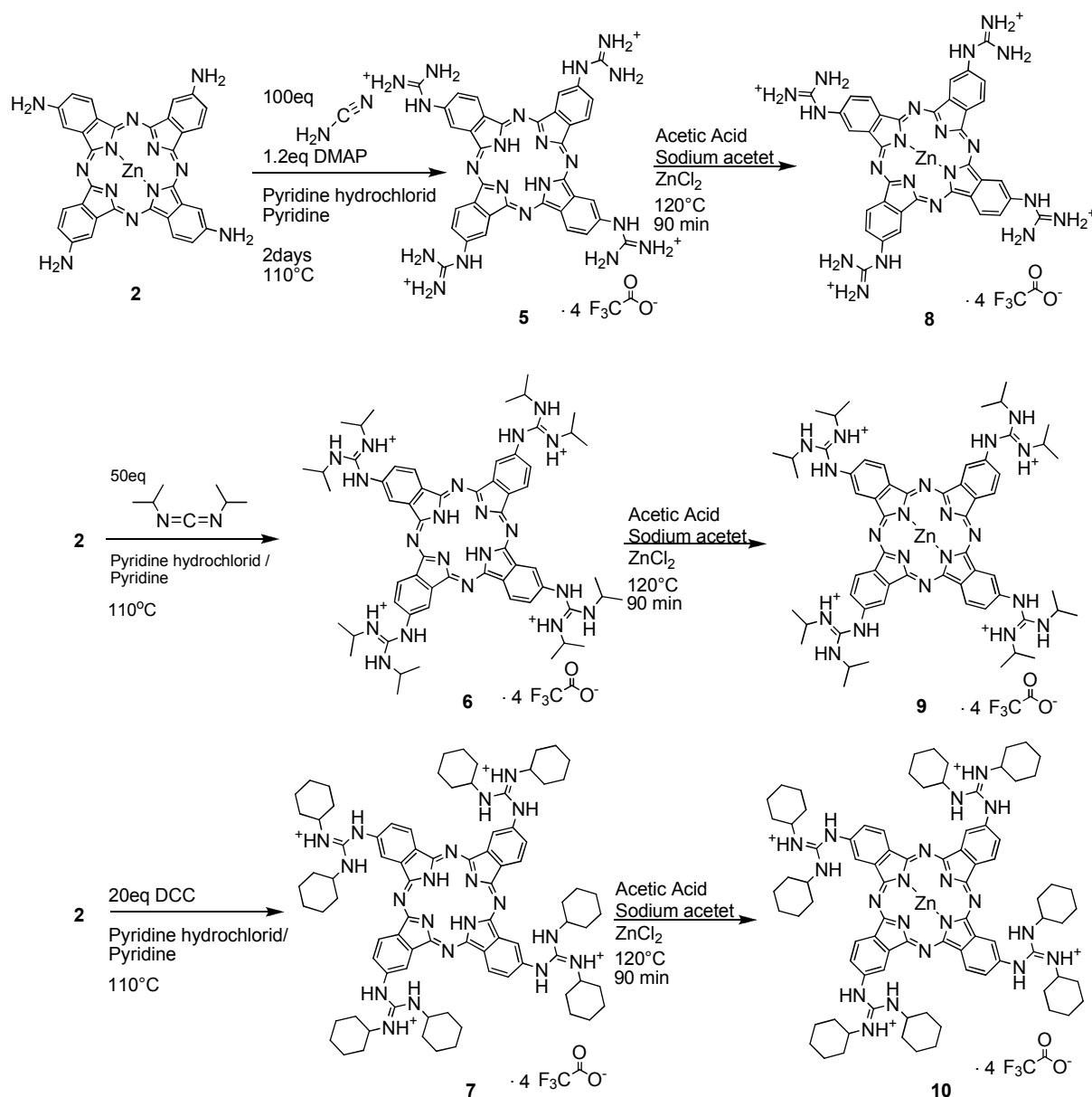


Fig. 22 Synthesis of tetraguanidino zinc phthalocyanines from 4,4',4'',4'''-tetraamino zinc phthalocyanine (**2**)

3.2.1 Yields

According to analytical HPLC, yields for the zinc-free GPCs (**5-7**) and zinc-containing GPCs (**8-10**) were over 80% in each crude reaction mixture, while the isolated yields for **5**, **6**, **7**, **8**, **9** and **10** were 22%, 25%, 16%, 34%, 68% and 32%, respectively. The lower isolated yields reflect the solubility difficulties encountered with compounds without zinc (**5-7**) and **8** and **10**. Compounds **5**, **7**, **8** and **10** exhibit good solubility in DMSO, DMF, and pyridine, but were insoluble in water.

3.2.2 Purification

The solubility properties of the diisopropyl derivatives **6** and **9** were used for developing a non-chromatographic purification which gave higher yields. The solubility properties of **6**

and **9** are highly dependent on the counterions present. The chloride, citrate and acetate salts of **6** and **9** are highly water soluble. On the other hand the perchlorate, iodide, and trifluoroacetate salts of **6** and **9** are water insoluble. The most usual approach of cleaning **6** and **9** was to dissolve the crude material of the reaction in an aqueous chloride solution and precipitate by addition of trifluoroacetic acid (TFA). The precipitate is then dried, dissolved into neat TFA and precipitated upon addition of water.

Unfortunately, the same purification procedure was not effective for compounds **5**, **7**, **8** and **10**. Pure products were obtained by HPLC Chromatography.

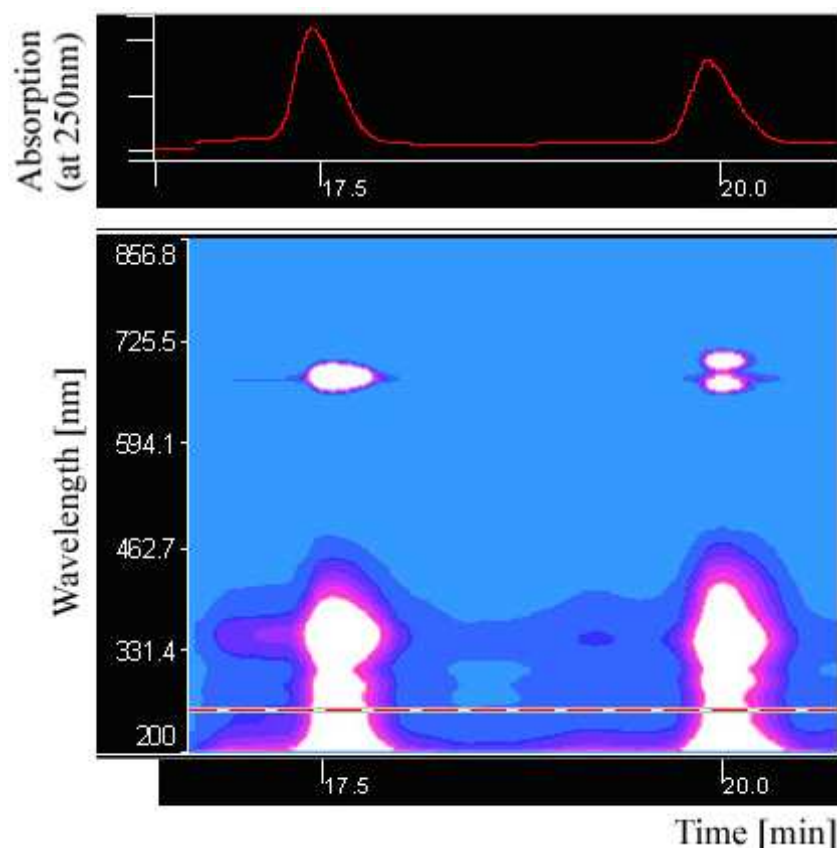


Fig. 23 Analytical HPLC of a partial de-metalation of the diisopropyl derivative (**9**) were the z axis is the absorption. The first peak is the zinc containing molecule (**9**) and the second peak is the metal-free compound (**6**).

3.2.3 NMR spectrums

A comparison of the NMR spectra (Fig. 24 & 25) reveals a correlation between the number of aromatic signals and the increasing steric bulk of each side chain. Compound **8** exhibits a simple NMR spectrum consistent with C_{4h} symmetry and a co-planar arrangement of guanidinium groups. The NMR spectra of the diisopropyl- and dicyclohexyl- derivatives grow increasingly more complex. Molecular modelling indicates that bulky substituents force the guanidinium groups above or below the plane of the macrocycle, resulting in four rotameric isomers. To get nice NMR spectras the GPCs were measured at a very low concentration.

Heating the NMR samples of diisopropyl- and dicyclohexyl- derivatives didn't simplify the spectra. Perhaps this is related to the tendency of Pcs to self aggregate in solution, which hinders the flipping of the bulky substituents at the guanidinium group. When the NMR sample was 800 fold diluted, the influence of the staking was still notable (determination of the molar extinction coefficient in chapter 4).

By analysing all spectra in Fig. 24 and 25 we observed a shift to the right of the NH proton **a** and a shift to the left of protons **b**. The substitution pattern on the guanidine has an effect on the acidity of the NH **a** and **b**. The shifting of the protons **b** is similar if the substituent is a diisopropyl (**6**, **9**) or dicyclohexyl (**7**, **10**). With the proton **a** it shifts more to the right with the bulkier substituent. The alkyl group (diisopropyl or dicyclohexyl) on the guanidine increases the electron density on the NH of **a** and this will have an impact on the acidity. The bulky groups on the guanidine exhibit a more hindered rotation around the N-Phenylgroup, which prevent electron delocalization into phenylgroup, making it more basic. The NMR spectra of the metal-free GPCs and the ones with zinc are nearly identical, but the spectra with zinc are less broadened (compare **A** from Fig. 24 with **A** from Fig. 25). This is consistent with the limited solubility of the metal-free GPCs.

By addition of some drops of d_3 MeOD to the NMR probe the NH protons are exchanged (Fig. 26). The NMR of the diisopropyl derivative with zinc (**9**) gets sharper and the four rotameric conformational isomers get more evident (Proton 4 and 3 in Fig. 26).

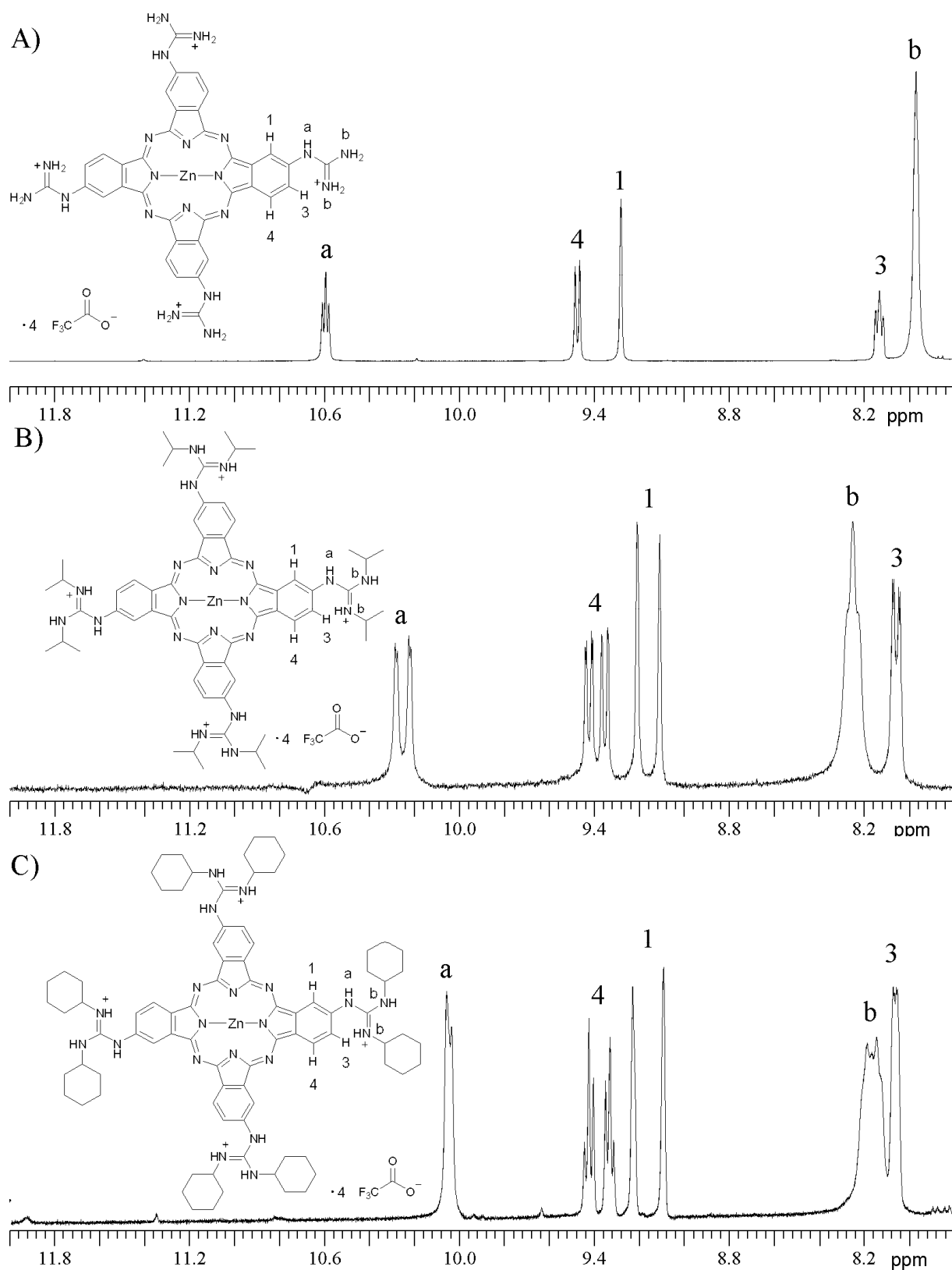


Fig. 24 Partial ^1H NMR spectra of tetraguanidino zinc phthalocyanines where: A) R = H (**8**) (0.14 mM), B) R = isopropyl (**9**) (0.22 mM), C) R = dicyclohexyl (**10**) (0.51 mM). All spectra were collected in d_6 -DMSO. Protons a and b exhibiting exchange with d_3 MeOD.

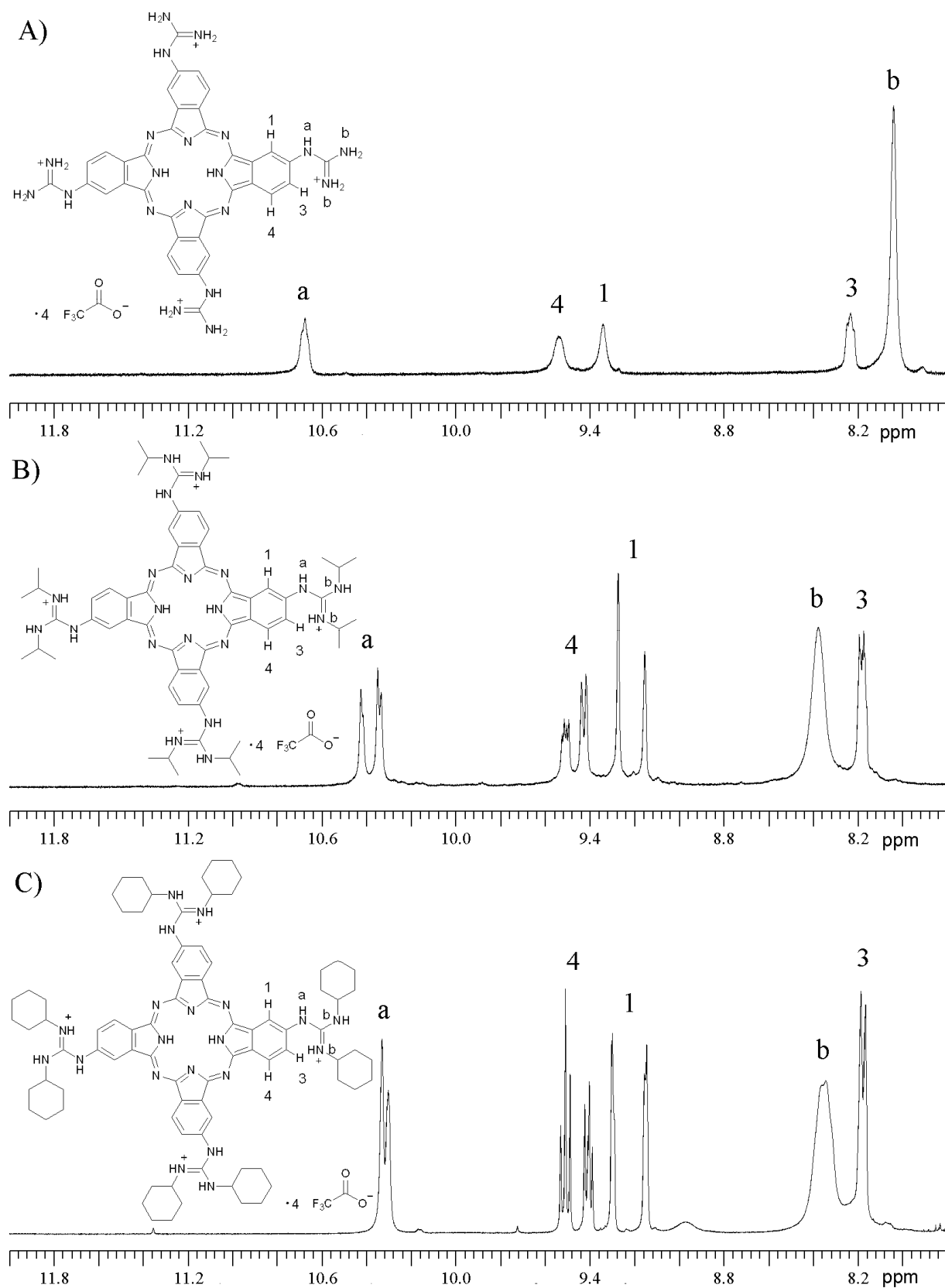


Fig. 25 Partial ^1H NMR spectra of tetraguanidino metal-free phthalocyanines where: A) R = H (**5**)(0.38mM), B) R = isopropyl (**6**)(0.29mM), C) R = dicyclohexyl (**7**)(0.84mM). All spectra were collected in d_6 -DMSO. Protons a and b exhibiting exchange with d_3MeOD .

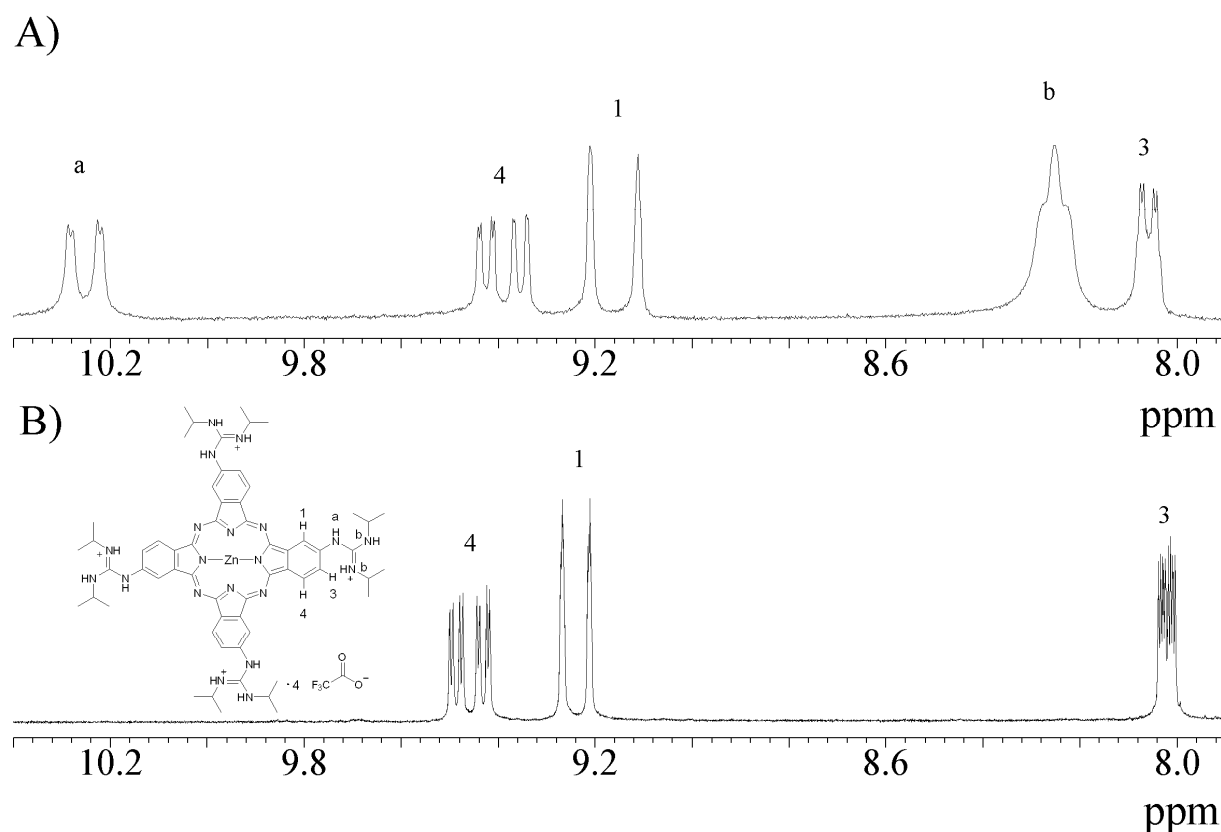


Fig. 26 Partial ^1H NMR spectra of (**9**) in **A)** d_6 -DMSO; **B)** d_6 -DMSO with three drops of d_3MeOD .

3.2.4 Mass spectroscopy

Mass spectroscopy, which has become a great tool for analysis of Pcs, was used to verify if the guanidinylation reaction was completed or if it stopped at the 3 substituted guanidinylation as with the unsubstituted guanidinium **5** without the help of the catalyst. ESI MS data gave us a very special pattern in all the GPcs (Fig. 27), which is simplified by the lost of zinc (compare **B** and **D** in Fig. 27). The isotope pattern which always starts with $[\text{M}+\text{H}]^+$ is the same as the simulated.

In summary we found carbodiimides in pyridine, pyridine-HCl are suitable for guanidinylation of aryl amines, to our surprise, these conditions removed zinc metal from phthalocyanines providing the first examples of zinc removal from phthalocyanines. The scope of this reaction is being evaluated for other phthalocyanin substituents.

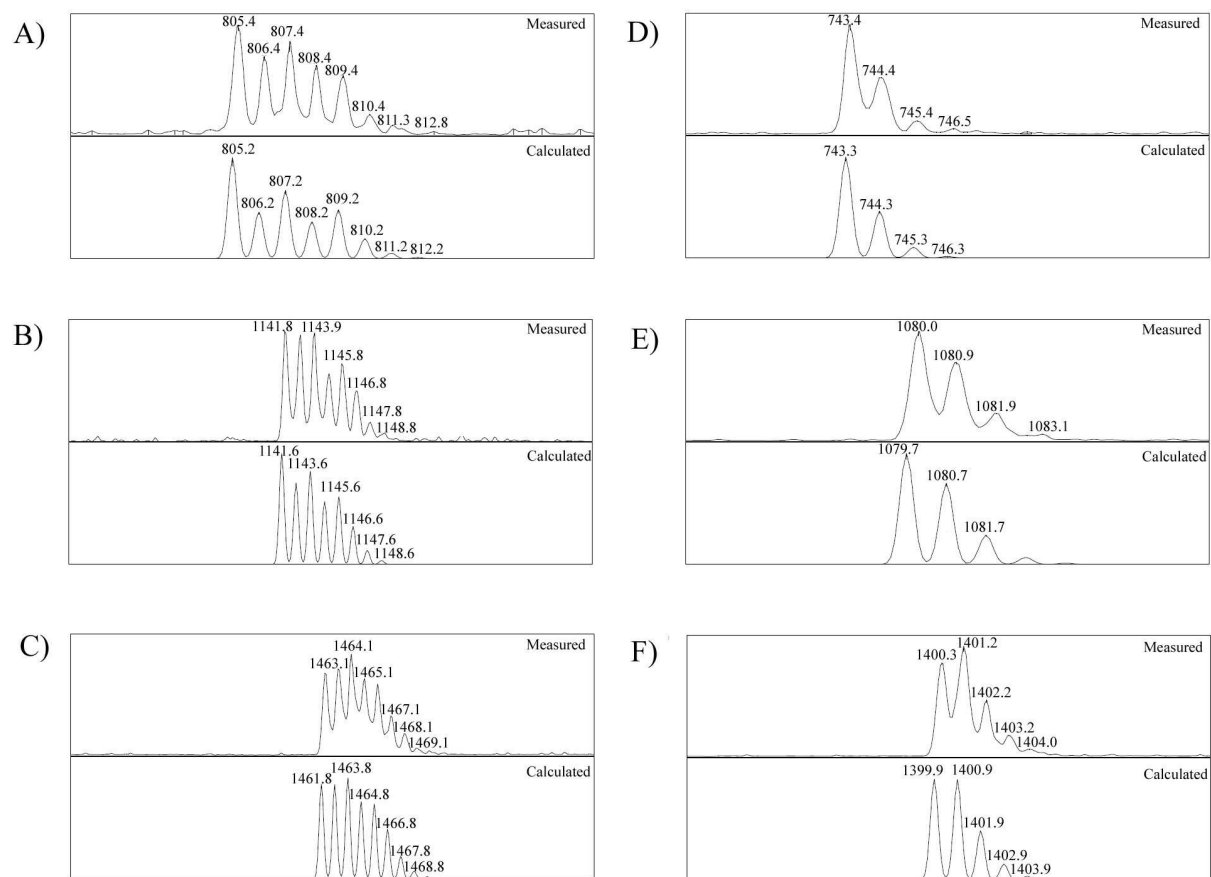


Fig. 27 ESI MS data of: **A)** Compound **8**; **B)** Compound **9**; **C)** Compound **10**; **D)** Compound **5**; **E)** Compound **6**; **F)** Compound **7**. Isotope pattern of the measured (up) and simulated (down) GPs.

4. Fluorescence assays

4.1 General features

Fluorescence is used in environmental monitoring, clinical chemistry, DNA sequencing, and genetic analysis by fluorescence in situ hybridisation (FISH). Fluorescence is also used for cell identification and sorting in flow cytometry, and in cellular imaging revealing the localization and movement of intracellular substances by means of fluorescence microscopy. There is a continuing development of medical tests based on the phenomenon of fluorescence. Fluorescence typically occurs from aromatic molecules (Fig. 28). Fluorescence occurs when a molecule relaxes to its ground state after being electronically excited. Returning to the ground state is normally spin-allowed and can occur rapidly by emission of a photon. Many fluorophores display subnanosecond lifetimes, that's why measurements of the time resolved emission requires sophisticated optics and electronics.

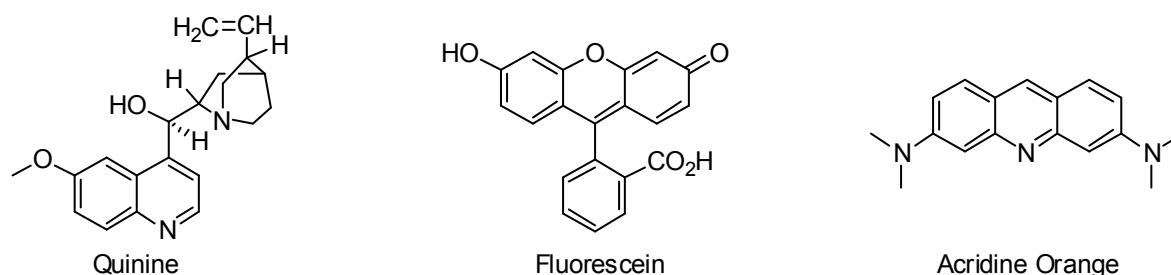


Fig. 28 Structures of some fluorescent substances.

The energy of the emission is typically less than of absorption. Usually the absorbed photon is in the ultraviolet range, and the emitted light is in the visible range, but this depends on the absorbance curve and Stokes shift of the particular fluorophore. Because of the rapid relaxation, emission spectra are usually independent of the excitation wavelength. The time span between the absorption of light and its subsequent reemission allows time for several processes, each of which results in change of fluorescence spectral observables. Some dynamic processes can affect the fluorescence anisotropies, quantum yields, lifetimes, and emission spectra. Resonance energy transfer provides a reliable indicator of molecular proximity on the angstrom size scale. The spectral characteristics of fluorophores can provide a great deal of information on the solution behaviour of macromolecules.

An important feature of fluorescence is that there is a rather direct connection between the spectral observables and molecular features of the sample. It is therefore easy to visualize how the spectral properties are affected by the local environment, accessibility to quenchers, or the presence of nearby acceptors.

4.2 UV-vis spectroscopy

The first UV-vis data on transition-metal phthalocyanines (PcM) were reported by Linstead and co-workers more than 60 years ago. PcZn is often used as a good starting model for the understanding of phthalocyanine-based excited-state properties because of the presence of a closed-shell d^{10} configuration of the central atom (which simplifies UV-vis spectra due to the absence of additional metal-to-ligand charge-transfer and ligand-to-metal charge-transfer transitions) and the high symmetry (D_{4h}) of the complex. The first spectral assignment of PcZn were provided by Edward and Guaterman for the gas-phase high-temperature spectra in which the Q, B, N, L, and C bands were identified in the UV-vis spectrum. It has been suggested that the Q, B, N, and L bands consist of almost pure π - π^* single-electron transition configurations. ^[50]

The UV/VIS spectrums of compounds **5** – **10** were determined (Fig. 29). These spectra are very similar to the UV-vis spectrum of PcZn. ^[51] The NMR sample was diluted 200 fold in DMSO to obtain the first set of data. In each subsequent step the concentration was halved. The OD values at 360 nm were also halved. We observe a red shift after every dilution in the Q-band (which are shown with black arrows in Fig. 29). The Q-band is sensitive to stacking, indicating the strong tendency of Pcs derivatives to self aggregate in solution down to very low concentrations.

The extinction coefficients were determined at 360 nm. The B-Band (which is shown with red arrows in Fig. 29) did not shift when the concentration was decreased because it is insensitive to stacking interactions.

The UV/VIS spectra of the compounds with zinc (**8**, **9**, **10**) and the ones without (**5**, **6**, **7**) had one notable difference which is pointed out with the blue arrow in Fig. 29. This absorption maxima is also present in the spectrums of the metal free compounds but it is more broadened. This is consistent with the limited solubility of the metal-free GPcs.

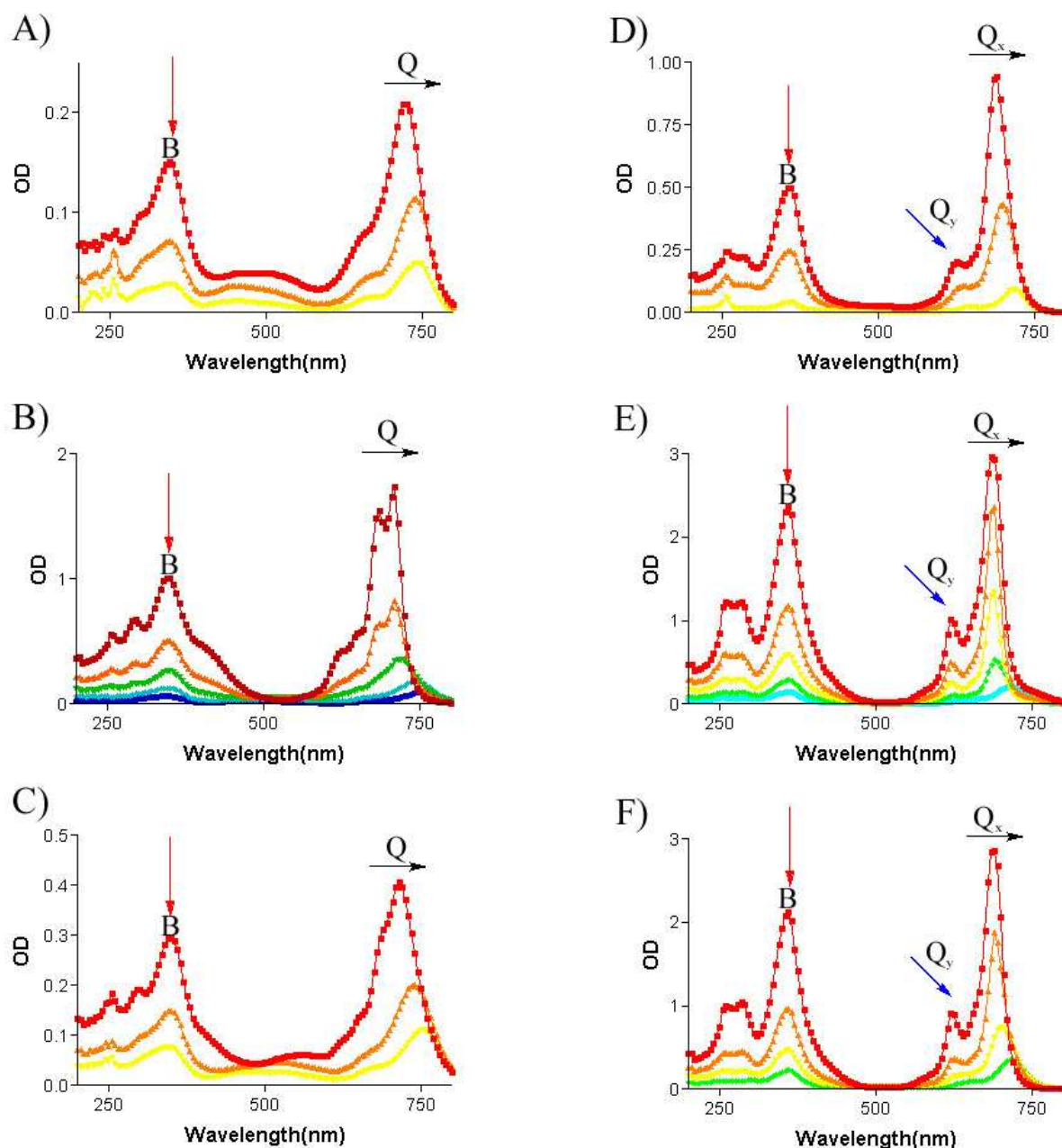


Fig. 29 UV/VIS spectra of tetraguanidino phthalocyanine: **A)** **5** ($2.82 \cdot 10^{-6} - 7.07 \cdot 10^{-7}$ M); **B)** **6** ($1.33 \cdot 10^{-5} - 8.32 \cdot 10^{-7}$ M); **C)** **7** ($7.16 \cdot 10^{-6} - 1.79 \cdot 10^{-6}$ M); **D)** **8** ($8.91 \cdot 10^{-6} - 2.22 \cdot 10^{-6}$ M); **E)** **9** ($2.17 \cdot 10^{-5} - 1.36 \cdot 10^{-6}$ M); **F)** **10** ($9.05 \cdot 10^{-6} - 1.13 \cdot 10^{-6}$ M). All spectra were taken in DMSO. Q- and B-Bands are shown.

4.3 Fluorescence assays: Comparison of all compounds

4.3.1 Fluorescence enhancement assays

Our compounds (**5** – **10**) become fluorescent when they bind to DNA ($E_x = 400\text{--}625$ nm, $E_m = 700\text{--}730$ nm) and could be detected down to concentrations in the nM range. Thanks to these fluorescence properties, fluorescence enhancement experiments could be carried out to obtain K_d values (Fig. 30; see Chapter 5 for experimental details). Upon saturation with DNA or RNA in the presence of a detergent and DMSO, a 8-, 9-, 28-, 4-, and 1.5-fold increases in

fluorescence emission was observed for compound **6**, **7**, **8**, **9** and **10** respectively. In the absence of a detergent or DMSO the diisopropyl derivative (**6**) and (**9**) exhibited 20-, 23-fold increases respectively.

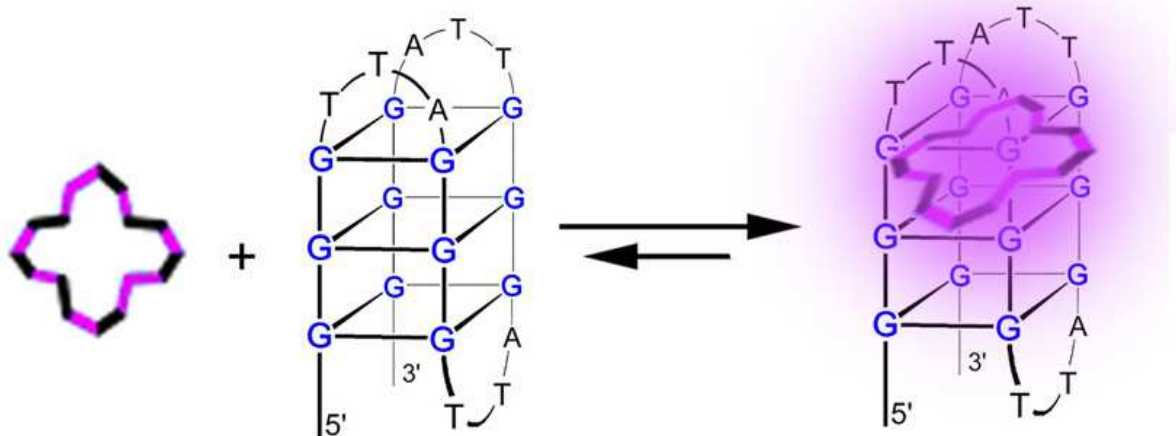


Fig. 30 Fluorescence enhancement. When the molecule binds to the DNA it becomes fluorescent.

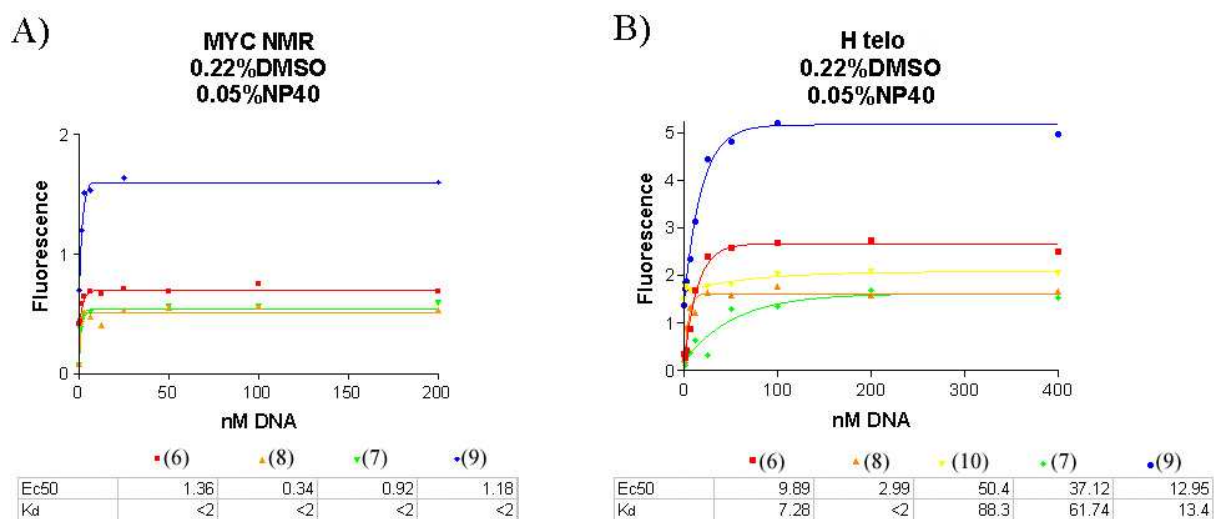


Fig. 31 Fluorescence enhancement experiment using A) 10 nM solutions of **6**, **7**, **8** and **9** (Ex 620nm, Em. 705nm) upon titration with Myc NMR; B) 25 nM solutions of **6**, **7**, **8**, **9** and **10** (Ex 620nm, Em. 705nm) upon titration with H telo. Experiments were in TKE buffer with 0.05% NP40 and 0.22% DMSO. Multiple readings at variable times indicated equilibrium was reached.

Compounds **5** – **10** were measured under the same conditions to compare their K_d/EC_{50} values. The tetraguanidine derivative without zinc (**5**) was insoluble in almost all cases. Different buffers, pHs, and alcohols were tried. DMSO and different detergents were added. The conditions allowing a direct comparison of compounds **6** – **10** were 0.22% DMSO and 0.05% NP40 in the TKE buffer. NP40 is a well known detergent in Biochemistry. The

role of the detergents was to avoid the staking of the compound to the walls of the black polystyrene assay plates and the pipette caps.

We measured the EC₅₀ of **6** - **10** upon adding DNA derived from the c-Myc oncogene promoter (Myc NMR) and the DNA of the human telomeric repeat (H telo). Compounds were held constant at 25 nM. The K_d values obtained showed very clearly that the dicyclohexyl derivatives (**7** and **10**) had the lowest G-quadruplex affinity (Fig. 31). The strongest binder is the tetraguanidine derivative **8** which gives K_d values < 2 for Myc NMR as well as for Htelo, to our knowledge the lowest ever measured. The diisopropyl derivatives (**6** and **9**) give also very low K_d values. If we compare the K_d values of the macrocycles with zinc to the macrocycles without zinc we notice that the molecules without zinc have higher affinity than those containing zinc in the presence of detergents.

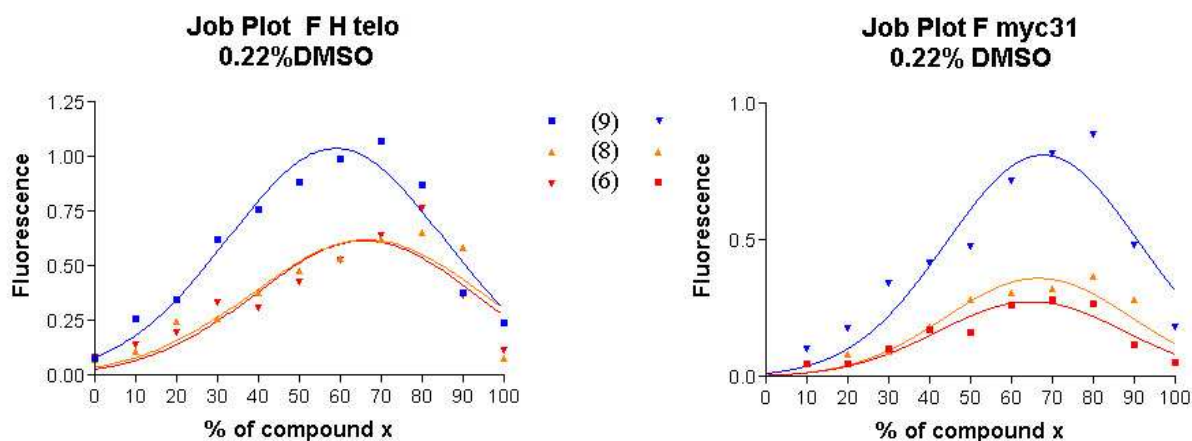


Fig. 32 Job Plot for **6**, **8** and **9** at pH 7.4 with 0.22% DMSO in the TKE buffer. The sum of the concentrations of the ligand and DNA was kept constant at [ligand] + [DNA] = 100 μ M. Fluorescence measurements were made at excitation wavelengths of 495 nm and emission of 520 nm. Multiple readings at variable times indicated equilibrium was reached.

To estimate the binding stoichiometry of compounds **6**, **8** and **9** to the Myc NMR- and H telo DNA we conducted Job Plot experiments (Fig. 32). Based on the data of the Job Plot we can be certain that these interactions do not have a 1:1 stoichiometry. If the fluorescence maximum is at 50%, 66%, or 75% they represent binding stoichiometries of 1:1, 2:1 or 3:1 respectively. Based on these results we can not be certain if it is a 2:1 or 3:1. Upon other stoichiometric experiments made by Alzeer and Luedtke, we know that it is a 2:1 stoichiometry. The fluorescence data was analysed using an independent 2:1 binding model to calculate K_d values from the EC₅₀ values.

In figure 33 all fluorescence enhancement experiments with the guanidine Pc **8** under variable conditions are shown. The mutant (F Hum telo-Mu; Fig. 33) of the Human telo sequence was also evaluated. The mutant sequence is not able to form a G-quadruplex. A low K_d /EC₅₀ for the Mutant sequence would indicate that our compound does not bind

specifically to this G-quadruplex. The K_d value of the mutant is 10-times higher than the Human telo sequence. Indicating a good specificity of **8** towards G-quadruplex.

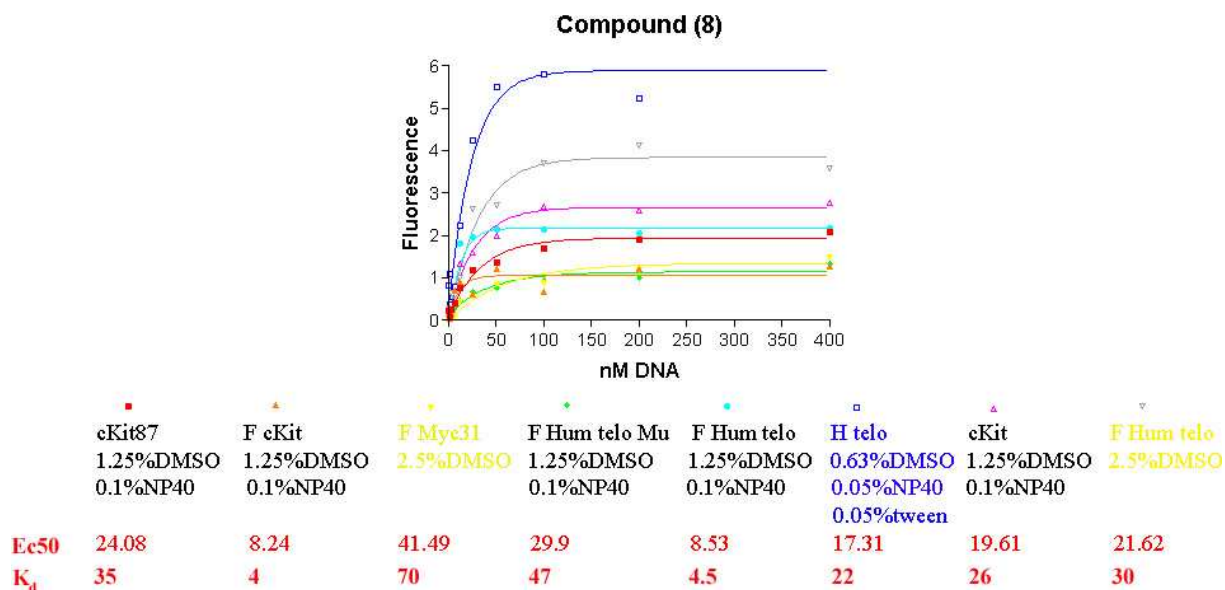


Fig. 33 Fluorescence enhancement experiments of a 25 nM solution of the tetraguanidine derivative **8** (Ex. 620 nm, Em. 705 nm) upon titration with different nucleic acids. All experiments were conducted in TKE buffer only the detergents are varied. The experiments with the same conditions are indicated by color. Multiple readings at variable times indicated equilibrium was reached.

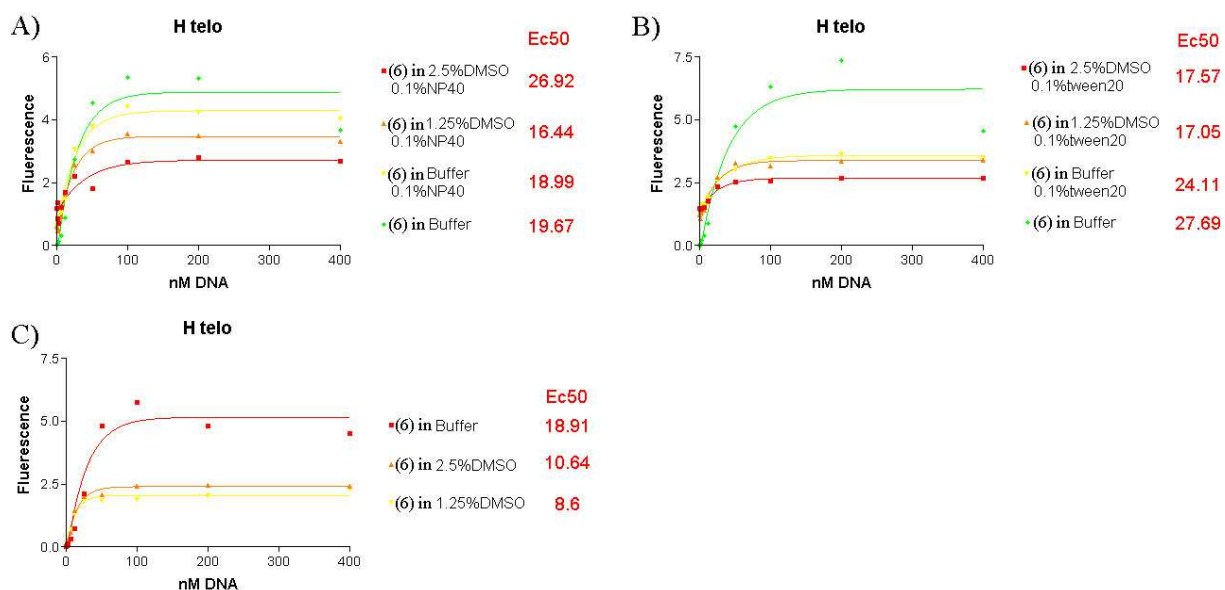


Fig. 34 A) - C) Influence of detergents to the EC₅₀ values of the diisopropyl derivative without zinc (**6**) (Ex. 620 nm, Em. 705 nm) and the DNA of the human telomeric repeat (H telo). Multiple readings at variable times indicated equilibrium was reached.

Given the conditions with DMSO and a detergent we were curious how much they influence the EC₅₀/ K_d values especially for the diisopropyl derivative without zinc (**6**), which is one of our best compounds based on the K_d /EC₅₀ values and solubility properties (Fig. 34). By addition of DMSO the EC₅₀/ K_d value gets smaller, which suggests a lower self-

association. The addition of a detergent (NP40 or tween20) also improves the EC50 value as it decreases. The combination of DMSO and the detergent NP40 gave the lowest EC50 values.

Based on the solubility properties of our compounds we concentrated our efforts upon the diisopropyl derivatives (**6** and **9**), which were soluble in water without the help of a detergent or DMSO. We obtained the absorbance and fluorescence of **6** and **9** in the absence of a detergent monitored upon adding DNA derived from the c-Myc oncogenic promoter (Myc NMR) or the human telomeric repeat (H telo). Gaining information if the molecules have a high affinity to these G-quadruplex forming sequences. To determine the specificity towards G-quadruplex we evaluated a mutant of the H telo sequence (H telo-Mu), calf thymus DNA (CT DNA) and a mixture of yeast tRNA (tRNA).

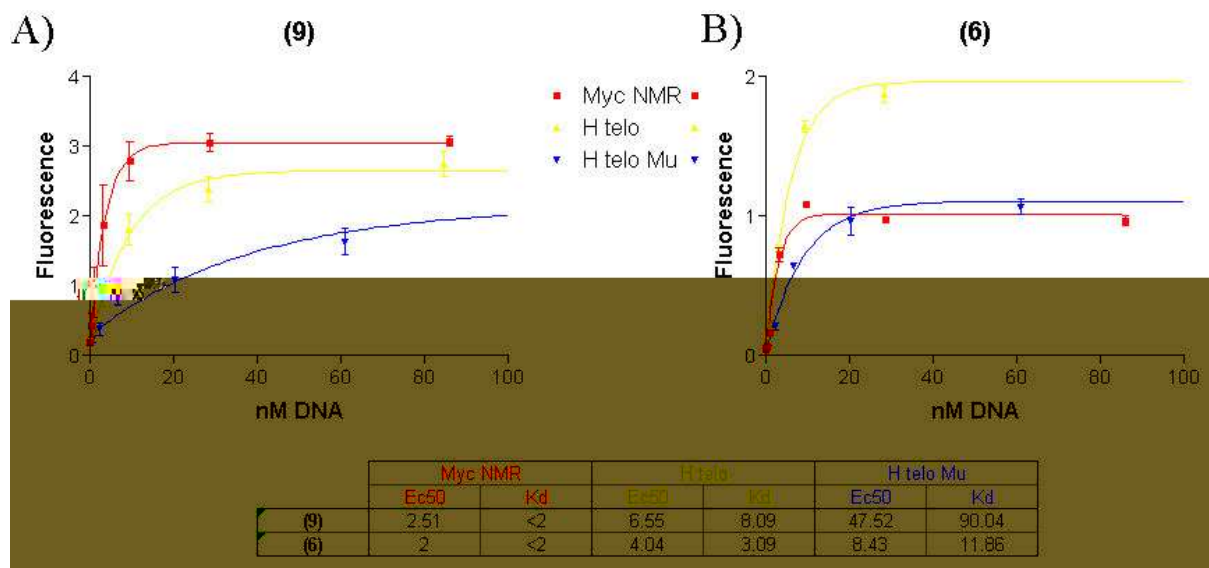


Fig. 35 Fluorescence enhancement of 10 nM solutions of **A) 9** (Ex. 620 nm, Em. 705 nm) and **B) 6** (Ex. 620 nm, Em. 720 nm) upon titration with the nucleic acids: c-Myc, H telo and H telo-Mu in TKE buffer. Multiple readings at variable times indicated equilibrium was reached.

Upon saturation with DNA or RNA, an approximate 100-fold increase in fluorescence emission from **6** and **9** was observed (Fig. 35). Analysis of **9** absorbance changes by Luedtke and Alzeer indicated a 2:1 binding stoichiometry for **9**/c-Myc, a 1:1 stoichiometry for **9**/H telo, and about a 4:1 stoichiometry for **9**/H telo-Mu. For **6** we assume the same stoichiometries. The fluorescence data for both compounds were analysed using an independent 2:1 binding model. Both compounds were measured in a concentration of 10 nM. We estimated a **9**/c-Myc equilibrium dissociation constant of $K_d < 2$ nM for each site. The **9**/H telo equilibrium dissociation constant K_d was around 8 ± 5 nM. H telo-Mu bound to **9** with an apparent K_d of 90 ± 12 nM. As for **6** we got a $K_d < 2$ nM, 3 ± 2 nM 12 ± 5 nM respectively. This suggests a lower quadruplex specificity of **6** vs **9**.

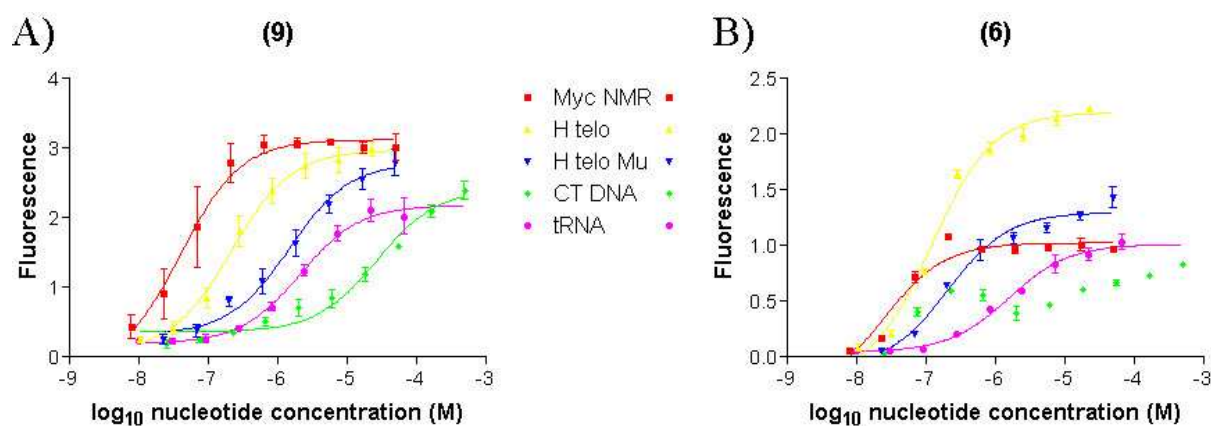


Fig. 36 Fluorescence intensities of 10 nM solutions of **A) 9** (Ex. 620 nm, Em. 705 nm) and **B) 6** (Ex. 620 nm, Em. 720 nm) upon titration with Myc NMR, H telo, H telo Mu, CT DNA and tRNA in TKE buffer. Multiple readings at variable times indicated equilibrium was reached.

We got a 100- and 10000 fold lower **9** affinity for tRNA and CT DNA compared to c-Myc quadruplex DNA (Fig. 36). This pointed out the highly selective G-quadruplex binding of the diisopropyl derivatives (**6** and **9**) (G-quadruplex > single strand > duplex).

Interestingly the fluorescence intensity curve of the compound without zinc (**6**) and CT DNA is multiphasic. We speculate that this phenomenon is due to the presence of variable sequences/structures in the CT DNA. The compound with zinc (**9**) doesn't show this bi-phasic behaviour which could be the explanation for the different biological activities of the diisopropyl derivatives (**6** and **9**).

4.3.2 Fluorescence quenching assay

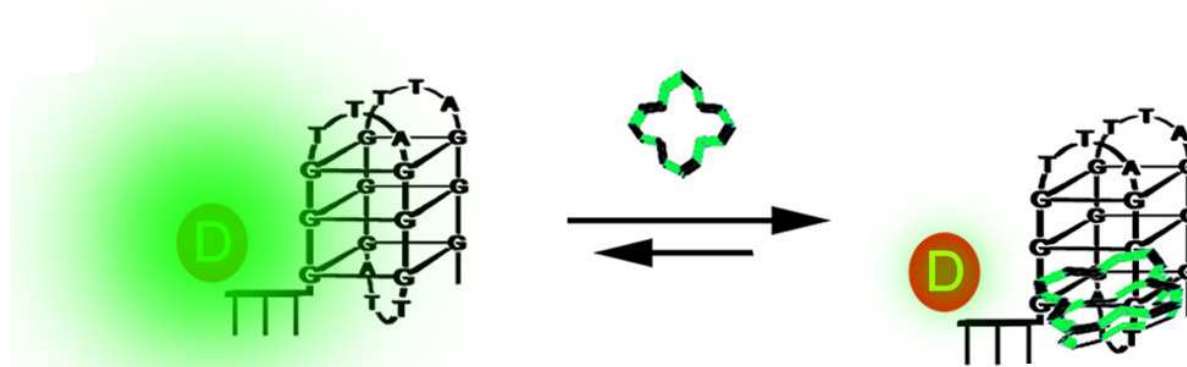


Fig. 37 Fluorescence quenching. The fluorescence labeled DNA is quenched if the molecule binds near to the fluorescein.

To provide an orthogonal assay to measure affinity and specificity we have measured the fluorescence intensity of fluorescein-labeled DNAs upon adding of our compounds (**6** – **9**). Fluorescein (which is shown in Fig. 28; Ex = 495 nm, Em = 520 nm) is quenched if the

molecule binds near to the fluorescein (Fig. 37). By addition of a G-quadruplex stabilising molecule quenching of the fluorescence is observed.

The affinity towards the G-quadruplex for compounds **6** to **9** in the presence of detergents was confirmed by fluorescence quenching experiments (Fig. 38). For determining the specificity toward G-quadruplex we added a 1000 fold nucleotide excess of calf thymus DNA (CT DNA) or a 1000 fold excess of a mixture of yeast tRNA (tRNA). There was almost no loss in the apparent binding of our compounds in the presence of competitor CT DNA or tRNA indicating that our compounds were very specific towards G-quadruplex. The diisopropyl derivative without zinc (**6**) is more specific to G-quadruplex and binds stronger than the diisopropyl derivative with zinc (**9**), which loses its specificity as soon as there is tRNA present.

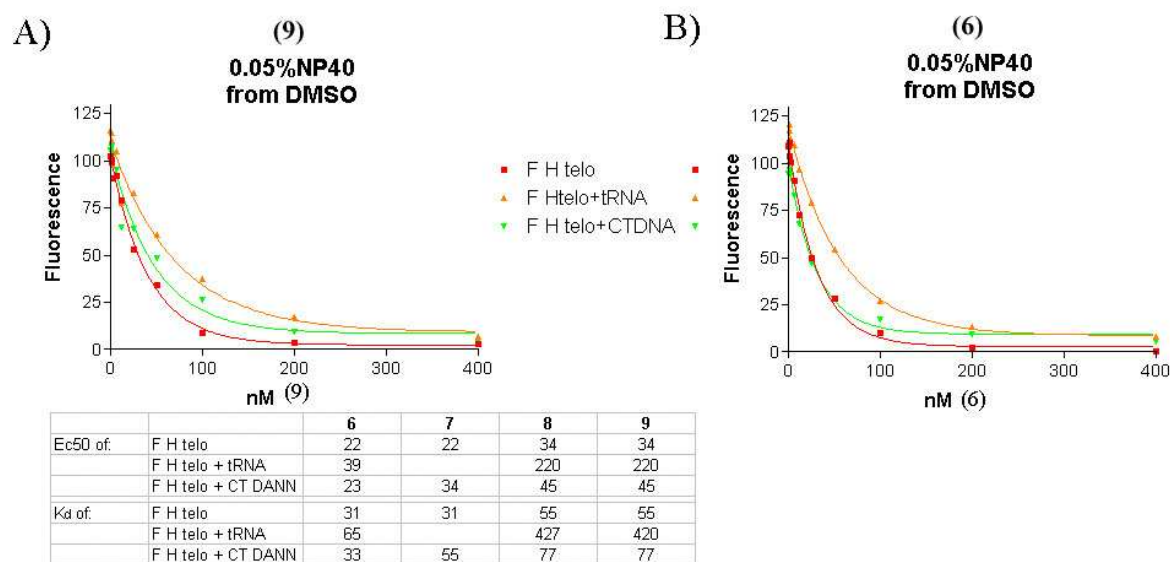


Fig. 38 Fluorescence quenching of a 25 nM solution of the 5' fluorescein end-labeled H telo (Ex 495 nm, Em 520 nm) upon titration with **6**, **7**, **8** or **9** in the presence or absence of 50 μ M CT-DNA or 50 μ M tRNA. Fluorescence quenching with **A**) **9** and **B**) **6**. Experiments were in TKE buffer with 0.05% NP40 and 0.22% DMSO. Multiple readings at variable times indicated equilibrium was reached.

The G-quadruplex affinity and specificity of **6** and **9** in the absence of detergents were confirmed with fluorescence quenching experiment (Fig. 39 & Table 1). It was carried out with a 5'-fluorescein-labeled c-Myc DNA, H telo or H telo-Mu upon titration of **6** or **9** in the presence or absence of a 1000 fold nucleotide excess of CT DNA or tRNA. As a control, we evaluated the very well known cationic porphyrin 5,10,15,20-tetra(N-methyl-4-pyridyl) zinc porphyrin (Zn-TMPy4 shown in Table 1 as NL077; Fig. 10, chapter 1) and the cationic porphyrin 5,10,15,20-tetra(N-methyl-4-pyridyl) porphyrin (TMPy4; Fig. 10, chapter 1). Having these two controls allowed us to make another comparison of zinc vs. metal-free. The binding of Zn-TMPy4 with the nucleic acids is consistent with the values of the literature. By addition

of the competitor CT DNA to the Zn-TMPy4 a 300-fold loss of the apparent binding is observed. As for **9** the high apparent affinity of **9**/cMyc was measured even in the presence of a 1000-fold excess of CT DNA. As for **6** we observed the similar behaviour only that the K_d are higher for **6** than for **9**, indicating that the macrocycle with zinc is more specific (Tabel 1). The diisopropyl derivative with zinc binds stronger to the G-quadruplex. With the apparent affinity of **6**/H telo and **9**/H telo a 100 fold loss of the apparent binding is observed when CT DNA or tRNA is added. The diisopropyl derivative is much more specific towards the G-quadruplex formed from the Myc promoter and less specific for H telo.

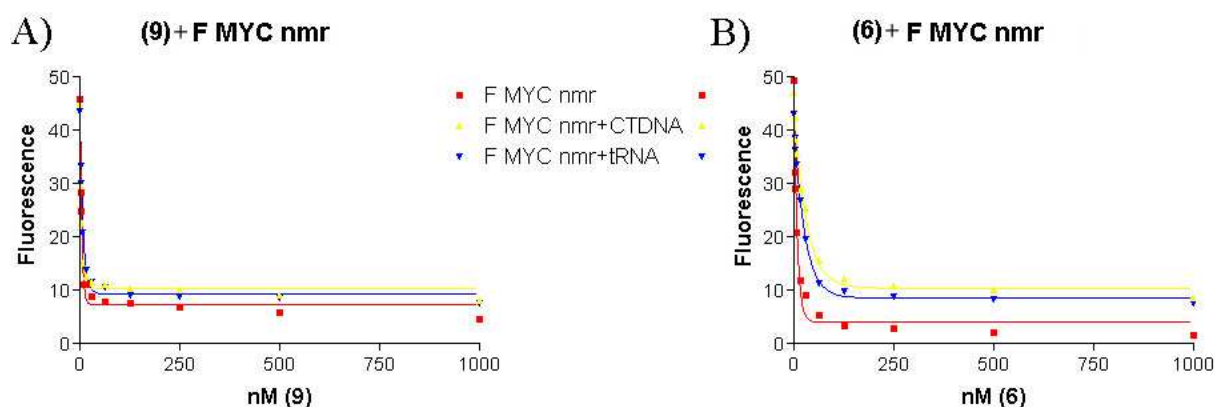


Fig. 39 Fluorescence quenching of a 10 nM solution of the 5' fluorescein end-labeled Myc NMR (Ex 495 nm, Em 520 nm) upon titration with **6** or **9** in the presence or absence of 220 μ M CT-DNA or 220 μ M tRNA. Fluorescence quenching with **A) 9** and **B) 6** in TKE buffer. Multiple readings at variable times indicated equilibrium was reached.

			DNA	DNA+CTDNA	DNA+tRNA	
F M YC nmr	TMPyP4	K	0.171	0.005	0.006	
		EC50	4.028	151.815	124.414	
		Kd	0.906	296.480	241.678	
	NL077	K	0.055	0.002	0.003	
		EC50	12.552	374.187	198.905	
		Kd	17.955	741.223	390.659	
	PR 001 (6)	K	0.122	0.032	0.037	
		EC50	5.651	21.746	18.528	
		Kd	4.152	36.342	29.907	
	PR 006 (9)	K	0.243	0.269	0.133	
		EC50	2.837	2.561	5.188	
		Kd	<2	<2	3.226	
				DNA	DNA+CTDNA	DNA+tRNA
	F H Telo	TMPyP4	K	0.037	0.001	0.001
EC50			18.847	499.276	616.622	
Kd			31.945	992.803	>1000	
NL077		K	0.013	0.000	0.001	
		EC50	52.194	4020.979	885.069	
		Kd	98.637	>1000	>1000	
PR 001 (6)		K	0.194	0.005	0.005	
		EC50	3.557	140.387	139.648	
		Kd	1.363	275.023	273.546	
PR 006 (9)		K	0.148	0.006	0.004	
		EC50	4.672	125.113	195.856	
		Kd	3.593	244.477	385.962	
			DNA	DNA+CTDNA	DNA+tRNA	
F H Telo Mu		TMPyP4	K	0.014	0.000	0.003
	EC50		49.676	>1000	219.955	
	Kd		93.602	>1000	434.161	
	NL077	K	0.004	0.000	0.001	
		EC50	185.784	>1000	915.484	
		Kd	365.817	>1000	>1000	
	PR 001 (6)	K	0.058	0.003	0.002	
		EC50	11.977	197.708	370.370	
		Kd	18.204	389.665	734.991	
	PR 006 (9)	K	0.061	0.000	0.000	
		EC50	11.258	>1000	>1000	
		Kd	16.766	>1000	>1000	

Table 1 Fluorescence quenching of a 10nM solution of the 5' fluorescein end-labeled DNA (Ex 495 nm, Em520 nm) upon titration with **6**, **9**, TMPyP4 and Zn-TMPyP4 in the presence or absence of 220 μ M CT DNA or 220 μ M tRNA in TKE buffer. Multiple readings at variable times indicated equilibrium was reached.

In summary, we have created a series of molecules which have a high affinity and specificity to the G-quadruplex. The tetraguanidine derivative **8** was the molecule with the highest affinity. However its limited solubility has prevented its full characterization. Balayeshwanth R. Vummidi showed that the diisopropyl derivatives (**6** and **9**) go into the cells (Fig. 40). **6** and **9** had the best EC₅₀/K_d values without the addition of DMSO and/or a detergent. Excellent K_d values were obtained, even in the presence of a competing nucleic acids. **6** and **9** had the best solubility properties of our synthesised compounds, especially in water.

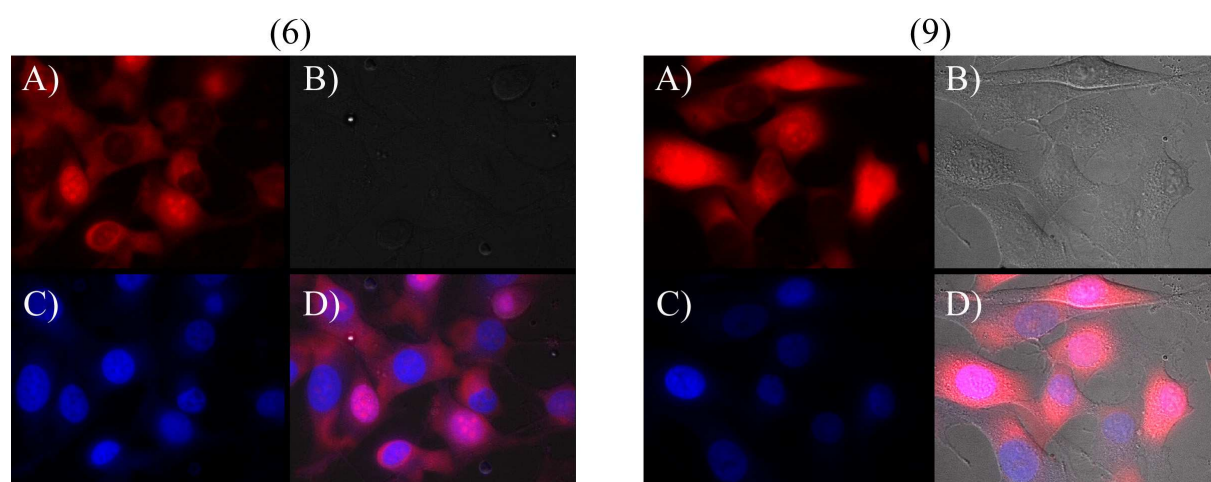


Fig. 40 Fixed SK-Mel-28 stained with 3 M of **6** and **9**, and 180 M of Hoechst 33342. **A)** **6/9** fluorescence (Ex = 620 nm, Em = 700 nm). **B)** White light absorbance. **C)** Hoechst 33342 fluorescence (Ex = 360 nm, Em = 470 nm). **D)** Composite image of A) – C). All these data was obtained by Balayeshwanth R. Vummidi.

5. Experimental Part

5.1 General Remarks

5.1.1 Reaction conditions, solvents, chemicals

Reagents were obtained in the highest commercially available grades from *Sigma Aldrich*. Reaction solvents were purchased from *Aldrich*, *Fisher Scientific*.

Acetonitrile (HPLC grade) was purchased from *Fisher Scientific*. MeOH (HPLC grade) was purchased from *Sigma Aldrich*.

Oligonucleotide DNAs were purchased as the HPLC-purified products from *Genosys*.

5.1.2 Chromatography, and recording of spectrums

For purification and analysis, reversed-phase high performance liquid chromatography (RP-HPLC) was performed using a dual pump Varian (*ProStar*) system. The columns used were a C18 Interchrom (250mm x 21.2mmID; column A), C18 Daisopak (250mm x 10mmID; column B) and C18 YMC basic (150mm x 10mmID; column C) for preparative separations and C18 Interchrom (250mm x 4.6mmID; column D) for analytical separation. Solvents used were acetonitrile from *Fisher Scientific* and doubly distilled water, each containing 0.1% trifluoroacetic acid (TFA).

¹H-NMR spectra were measured on *Bruker ARX-300* or *AV-400* or *AV-500* spectrometers (*Bruker*, Karlsruhe, Germany). The chemical shift values are given in ppm relative to the internal standard tetramethylsilane (TMS; $\delta = 0.00$ ppm) or the solvents resonance. The coupling constant *J* are given in Hz and resonance multiplicity is described as *s* for singlet, *d* for doublet, *dd* for doublet doublet, *t* for triplet and *m* for multiplet and *br* is used for broad signals. All data processing was carried out with Topspin and Xeasy (*Bruker*).

The mass spectrums were measured by the MS-team of the Organic Chemistry Institute of the University of Zürich. For the matrix-assisted laser desorption/ionization (MALDI) a *Bruker* Autoflex was used, electrospray ionization (ESI) was measured on the Esquire LC from *Bruker*. ESI high resolution was measured on the MAT 900 from *Finnigan*.

Absorbance and emission spectra were collected using a *SpectraMax* MP5 spectrophotometer in *Greiner* Bio-one UV-Star 96-well plates (final volume = 200 μ L). Binding assays were conducted in Canning 384-well black polystyrene assay plates with non-binding surfaces

(final volume = 70 or 80 μL). All data processing was carried out with *Microsoft Office Excel* and *Graph Pad Prism*.

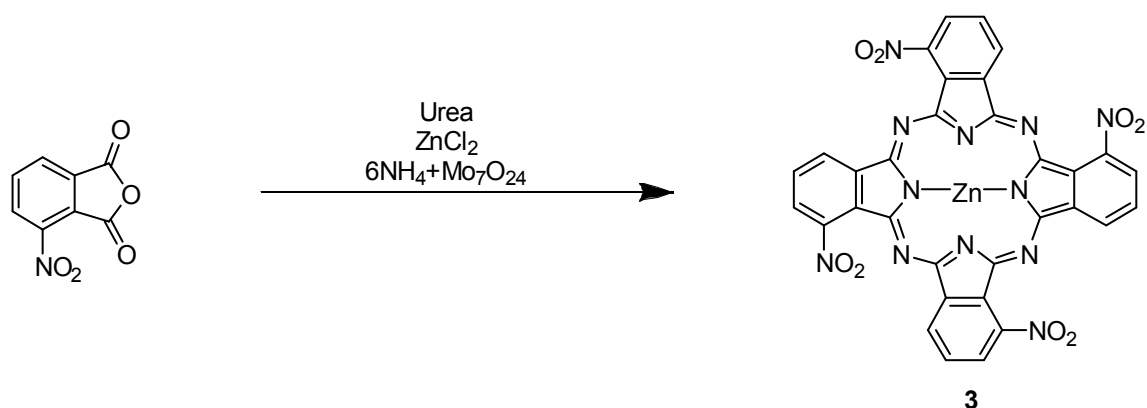
5.1.3 Other machines used.

The sonications were carried out in a TPC-15 bath sonicator from *Telsonic Ultrasonics*.

The centrifugations were performed in an *Eppendorf Centrifuge 5804*.

5.2 Synthesis of Phthalocyanines

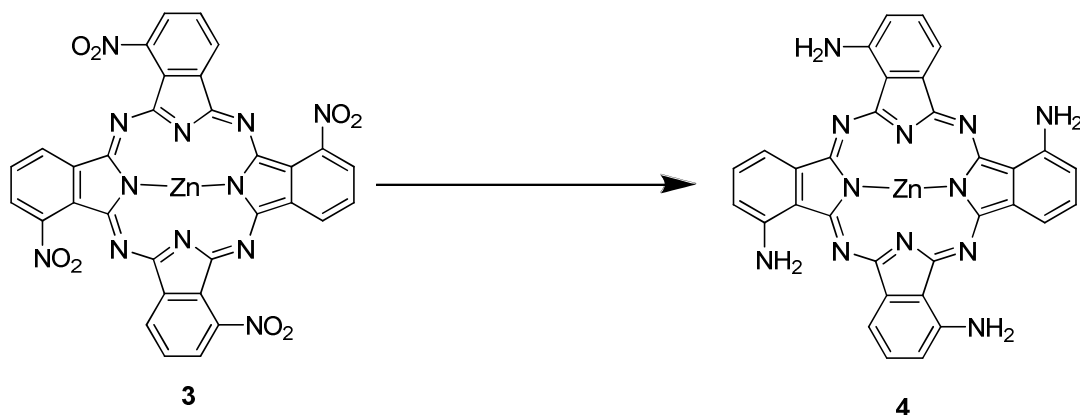
5.2.1 Synthesis of 3,3',3'',3'''-tetranitro zinc phthalocyanine (3)



3-nitro-phthalic anhydride (7 g, 36.2 mmol), urea (3.33 g, 289.9 mmol), ammonium molybdate (91 mg, 0.07 mmol) and zinc chloride (1.2 g, 8.8 mmol) were finely ground and mixed. The mixture was heated at 150°C. After bubbling disappeared completely, the reaction mixture was cooled and centrifuged. The precipitate was repeatedly washed with water, methanol, ethyl acetate and dried to afford **3** (6.732 g, 98%) as a dark green solid.

MALDI TIF MS (m/z): $[M+H]^+$ calcd for $\text{C}_{32}\text{H}_{13}\text{N}_{12}\text{O}_8\text{Zn}$, 757.02; found 757.10

5.2.2 Synthesis of 3,3',3'',3'''-tetraamino zinc phthalocyanine (4)



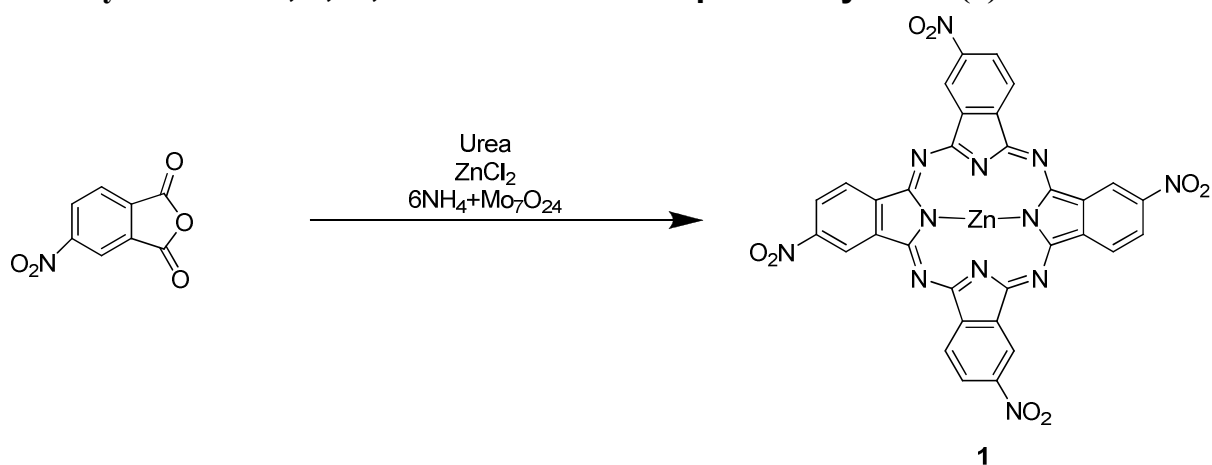
Sodium sulfide nonahydrate (25.59 g, 106.6 mmol) was added to a solution of **3** (6.73 g, 8.88 mmol) in DMF (200 mL). The reaction mixture was stirred under N_2 and heated at 60°C. After 1.5 h, the mixture was cooled to room temperature. The solvent was removed under

reduced pressure. Precipitate was caused by adding cold water and was collected by centrifugation. The precipitate was repeatedly washed with MeOH/ether (1:9), water and dried to afford **4** (2.44 g, 43%) as a dark green solid.

$^1\text{H-NMR}$ (300 MHz, d_6 -DMSO) δ 8.55 (m, 4H), 7.89 (m, 4H), 7.64 (br. s, 4NH), 7.41 (dd, J = 6.0, 9.0 Hz, 4H), 7.27 (br. s, 4(NH)).

MALDI TIF MS (m/z): $[\text{M}+\text{H}]^+$ calcd for $\text{C}_{32}\text{H}_{21}\text{N}_{12}\text{Zn}$, 637.12; found 637.20

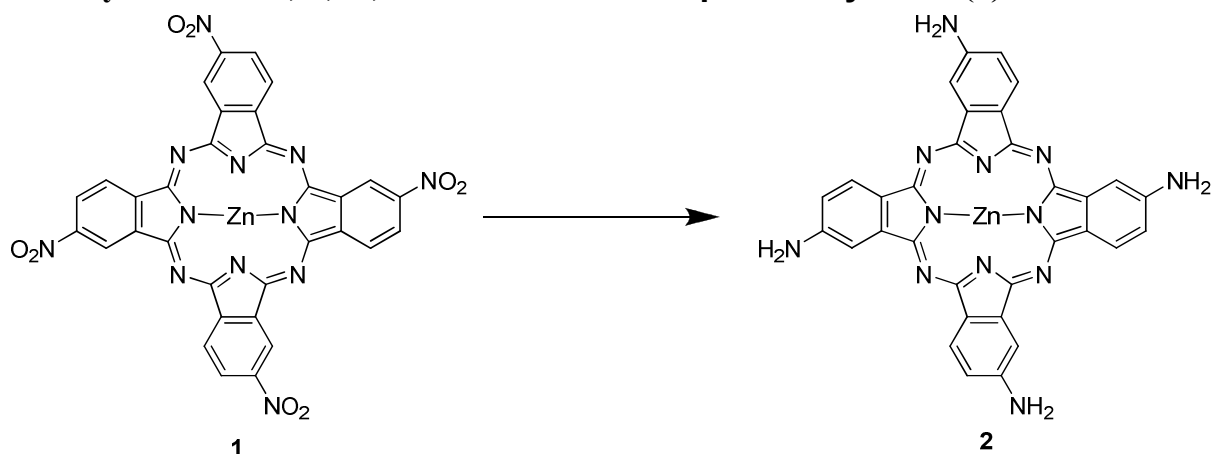
5.2.3 Synthesis of 4,4',4'',4'''-nitrotetrad zinc phthalocyanine (**1**)



Ammonium molybdate (32 mg, 0.025 mmol) was added to a solution of 4-nitro-phthalic anhydride (4.98 g, 260 mmol), urea (7.5 g, 125 mmol), and zinc chloride (879 mg, 6.45 mmol) in nitrobenzene (40 mL). The mixture was stirred under N_2 and heated at 185°C . After 4 h, the reaction mixture was cooled. Addition of water caused precipitation. The precipitate was collected by centrifugation. The solid was washed with water, MeOH/ether (1:20), EtOAc/hexane (2:1), toluene, hexan and dried to afford **1** (3.154 g, 65%) as a dark green solid.

MALDI TIF MS (m/z): $[\text{M}+\text{H}]^+$ calcd for $\text{C}_{32}\text{H}_{13}\text{N}_{12}\text{O}_8\text{Zn}$, 757.02; found 757.10

5.2.4 Synthesis of 4,4',4'',4'''-tetraamino zinc phthalocyanine (**2**)



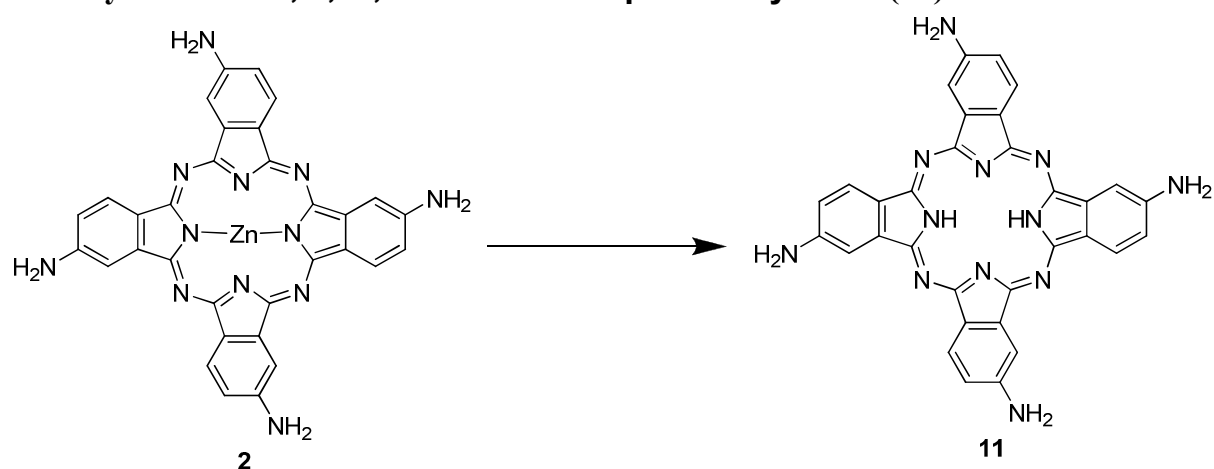
Sodium sulfide nonahydrate (11.94 g, 49.94 mmol) was added to a solution of **1** (3.154 g,

4.16 mmol) in DMF (100 mL). The reaction mixture was stirred under N₂ and heated at 60°C. After 1.5 h, the mixture was cooled to room temperature. The solvent was removed under reduced pressure. Ice water (200 mL) was added and the resulting precipitate was collected by centrifugation. The precipitate was repeatedly washed with water, MeOH/ether (1:15), MeOH/EtOAc (1:1), hexane and dried to afford **2** (2.322 g, 87.5%) as a dark green solid.

¹H-NMR (300 MHz, d₆-DMSO) δ 8.88 (t, *J* = 9.0 Hz, 4H), 8.42 (d, *J* = 12.0 Hz, 4H), 7.35 (d, *J* = 9.0 Hz, 4H), 6.18 (br. s, 4(NH₂)).

MALDI TIF MS (*m/z*): [M+H]⁺ calcd for C₃₂H₂₁N₁₂Zn, 637.12; found 637.10

5.2.5 Synthesis of 4,4',4'',4'''-tetraamino phthalocyanine (**11**)

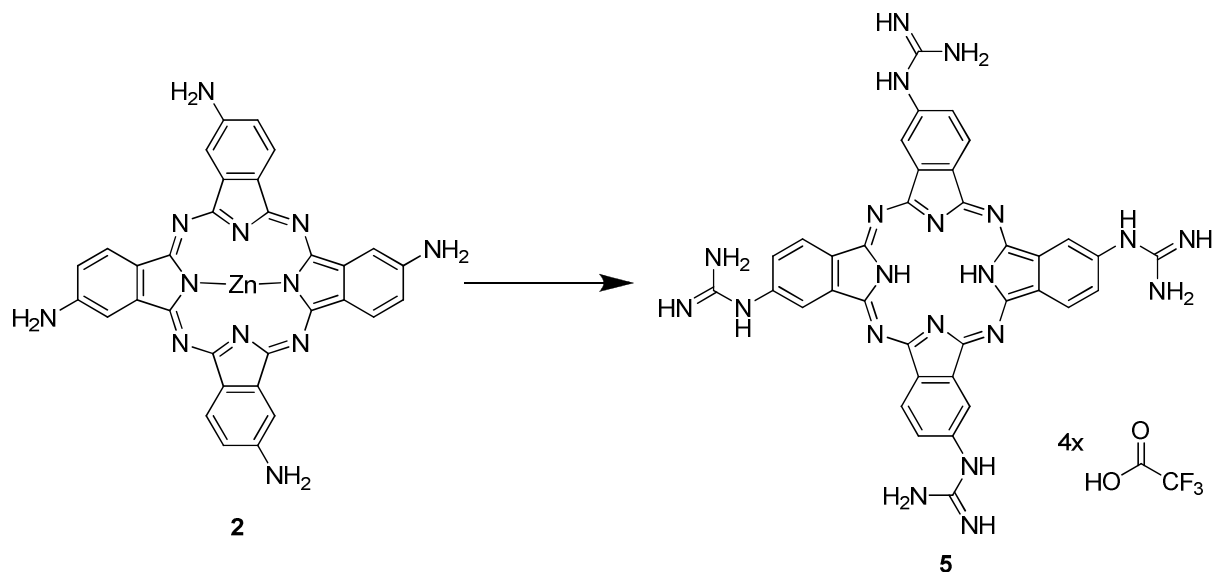


2 (35 mg, 0.055 mmol), pyridine (2mL), and pyridinium-HCl (1 g) were stirred under N₂ at 110°C for 17h. The reaction was removed from the heat and 10 mL of H₂O was used to transfer the hot mixture into a polypropylene centrifuge tube, and the resulting precipitate was collected by centrifugation at 6'500 r.p.m. The dark precipitate was washed repeatedly with H₂O, MeOH, EtOAc, and dried under high vacuum to yield 30.2mg (95%).

MALDI TOF MS (*m/z*): [M]⁺ calcd for C₃₂H₂₂N₁₂, 574.2; found 574.2.

5.3 Synthesis of Guanidino Phthalocyanines

5.3.1 Synthesis of tetra-guanidino phthalocyanine (5)



2 (42.6 mg, 0.067 mmol), pyridine (3 mL), pyridinium-HCl (1.5 g), cyanoamid (22.5 mg, 0.53 mmol, 8 equiv) and DMAP (9.8 mg, 0.080 mmol, 1.2 equiv) were stirred under N_2 at 110 °C. At intervals (after 2h, 6h and 10h) cyanoamid (67.4 mg, 1.59 mmol, 24 equiv) was added to the reaction mixture. The reaction was removed from the heat after 2 days. DMF (7 mL) was used to transfer the hot mixture into a polypropylene centrifuge tube. Ether (35 mL) was added and the resulting precipitate was collected by centrifugation at 6'500 r.p.m. The precipitate was washed with ether (10 mL) water/methanol/ether (2:3:3, 2x, 40 mL) and methanol (2x, 20 mL). Ether (20 mL) was added to the supernatant of the last wash. The precipitate was collected. All collected precipitates were washed with hexane (2x, 20mL). The crude product was dried under high vacuum over night. For HPLC purification 3mg of 79 mg were dissolved in DMSO (3 mL). A 6:1 mixture of water and MeOH containing 0.1% TFA (3.5 mL) was added. After passing the solution through a filter it was purified by HPLC with column A at a flow rate of 10 ml/min with the following gradient: linear 18-35% acetonitrile containing 0.1% TFA over 25 min. The peak of **5**, eluting between 17-18 min, was collected. The solvents were removed under reduced pressure. The resulting powder was dissolved in water containing 0.1% TFA (1 mL), and lyophilized to obtain of a dark green powder. The total yield was 15.8mg (21.7%).

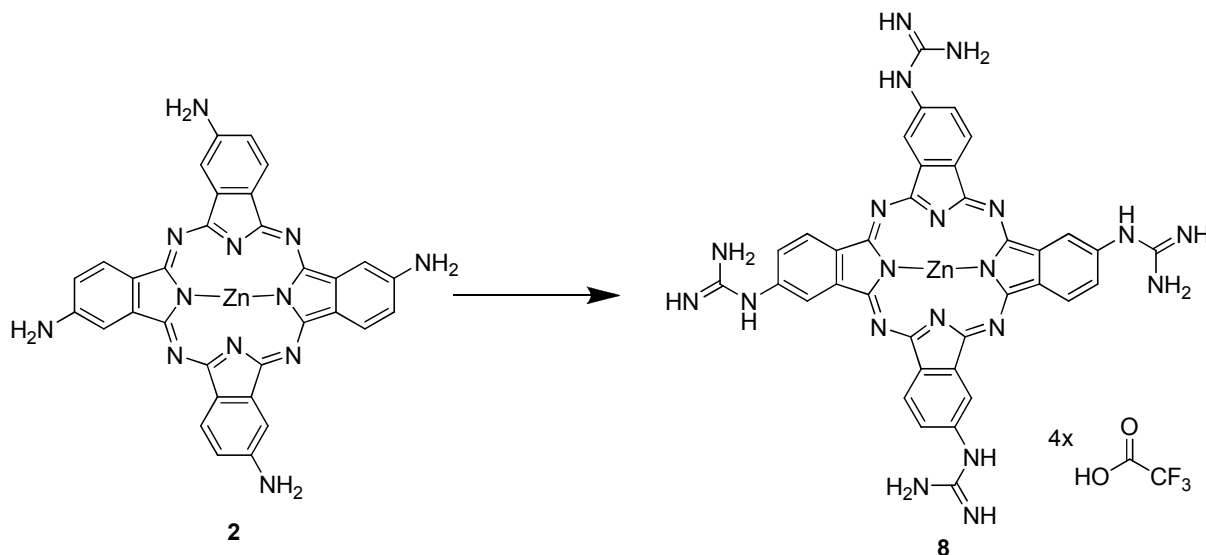
1H -NMR (400 MHz, d_6 -DMSO) δ 10.68 (br. s, 4NH), 9.55 (br. s, 4H), 9.34 (br. s, 4H), 8.24 (br. s, 4H), 8.04 (br. s, 12NH).

MALDI TIF MS (m/z): $[M+H]^+$ calcd for $C_{36}H_{31}N_{20}$, 743.3; found 743.3.

HR-ESI (m/z): $[M+H]^+$ calcd for $C_{36}H_{31}N_{20}$ 743.3041; found 743.3037.

UV-Vis (DMSO) λ_{max} (nm) and ϵ ($\text{cm}^{-1}\text{M}^{-1}$): 344 (5.18×10^5)

5.3.2 Synthesis of tetra-guanidine zinc phthalocyanine (**8**)



Zn(II) was re-introduced into **5** (65.93 mg, 0.055 mmoles) by heating the precipitate in acetic acid (3 mL), anhydrous sodium acetate (1 g), and ZnCl_2 (150 mg, 1.1 mmoles, 20 equiv) at 120 °C for 4 h. The reaction mixture was transferred while hot into a polypropylene centrifuge tube and cooled to r.t. After centrifugation the precipitate was collected and the supernatant was placed in the fridge for 12 hours. White crystals formed which were thrown away after collecting them by centrifugation. After adding methanol (100 mL) the solvents were removed under reduced pressure. The supernatant was passed through the reverse phase column with a gradient from 5% till 25% of acetonitrile containing 0.1% TFA. Every fraction which was coloured green was collected. The solvents were removed under reduced pressure. For HPLC purification 6 mg of 65 mg powder were dissolved in water containing 0.1% TFA (10 mL), passed through a filter and purified by HPLC with column A at a flow rate of 10 mL/min with the following gradient: linear 18-35% acetonitrile containing 0.1% TFA over 25 min. The peak of **8**, eluting between 15-16 min, was collected. The solvents were removed under reduced pressure. The resulting powder was dissolved in water containing 0.1% TFA (1 mL), and lyophilized to obtain a dark green powder. The total yield was 23.8 mg (34.3%).

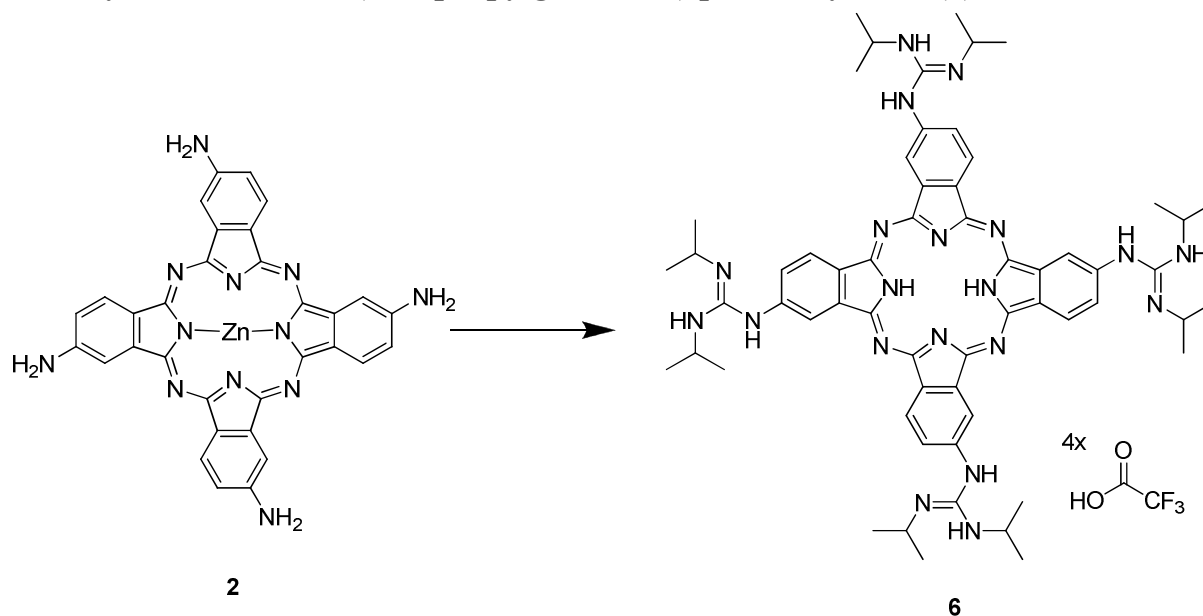
$^1\text{H-NMR}$ (400 MHz, d_6 -DMSO) δ 10.60 (t, $J = 5.8$, 4NH), 9.48 (d, $J = 8.4$, 4H), 9.29 (s, 4H), 8.13 (t, $J = 7.4$, 4H), 7.97 (br. s, 16NH).

MALDI TIF MS (m/z): $[\text{M}+\text{H}]^+$ calcd for $\text{C}_{36}\text{H}_{31}\text{N}_{20}\text{Zn}$, 805.21; found 805.3.

HR-ESI (m/z): $[\text{M}+\text{H}]^+$ calcd for $\text{C}_{36}\text{H}_{31}\text{N}_{20}\text{Zn}$, 805.2175; found 805.2177

UV-Vis (DMSO) λ_{max} (nm) and ϵ ($\text{cm}^{-1}\text{M}^{-1}$): 345 (5.68×10^5)

5.3.3 Synthesis of tetra-(diisopropylguanidine) phthalocyanine (6)



2 (100 mg, 0.157 mmol), pyridine (8 mL), pyridinium-HCl (4 g), and diisopropylcarbodiimide (1.214 mL, 7.83 mmol, 50 equiv) were stirred under N₂ at 110 °C for 19 h. The reaction was removed from the heat and 20 mL of H₂O was used to transfer the hot mixture into a polypropylene centrifuge tube. While vortexing, 1 mL of trifluoroacetic acid (TFA) was added and the resulting precipitate was collected by centrifugation at 6'500 r.p.m. The crude product was dried under high vacuum over night. The supernatant was passed through the reverse phase column with a gradient from 5% till 45% of acetonitrile containing 0.1% TFA. Every fraction which was coloured green was collected. The solvents were removed under reduced pressure. The product obtained from the supernatant was washed two times with 25 mL of a 1:1 mixture of hexane and ethyl acetate. The precipitate was then dissolved in 2 mL of Methanol and 10 mL of Ethyl acetate and heated to 50°C. 67 mL of hexane were slowly added to the hot solution. Precipitation is formed when the mixture was cooled to r.t. The precipitate was collected by centrifugation. H₂O was added to the precipitate and while vortexing, 1 mL of TFA was added and the resulting precipitate was collected by centrifugation and dissolved in a 1:3 mixture of acetonitrile and water containing 0.1% TFA (9mL), and lyophilized to yield 60 mg (24.8%) of a dark green powder.

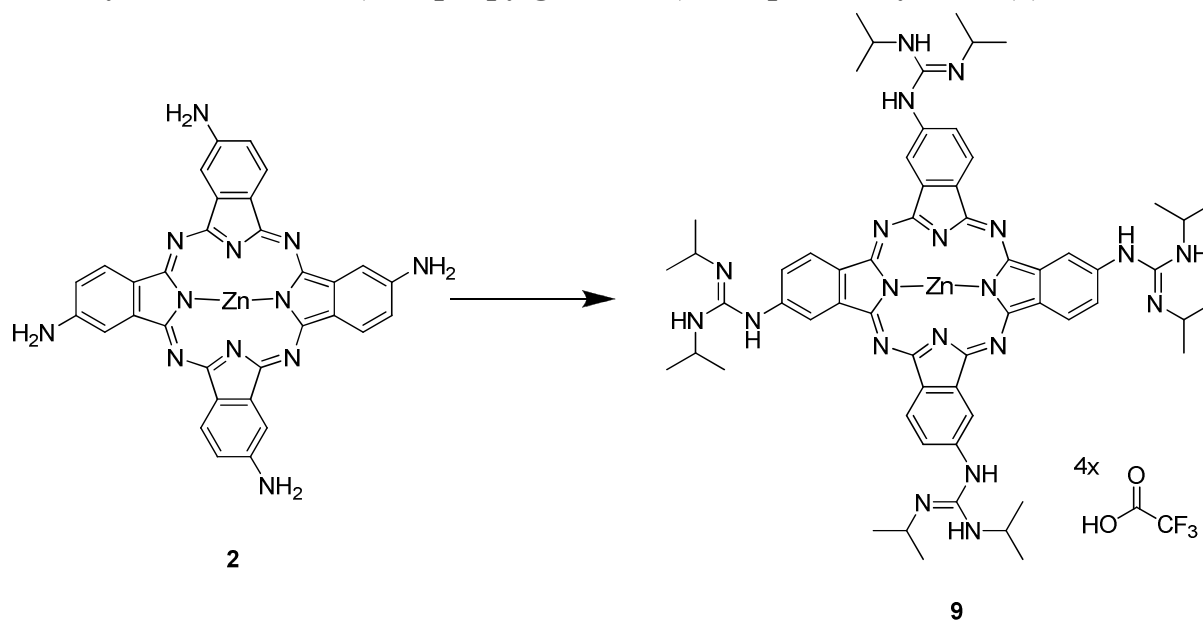
¹H-NMR (400 MHz, d₆-DMSO) δ 10.42, 10.34 (2d, $J_1 = 3.6$ Hz, $J_2 = 6$ Hz, 4NH, 4:5), 9.51, 9.43 (dd and d, $J_1 = 4$ Hz, $J_2 = 4$ Hz, $J_3 = 8.4$ Hz, 4H, 4:5), 9.28, 9.16 (2s, 4H, 6:4), 8.379 (br. s, 8NH), 8.18 (m, 4H), 4.23 (m, 8H), 1.40 (m, 38H).

MALDI TIF MS (m/z): [M+H]⁺ calcd for C₆₀H₇₉N₂₀, 1079.68; found 1079.6.

HR-ESI (m/z): [M+H]⁺ calcd for C₆₀H₇₉N₂₀, 1079.6797; found 1079.6798.

UV-Vis (DMSO) λ_{max} (nm) and ε (cm⁻¹M⁻¹): 345 (7,79x 10⁵)

5.3.4 Synthesis of tetra-(diisopropylguanidine) zinc phthalocyanine (9)



2 (36 mg, 0.056 mmol), pyridine (2 mL), pyridinium-HCl (1 g), and diisopropylcarbodiimide (437 μ L, 2.8 mmol, 50 equiv) were stirred under N_2 at 120 $^\circ$ C for 20 h. The reaction was removed from the heat and 10 mL of H_2O was used to transfer the hot mixture into a polypropylene centrifuge tube. While vortexing, 0.5 mL of trifluoroacetic acid (TFA) was added and the resulting precipitate was collected by centrifugation at 6'500 r.p.m. After repeating this step two times with the supernatant, the crude product was dried under high vacuum for 30 min. HPLC and MS analysis indicated partial loss of Zn(II) from the product. Zn(II) was re-introduced by heating the precipitate in acetic acid (3 mL), anhydrous sodium acetate (1 g), and $ZnCl_2$ (150 mg, 1.1 mmol, 20 equiv) at 120 $^\circ$ C for 90 min. The reaction was removed from the heat and 10 mL of H_2O was used to transfer the hot mixture into a polypropylene centrifuge tube. While vortexing, 1.0 mL of trifluoroacetic acid (TFA) was added and the resulting precipitate was collected by centrifugation. 1.0 mL of TFA was added to the supernatant and the resulting precipitate was collected as before. The precipitates were re-dissolved in 133 mM KCl in water (15 mL) by sonication. While vortexing, 1.0 mL of TFA was added drop-wise and the precipitate collected as before. The precipitate was partially suspended in 25 mL with vigorous shaking and 1 mL of TFA was added drop-wise. The resulting precipitate was collected by centrifugation, dissolved in a 1:3 mixture of acetonitrile and water containing 0.1% TFA (8 mL), and lyophilized to yield 60 mg (67.1 %) of a dark green powder.

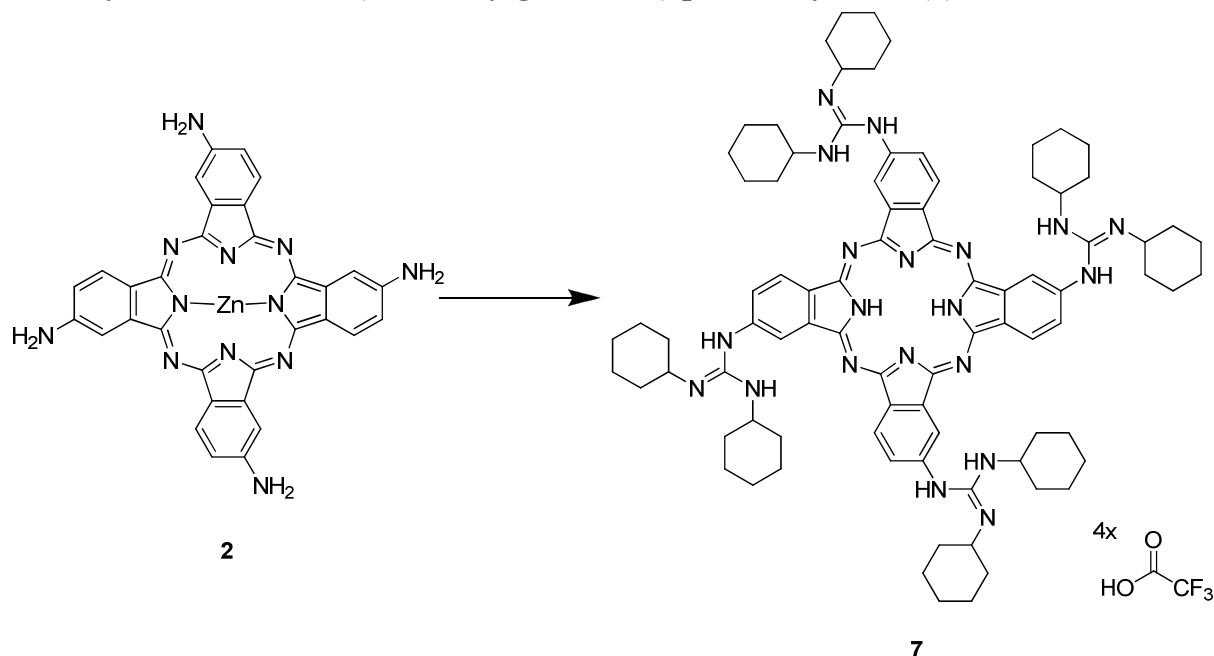
1H -NMR (400 MHz, MeOD) δ 9.50 (d, $J_1 = 2.8$ Hz, 1H), 9.48 (d, $J_1 = 2.4$ Hz, 1H), 9.44 (d, $J = 2.4$ Hz, 1H), 9.42 (d, $J = 2.4$ Hz, 1H), 9.27 (br. s, 2H), 9.21 (br. s, 2H), 9.42 (m, 4H), 4.16 – 4.28 (m, 8H), 1.36 – 1.44 (m, 48H).

MALDI TIF MS (m/z): $[M+H]^+$ calcd for $C_{60}H_{77}N_{20}Zn$, 1141.6; found 1141.6.

HR-ESI (m/z): $[M+H]^+$ calcd for $C_{60}H_{77}N_{20}Zn$, 1141.5932; found 1141.5923.

UV-Vis (DMSO) λ_{max} (nm) and ϵ ($cm^{-1}M^{-1}$): 358 (1.08×10^6)

5.3.4 Synthesis of tetra-(dicyclohexylguanidine) phthalocyanine (7)



2 (94 mg, 0.147 mmol), pyridine (8 mL), pyridinium-HCl (4 g), and *N,N'*-Dicyclohexylcarbodiimide (607.9 mg, 2.947 mmol, 20 equiv) were stirred under N_2 at 110 °C for 19 h. The reaction was removed from the heat and 10 mL of H_2O was used to transfer the hot mixture into a polypropylene centrifuge tube. While vortexing, 1 mL of trifluoroacetic acid (TFA) was added and the resulting precipitate was collected by centrifugation at 6'500 r.p.m. If the supernatant was still coloured green the last step was repeated, otherwise the supernatant is removed. The crude product was dried under high vacuum for 1 hour. The green powder was re-dissolved in the minimal amount of DMSO (2.5 mL). Water (22 mL) was added to the DMSO solution and while vortexing TFA (1 mL) was added dropwise. The obtained precipitate was collected by centrifugation. The washing-step with DMSO was repeated 2 times. For HPLC purification 10 mg of 255 mg were dissolved in DMSO (5 mL). A 5:3 mixture of water and MeOH containing 0.1% TFA (8 mL) was added. After passing the solution through a filter it was purified by HPLC with column B at a flow rate of 4 mL/min with the following gradient: linear 26-34% acetonitrile containing 0.1% TFA over 25 min. The peak of **7**, eluting between 18-19 min, was collected. The solvents were removed under reduced pressure. The resulting powder was dissolved in a 1:3 mixture of acetonitrile and water containing 0.1% TFA (8 mL), and lyophilized to give a dark green powder. The total yield was 33.2 mg (16.1%).

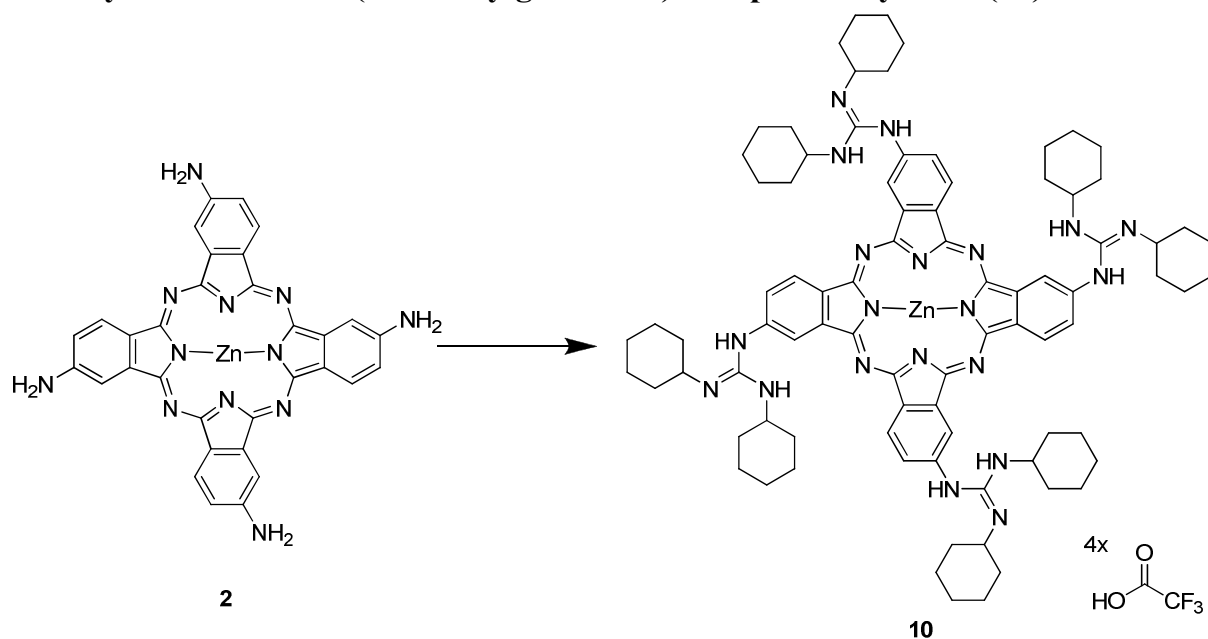
¹H-NMR (400 MHz, d₆-DMSO) δ 10.32 (br. s, 2NH), 10.30 (br. s, 2NH), 9.51 (dd, $J_1 = 8.8$ Hz, $J_2 = 8.4$ Hz 2H), 9.40 (dd, $J_1 = 8.0$ Hz, $J_2 = 5.2$ Hz 2H), 9.30 (s, 2H), 9.15 (br. s, 2H), 8.35 (m, 8NH), 8.19 (br. s, 2H), 8.17 (br. s, 2H) 3.87 (m, 8H), 2.13 (m, 16H), 1.84 (m, 16H), 1.65 (m, 8H), 1.52 (m, 16H), 1.39 (m, 16H), 1.17 (m, 8H), -0.139 (br. s, 2NH).

MALDI TIF MS (m/z): $[M+H]^+$ calcd for C₈₄H₁₁₁N₂₀, 1399.9; found 1399.8.

HR-ESI (m/z): $[M+H]^+$ calcd for C₈₄H₁₁₁N₂₀, 1399.9301; found 1399.9303.

UV-Vis (DMSO) λ_{max} (nm) and ϵ (cm⁻¹M⁻¹): 346 (8.48 x 10⁵)

5.3.6 Synthesis of tetra-(diclohexylguanidine) zinc phthalocyanine (10)



Meta-tetraminophthalocyanine PR008 (94 mg, 0.147 mmol), pyridine (8 mL), pyridinium-HCl (4 g), and *N,N'*-Dicyclohexylcarbodiimide (607.9 mg, 2.947 mmol, 20 equiv) were stirred under N₂ at 110 °C for 19 h. The reaction was removed from the heat and 10 mL of H₂O was used to transfer the hot mixture into a polypropylene centrifuge tube. While vortexing, 1 mL of trifluoroacetic acid (TFA) was added and the resulting precipitate was collected by centrifugation at 6'500 r.p.m. If the supernatant was still coloured green the last step was repeated, otherwise the supernatant is removed. The crude product was dried under high vacuum for 1 hour. HPLC and MS analysis indicated partial loss of Zn(II) from the product. Zn(II) was re-introduced by heating the precipitate in acetic acid (9 mL), anhydrous sodium acetate (3 g), and ZnCl₂ (450 mg, 3.3 mmol, 20.4 equiv) at 120 °C for 90 min. The reaction was removed from the heat and 20 mL of H₂O was used to transfer the hot mixture into two polypropylene centrifuge tubes. Both tubes were treated as followed: While vortexing, 1.0 mL of trifluoroacetic acid (TFA) was added and the resulting precipitate was collected by centrifugation. The precipitates were re-dissolved in 133 mM KCl in water (15

mL) by sonication. To get complete precipitation 1.0 mL of TFA was added while vortexing drop-wise and the precipitate collected as before. The precipitate was partially suspended in 25 mL with vigorous shaking and 1 mL of TFA was added drop-wise. The resulting precipitate was collected by centrifugation, dissolved in a 1:3 mixture of acetonitrile and water containing 0.1% TFA (8 mL), and lyophilized. The green powder was re-dissolved in the minimal amount of DMSO (2.5mL). Water (22mL) was added while vortexing. TFA (1 mL) was added to get a precipitate which was collected by centrifugation. The washing-step with DMSO was repeated 2 times. For HPLC purification 10 mg of 265 mg were dissolved in a 1:1 mixture of water and MeOH containing 0.1% TFA (15mL). After passing the solution through a filter it was purified by HPLC with column C at a flow rate of 4 ml/min with the following gradient: linear 48-58% acetonitrile containing 0.1% TFA over 25 min. The peak of **10**, eluting between 16-17 min, was collected. The solvents were removed under reduced pressure. The resulting powder was dissolved in a 1:3 mixture of acetonitrile and water containing 0.1% TFA (8 mL), and lyophilized to give a dark green powder. The total yield was 90.1 mg (31.9%) of a dark green powder.

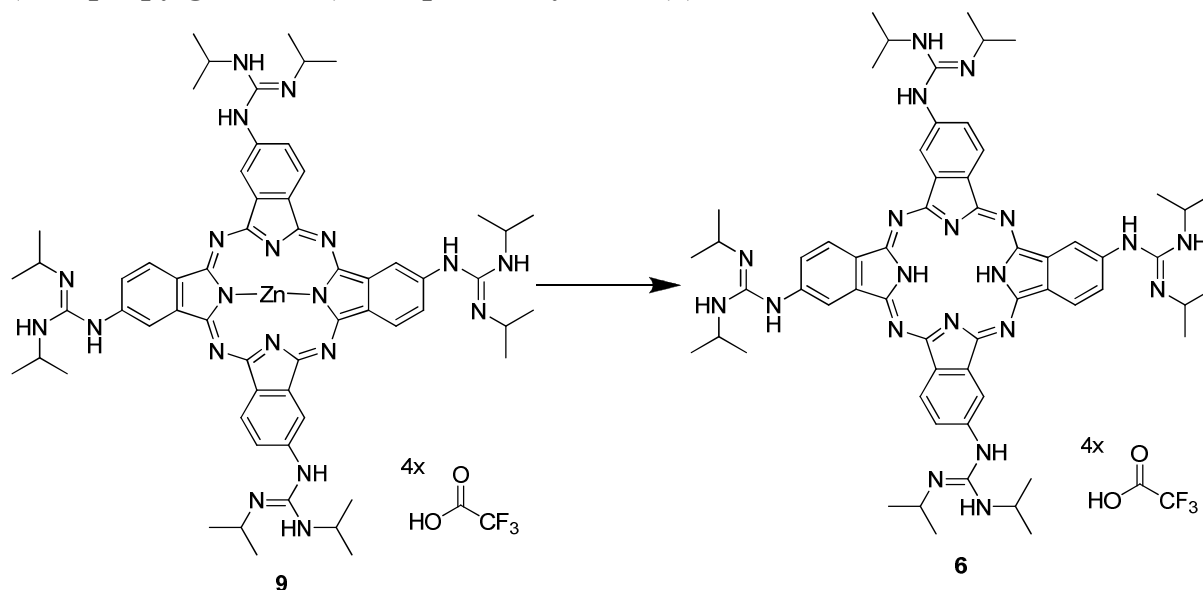
¹H-NMR (400 MHz, *d*₆-DMSO) δ 10.06 (br. s, 2NH), 10.04 (br. s, 2NH), 9.43 (dd, $J_1 = 6.8$ Hz, $J_2 = 8.8$ Hz 2H), 9.33 (t, $J = 7.6$ Hz 2H), 9.23 (s, 2H), 9.10 (s, 2H), 8.17 (m, 8NH), 8.07 (m, 4H), 3.84 (m, 8H), 2.12 (m, 16H), 1.83 (m, 16H), 1.64 (m, 8H), 1.51 (m, 16H), 1.39 (m, 16H), 1.16 (m, 8H).

MALDI TIF MS (*m/z*): [M+H]⁺ calcd for C₈₄H₁₀₉N₂₀Zn, 1461.8; found 1461.7.

HR-ESI (*m/z*): [M+H]⁺ calcd for C₈₄H₁₀₉N₂₀Zn, 1461.8436; found 1461.8423.

UV-Vis (DMSO) λ_{max} (nm) and ϵ (cm⁻¹M⁻¹): 345 (2.09 x 10⁶)

5.3.7 Synthesis of tetra-(diisopropylguanidine) phthalocyanine (**6**) from tetra-(diisopropylguanidine) zinc phthalocyanine (**9**)



9 (10 mg, 0.006 mM), pyridine (1 mL), and pyridinium-HCl (0.5 g) were stirred under N_2 at $110^\circ C$ for 17 h. The reaction was removed from the heat and 5 mL of H_2O was used to transfer the hot mixture into a polypropylene centrifuge tube. While vortexing, 0.5 mL of TFA was added and the resulting precipitate was collected by centrifugation at 6'500 r.p.m. The precipitate was re-dissolved in 133 mM KCl in water (6 mL) by sonication. While vortexing, 0.5 mL of TFA was added drop-wise and the precipitate collected as before. Water (5 ml) was added to the precipitate and while vortexing, 0.5 mL of TFA was added and the resulting precipitate was collected by centrifugation and dissolved in a 1:3 mixture of acetonitrile and water containing 0.1% TFA (3mL), and lyophilized to yield 30.2 mg (95%) of a dark green powder.

1H -NMR (400 MHz, d_6 -DMSO) δ 10.42, 10.34 (2d, $J_1 = 3.6$ Hz, $J_2 = 6$ Hz, 4NH, 4:5), 9.51, 9.43 (dd and d, $J_1 = 4$ Hz, $J_2 = 4$ Hz, $J_3 = 8.4$ Hz, 4H, 4:5), 9.28, 9.16 (2s, 4H, 6:4), 8.379 (br. s, 8NH), 8.18 (m, 4H), 4.23 (m, 8H), 1.40 (m, 38H).

MALDI TOF MS (m/z): $[M+H]^+$ calcd for $C_{60}H_{79}N_{20}$, 1079.68; found 1079.6.

5.4 Fluorescence experiments

5.4.1 Methods

To account for the hyperchromicity of G-quadruplex formation, quantifications were made at 99°C and the ϵ ($\text{cm}^{-1}\text{M}^{-1}$) values for 25°C calculated at 260 nm for the experiment for the diisopropyl derivatives (**6** and **9**) without detergents in the buffer:

<u>Oligo Name</u>	<u>Sequence</u>	<u>ϵ ($\text{cm}^{-1}\text{M}^{-1}$)(99°C)</u>	<u>ϵ ($\text{cm}^{-1}\text{M}^{-1}$)(25°C)</u>
Myc NMR	TGAGGGTGGGGAGGGTGGGGAA	229'900	160'900
Fl-Myc NMR	Flu- TGAGGGTGGGGAGGGTGGGGAA	262'400	193'400
Fl-Myc31	Flu-(GGGGAGGGT) ₂ GGGGAAGGTGGGG		
H telo	GTTA(GGGTTA) ₄ GG	306'900	276'200
Fl-H telo	Flu- GTTA(GGGTTA) ₄ GG		
H telo-mut	GTTA(GAGTTA) ₄ GG	319'300	287'400
Fl-H telo-mut	Flu- GTTA(GGGTTA) ₄ GG		
F Hum telo	Flu-[TTAGGG] ₄		
F Hum telo Mu	Flu-[TTAGAG] ₄		
c-Kit87	AGGGAGGGCGCTGGGAGGAGGG	226'700	
c-Kit	CCCGGGCGGGCGCGAGGGAGGGGAGG	253'400	
Fl-cKit	Flu-CCCGGGCGGGCGCGAGGGAGGGGAGG		

DNA oligos (~30 μM) were heated in a TKE buffer containing 50 mM Tris-HCl (pH 7.4) 150 mM KCl, and 0.5 mM EDTA to 99°C then slowly cooled to r.t. and quantified using $\epsilon = 9'600 \text{ cm}^{-1} \text{ M ntd}^{-1}$ (25°C) for the diisopropyl derivatives without a detergent. For all other experiments the ϵ ($\text{cm}^{-1}\text{M}^{-1}$)(99°C) are used. A correction for those K_d values is needed. For the quantification of the fluorescein tagged DNA we measured the OD at 260 and 490 nm. To the OD at 260 nm we subtracted half of the OD value at 490 nm and quantified using the ϵ from the same sequences without the fluorescein. Type I, highly polymerized calf thymus DNA (CT DNA) was dissolved into TKE at 37°C for 12 hrs, centrifuged at 20'000 x g, and the supernatant diluted 2X into TKE buffer. The solution was then sonicated for 2 minutes and the solution quantified using $\epsilon = 6'500 \text{ cm}^{-1} \text{ M ntd}^{-1}$ (25°C). The mixture of yeast tRNA (tRNA) was dissolved into TKE buffer at r.t. The solution was then sonicated and quantified using $\epsilon = 9640 \text{ cm}^{-1} \text{ M ntd}^{-1}$ (25°C).

5.4.2 Titrations

All titrations were conducted at room temperature. Buffer was measured as a blank in all assays. The Fluorescence data was analysed using an independent 2:1 binding model. The

titrations were conducted in TKE buffer containing 50 mM Tris-HCl (pH 7.4) 150 mM KCl, and 0.5 mM EDTA. If detergents were used it will be specified in the text.

Fluorescence enhancements assay

Fluorescence titrations were performed at a fixed concentration of ligand and the duplex concentration varied. A solution of a compound was added to the plate followed by one volume of DNA solution and mixed 3 times by pipette. The final volume was 70 μ L. Plates were read multiple times to ensure equilibrium was reached.

The fluorescence enhancements experiments were measured with a 25nM solution of the compounds. The DNA concentrations were: 400nM, 200nM, 100nM, 50nM, 25nM, 12.5nM, 6.25nM, 3.125nM, 1.563nM, 0.781nM and 0nM.

Fluorescence quenching assay

Fluorescence quenching of a 5' fluorescein end-labeled DNA (Ex 495nm, Em520nm) upon titration with ligands in the presence or absence of CT DNA or tRNA.

The fluorescence quenching experiment conducted for confirming the fluorescence enhancement experiments were measured with 25nM solution of the DNA. A solution of a compound was added to the plate followed by one volume of DNA solution and mixed 3 times by pipette. The final volume was 70 μ L. The concentration of the compounds were: 400nM, 200nM, 100nM, 50nM, 25nM, 12.5nM, 6.25nM, 3.125nM, 1.563nM, 0.781nM and 0nM

	<u>CT DNA</u>	<u>tRNA</u>
H telo	50 μ M	50 μ M

Fluorescence quenching of a 10nM solution of the 5' fluorescein end-labeled DNA (Ex 495nm, Em 520nm) upon titration with **6**, **9**, TMPyP4 and Zn-TMPyP4 in the presence or absence of CT DNA or tRNA.

The fluorescence quenching experiment conducted for confirming the direct assay experiments were measured with 10nM solution of the DNA. A solution of a compound was added to the plate followed by one volume of DNA solution and mixed 1 times by pipette. The final volume was 80 μ L. The concentration of the ligands (**6**, **9**, TMPyP4 and Zn-TMPyP4) were: 1000nM, 500nM, 250nM, 125nM, 62.5nM, 31.25nM, 15.625nM, 7.813nM, 3.906nM, 1.953nM and 0nM.

	<u>CT DNA</u>	<u>tRNA</u>
Flu-Myc nmr	220 μ M	220 μ M
Flu-H telo and Flu-H telo mu	300 μ M	300 μ M

Compounds from 1mM in DMSO.

Direct binding assay

A 2x solution of a compound was added to the plate followed by one volume of DNA solution and mixed once by pipette. The final volume was 80 μ L. Plates were read multiple times to ensure equilibrium was reached. This fluorescence enhancement experiment was measured with a 10nM solution of the compounds. The Myc NMR DNA concentrations were: 1622.22nM, 540.74nM, 180.25nM, 60.08nM, 20.03nM, 6.68nM, 2.23nM, 0.74nM, 0.25nM and 0nM. The H telo DNA concentrations were: 662.96nM, 220.99nM, 73.66nM, 24.55nM, 8.18nM, 2.73nM, 0.91nM, 0.30nM and 0nM. The H telo-Mu DNA concentrations were: 1429.63nM, 476.54nM, 158.85nM, 52.95nM, 17.65nM, 5.88nM, 1.96nM, 0.65nM and 0nM. The CT-DNA concentrations were: 490nM, 163.33nM, 54.44nM, 18.15nM, 6.05nM, 2.02nM, 0.67nM, 0.22nM, 0.07nM, 0.02nM and 0nM. The t-RNA concentrations were: 66nM, 22nM, 7.33nM, 2.44nM, 0.81nM, 0.27nM, 0.09nM, 0.03nM, 0.01nM and 0nM.

5.4.3 Job Plot

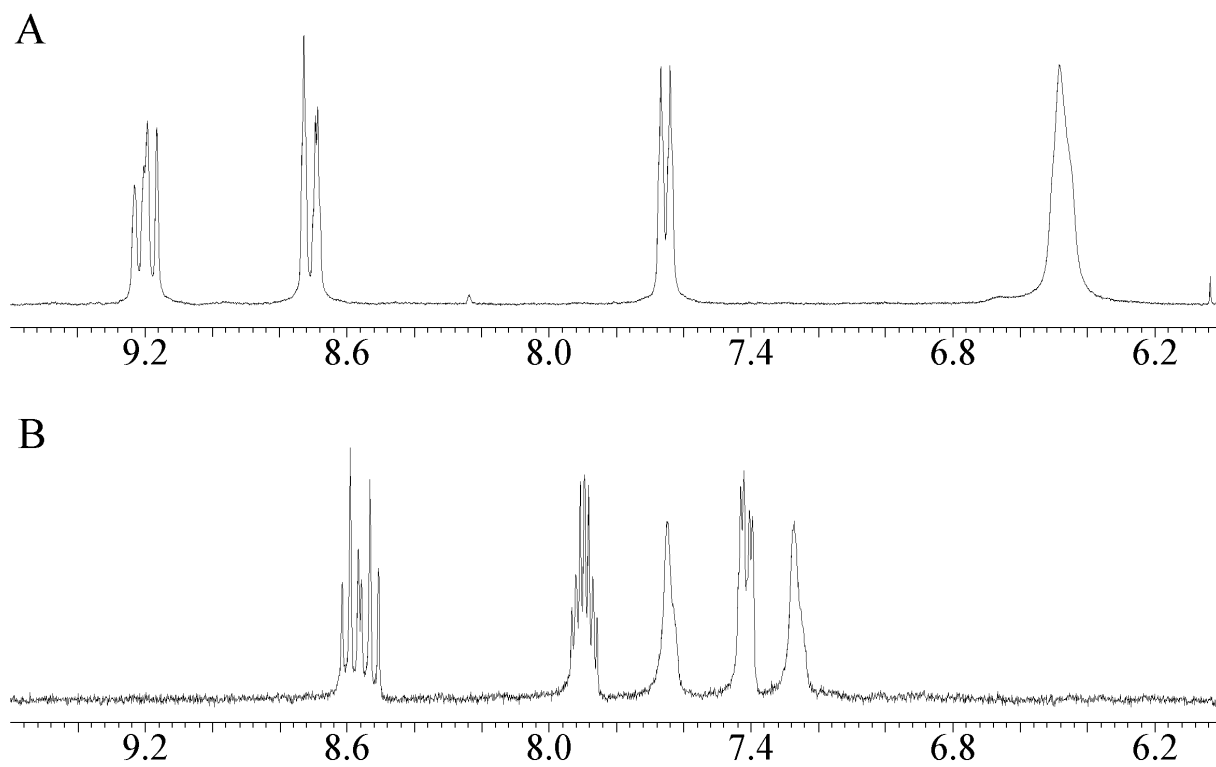
Binding stoichiometries were measured by continuous variation binding analysis by a method according to Job. ^[52] Both [compound] and [DNA] were varied for a fixed and constant summed concentration of 100nM. Different volumes of equimolar stock solution were mixed and made up to 70 μ L with the appropriate volumes to give mole fractions of the compound ranging from 0.1 to 1, in TKE buffer with 0.25% DMSO. Excitation wavelength is 495nm and the emission wavelength is 520nm.

6. Summary

We synthesised six different C_{4h} symmetric Guanidino Phthalocyanines (GPcs) which were characterized by MALDI TOF MS, high resolution ESI MS, NMR and UV-VIS. The G-quadruplex affinity and specificity of GPcs were evaluated by fluorescence testing. GPcs were synthesized by reacting a C_{4h} symmetric phthalocyanine 4,4',4'',4'''-tetraamino zinc phthalocyanine with various carbodiimides in the presence of pyridine-HCl at 120°C. During our efforts to synthesize GPcs we found that these conditions can de-metallate zinc-containing Pcs as well as catalyse the formation of mono- and trisubstituted guanines. The resulting derivatives have a high affinity and specificity for G-quadruplex DNA. The tetra-monosubstituted guanidine zinc phthalocyanine had the highest G-quadruplex affinity, but its limited solubility prevented its full characterization. We compared the binding affinities of tetra-diisopropylguanidine substituted phthalocyanines to other GPcs in the presence or absence of zinc metal. The K_d values determined by two types of fluorescence assays ranged 2 – 90 nM. The tetra-diisopropylguanidine substituted phthalocyanines were very water soluble, entered living cells, and had K_d values in the low nM range which surpassed all the K_d values published thus far. In addition to high affinity, the tetra-diisopropyl GPcs showed a high specificity for G-quadruplex DNA. These compounds also exhibit relatively low cytotoxicity, and anti-cancer activities *in vivo*.

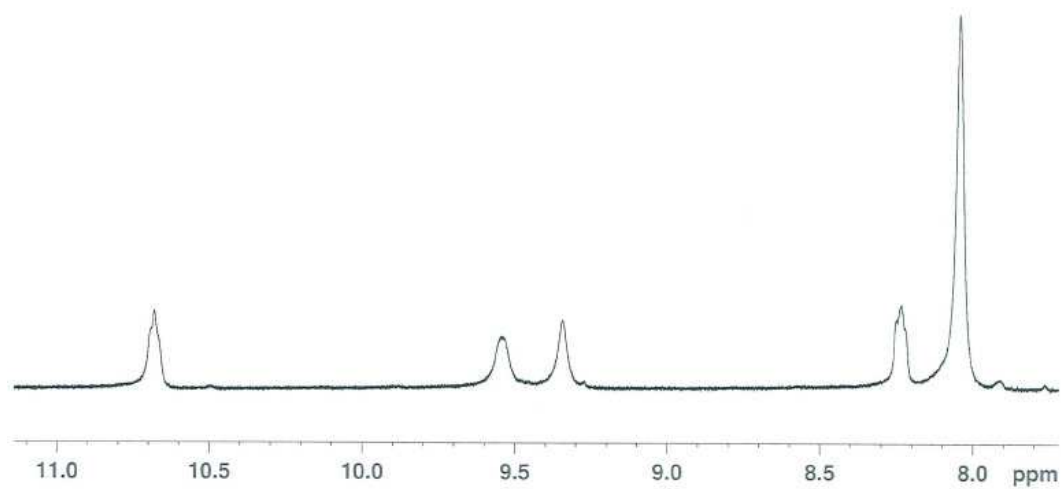
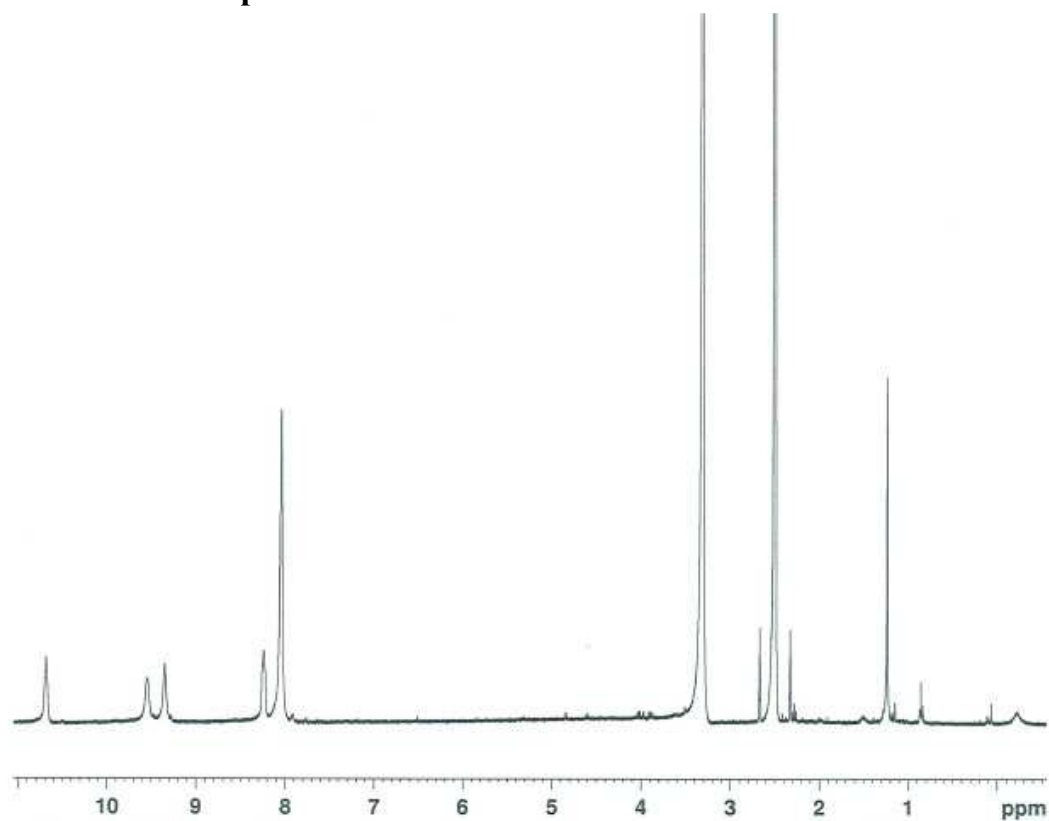
7. Appendix

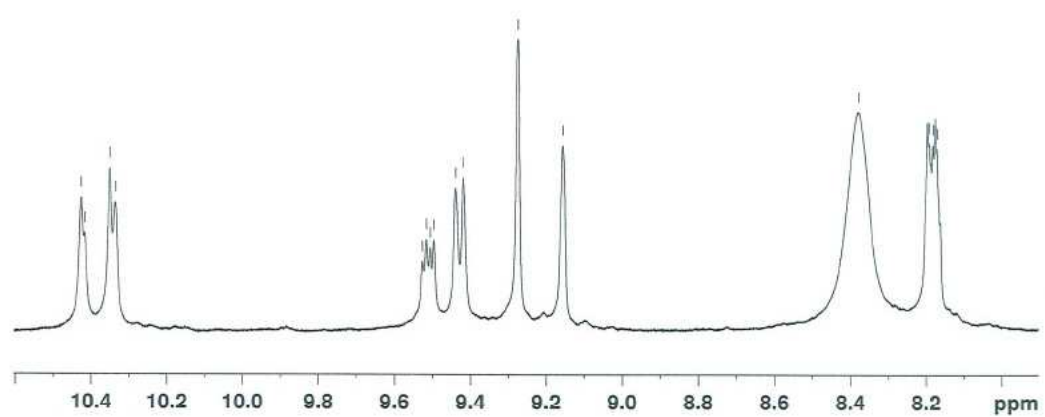
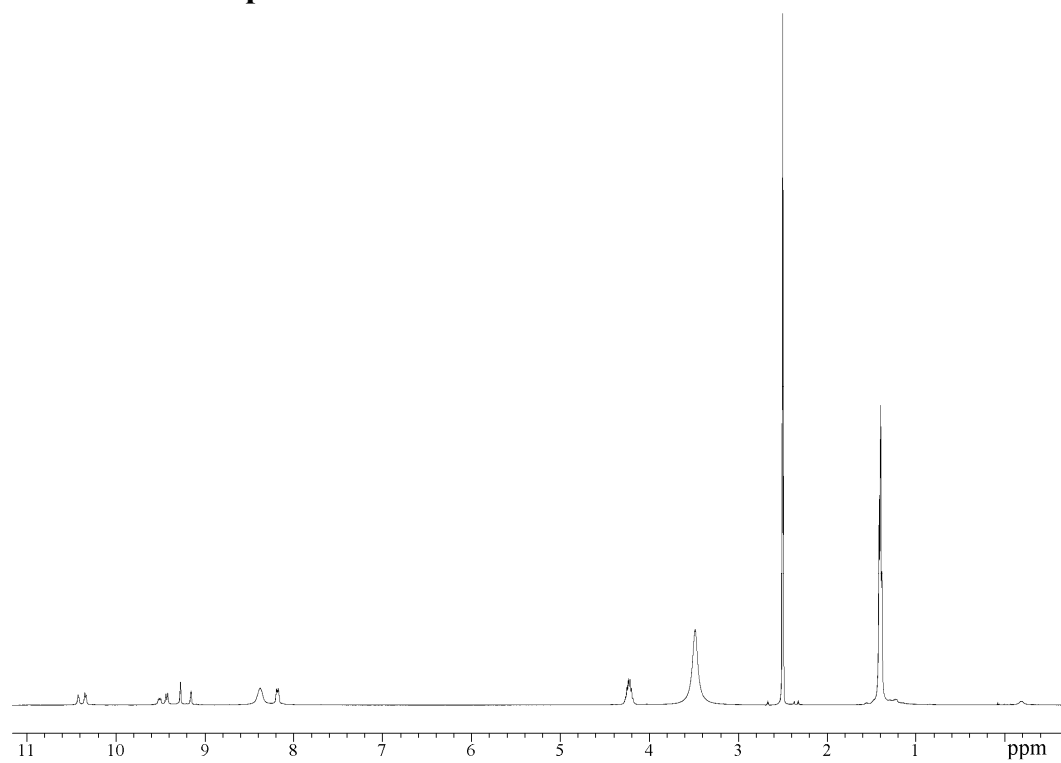
7.1 NMR spectra of 2 (A) and 4 (B)



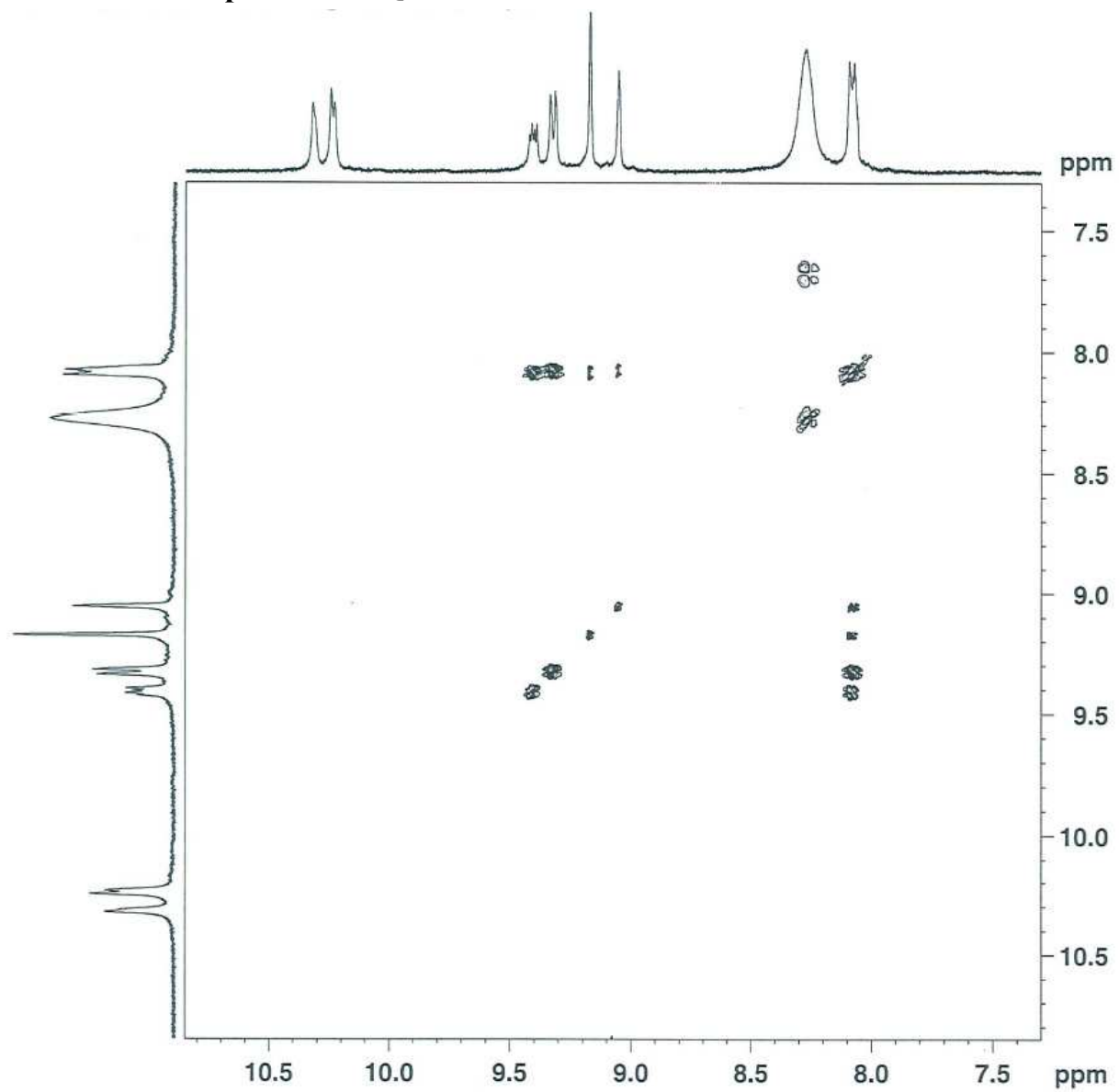
7.2 NMR spectra of 5

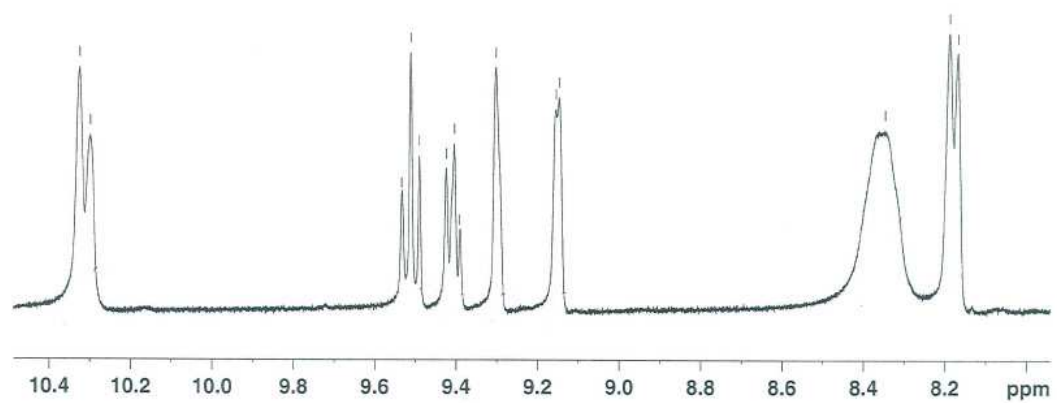
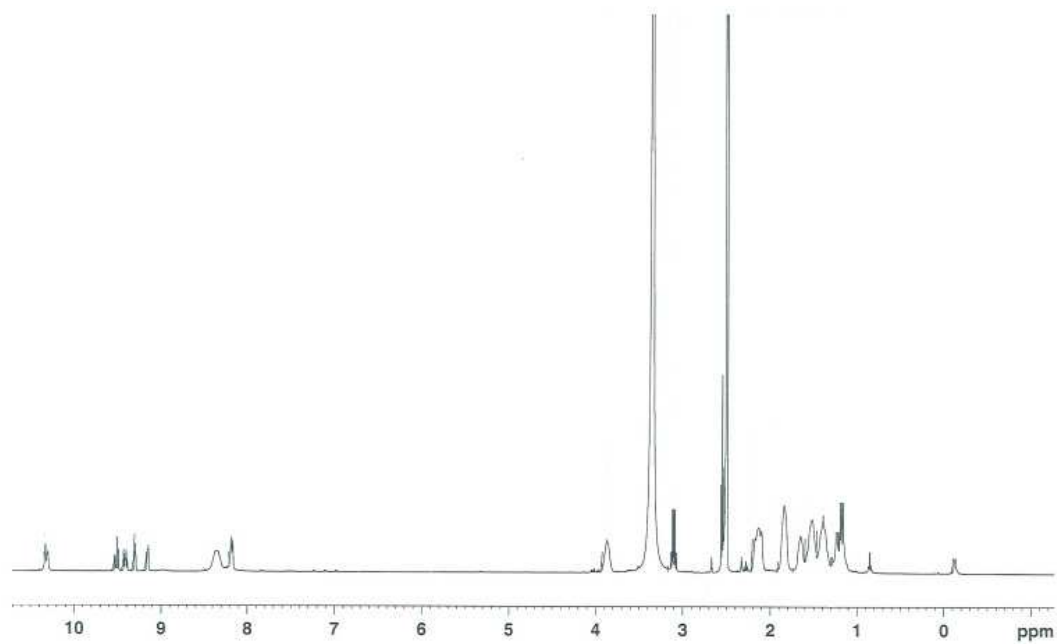
7.2.1 ^1H -NMR spectrum



7.3 NMR spectra of 6**7.3.1 ^1H -NMR spectrum**

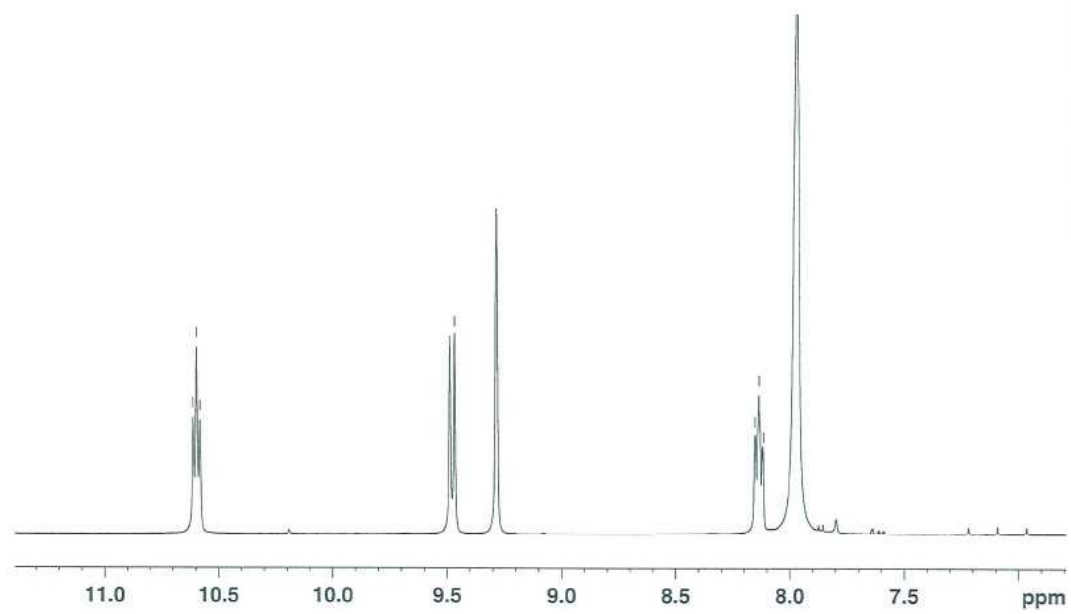
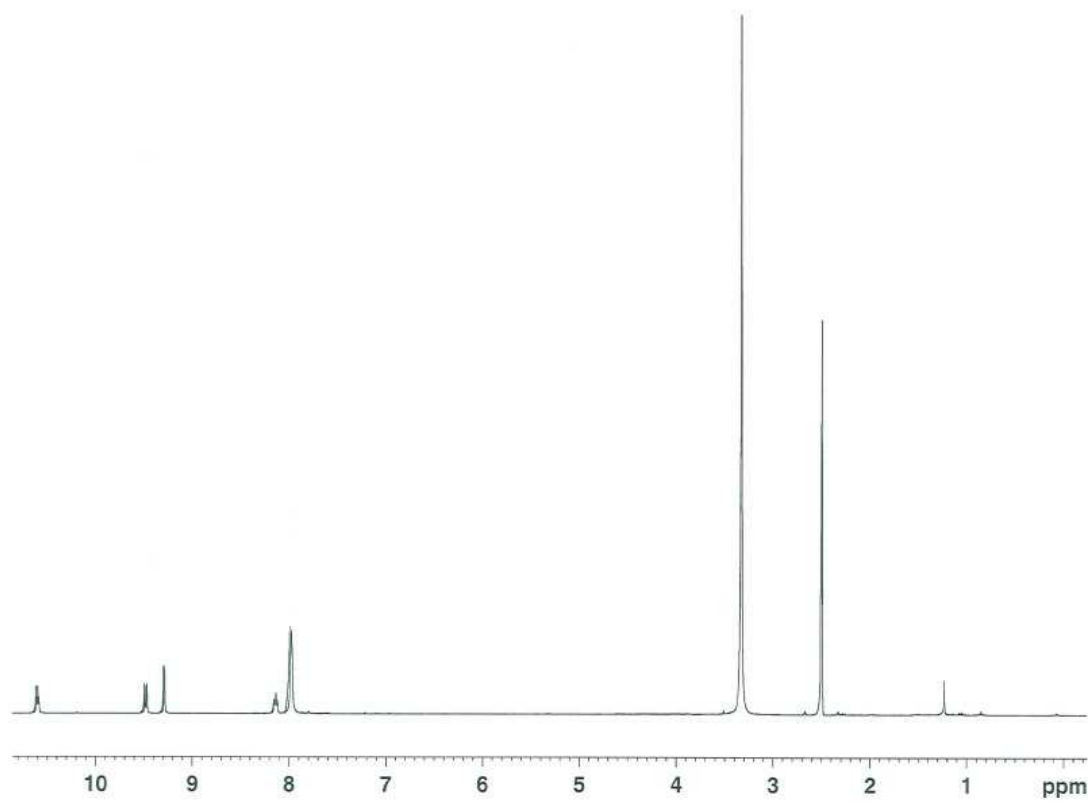
7.3.2 2D-NMR spectrum: DQF-COSY



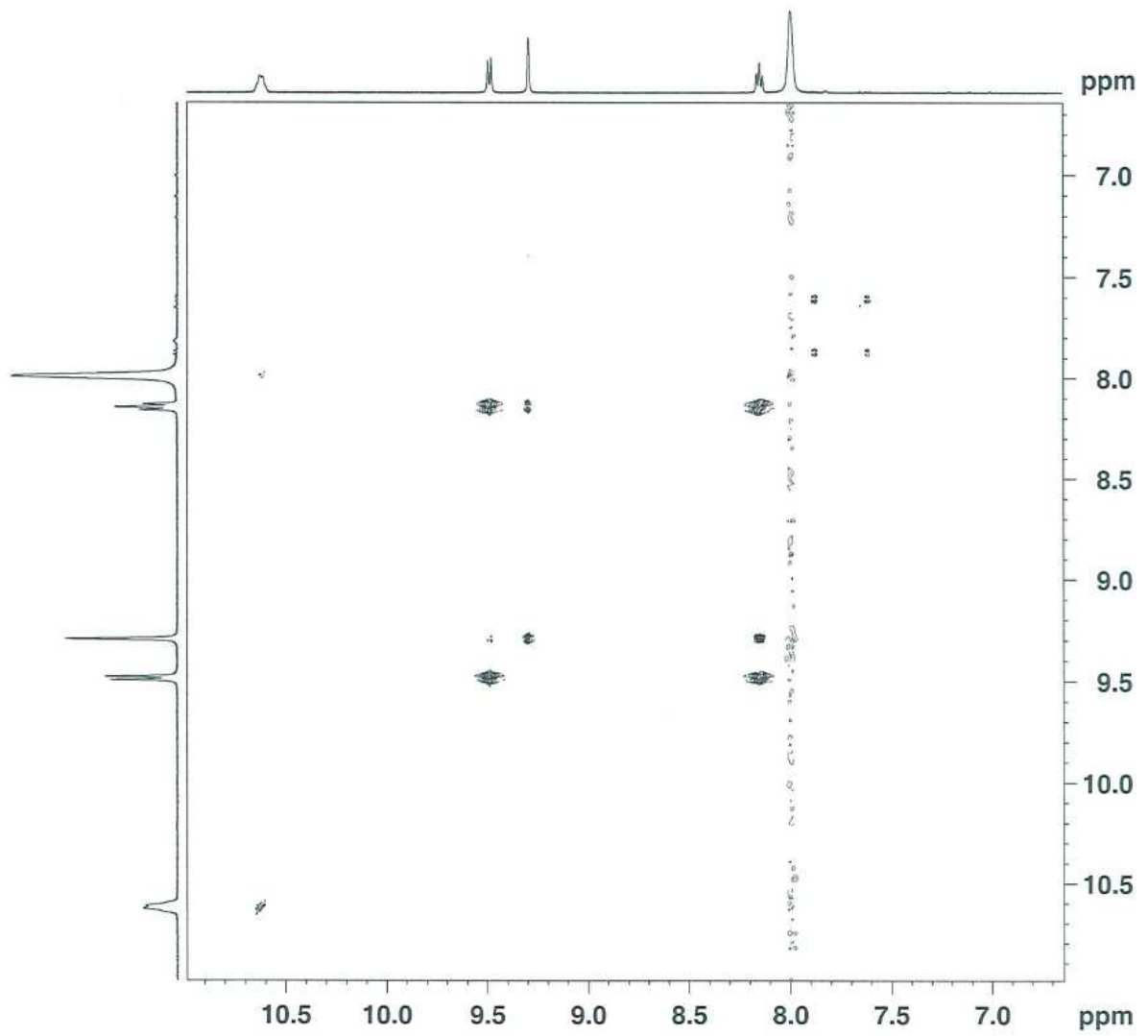
7.4 NMR spectra of 7**7.4.1 ^1H -NMR spectrum**

7.5 NMR spectra of **8**

7.5.1 ^1H -NMR spectrum

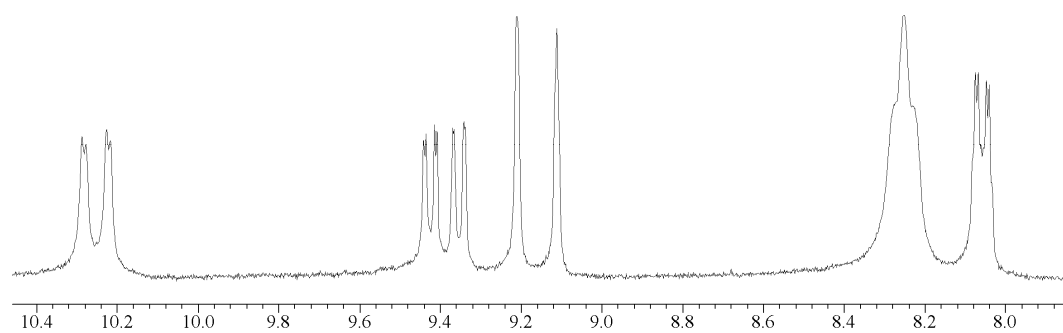
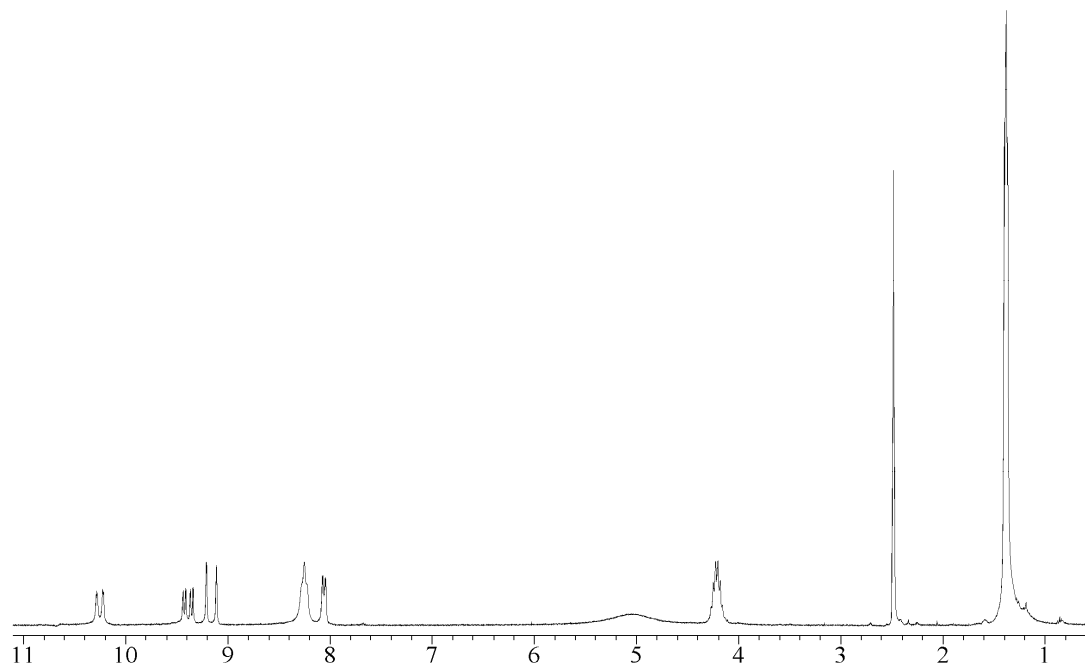


7.5.2 2D-NMR spectrum: DQF-COSY



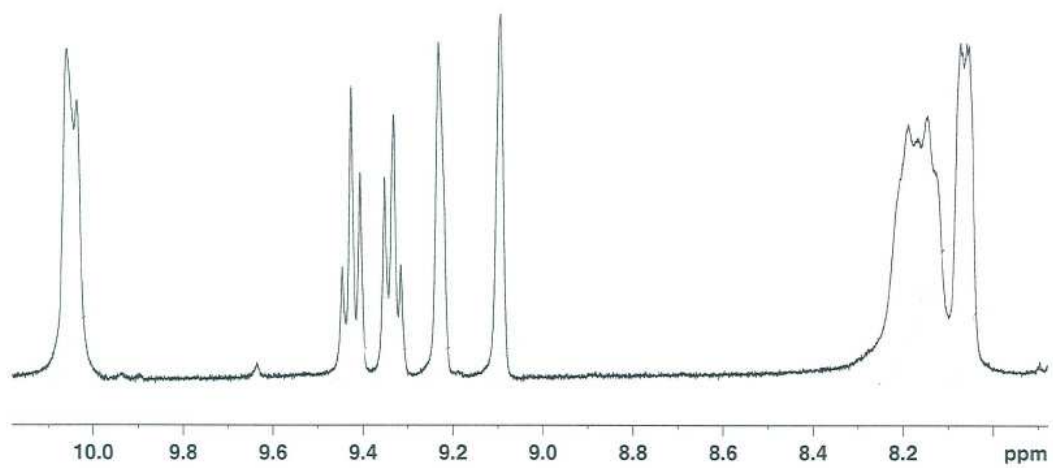
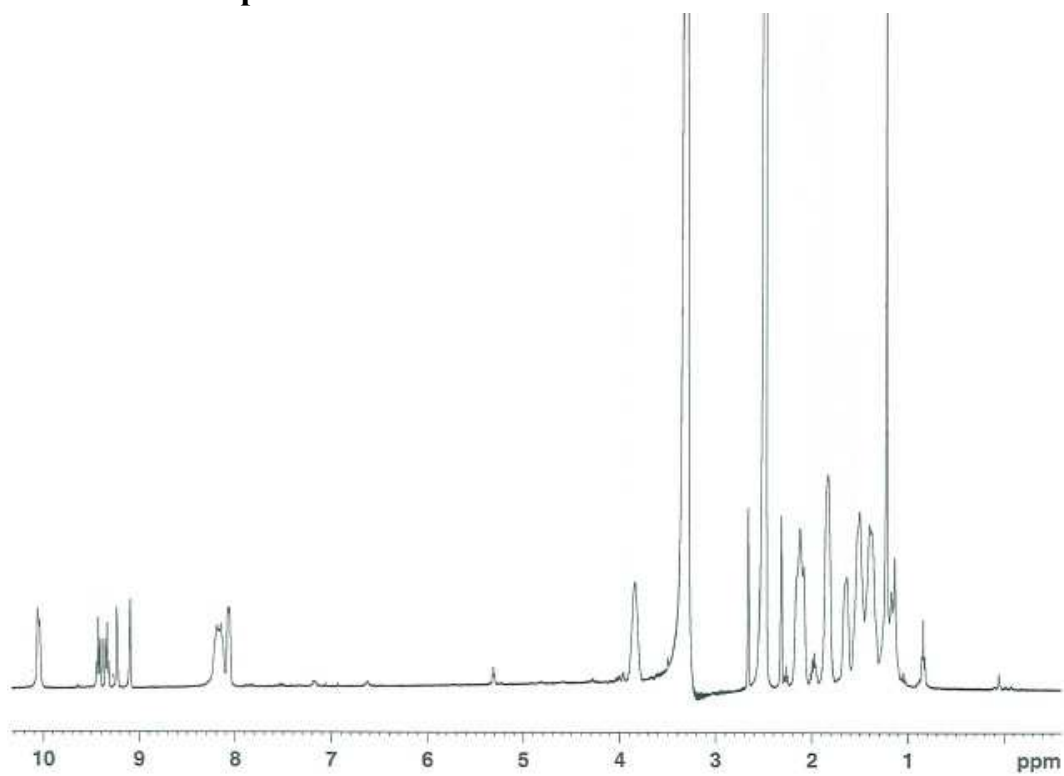
7.6 NMR spectra of 9

7.6.1 ^1H -NMR spectrum



7.7 NMR spectra of 10

7.7.1 ^1H -NMR spectrum



7.8 Fluorescence Quenching results of 9

			DNA_	DNA+CTDNA	DNA+HRNA
F Insulin	PR006 (9)	HalfLife	59.92	61.7	70.1
TKE buffer		Kd	107.34	110.9	127.7
F Myc31	PR006 (9)	HalfLife	35.23	37.71	40.62
TKE buffer		Kd	57.96	62.92	68.74
F cKit	PR006 (9)	HalfLife	16.83	22.19	27.36
TKE buffer		Kd	21.16	31.88	42.22
F Hum telo	PR006 (9)	HalfLife	50.96	148.1	1354
Mu		Kd	89.42	283.7	2695.5
TKE buffer					

7.9 Fluorescence enhancement results

			PR001 (6)	PR002 (5)	PR003 (8)	PR004 (10)	PR005 (7)
ckit	K		0.01784	0.0009194	0.03518	0.00011	0.007611
TKE buffer + 1.25%DMSO	Ec50		38.68	750.49	19.61	6272.73	90.66
0.1%NP40	Kd		64.85	1488.48	26.73	12532.95	168.82
			PR001 (6)	PR003 (8)	PR004 (10)	PR005 (7)	PR006 (9)
F Hum telo	K		0.0288	0.1042	0.01408	0.0003	0.0475
TKE buffer+ 0.1%NP40	Ec50		23.96	6.62	49.01	2300.00	14.53
1.25%DMSO	Kd		35.42	0.74	85.51	4587.50	16.55
F myc31	K		0.13	0.12	0.05	0.17	0.12
TKE buffer+ 0.22%DMSO	Ec50		5.13	5.95	15.30	4.12	5.95
0.05%NP40	Kd		<2	<2	18.10	<2	<2
				(from DMSO)			
F myc31	K		PR006 (9)	PR001 (6)	PR003 (8)		
TKE buffer	Ec50		0.07405	0.06877	0.5245		
	Kd		9.32	10.03	1.32		
			6.14	7.57	<2		
F Kit	K		0.02553	0.02464	0.1742		
TKE buffer	Ec50		27.03	28.00	3.96		
	Kd		41.55	43.51	<2		

8. Abbreviations

Bp	base pair
conc.	concentration
COSY	correlation spectroscopy
CT DNA	calf thymus DNA
DCC	N,N'-Dicyclohexylcarbodiimide
DMAE	dimethylaminoethanol
DMAP	4-(Dimethylamino)-pyridine
DMF	dimethylformamid
DMSO	dimethylsulfoxid
DNA	deoxyribonucleic acid
eq	equivalent
EC50	The molar concentration of an agonist, which produces 50% of the maximum possible response for that agonist.
ESI	electrospray ionization
EDTA	ethylenediaminetetraacetic acid
HPLC	high performance liquid chromatography
GPcs	Guanidino Phthalocyanines
H telo	DNA of the human telomeric repeat
H telo-Mu	Mutant DNA of the human telomeric repeat
HV	high vacuum
lit.	literature
MALDI	matrix-assisted laser desorption/ionization
MS	mass spectroscopy
Myc NMR	DNA derived from the c-Myc oncogene promoter
NMR	nuclear magnetic resonance
NP40	Nonidet P40 detergent
Pcs	Phthalocyanines
r.t.	room temperature
TAMPcs	Tetraaminometallophthylocyanines
TFA	trifluoroacetic acid
THF	tetrahydrofuran
TKE buffer	buffer containing 50 mM Tris-HCl (pH 7.4) 150mM KCl, and 0.5 mM EDTA
TMPy4	cationic porphyrin 5,10,15,20-tetra(N-methyl-4-pyridyl) porphin
tRNA	mixture of yeast tRNA
tween	tween®20 detergent
RP-HPLC	reverse phase high performance liquid chromatography
r.p.m.	rounds pair minute
UV/VIS	ultraviolet/visible spectroscopy
Zn-TMPy4	cationic porphyrin 5,10,15,20-tetra(N-methyl-4-pyridyl) zinc porphin

9. References

- [1] J. D. Watson, F. H. C. Crick, *Nature (London, United Kingdom)* **1953**, 171, 737.
- [2] Internet homepage: http://en.wikipedia.org/wiki/Image:A-DNA%2C_B-DNA_and_Z-DNA.png **2008**.
- [3] A. H. Wang, G. J. Quigley, F. J. Kolpak, J. L. Crawford, J. H. van Boom, G. van der Marel, A. Rich, *Nature FIELD Full Journal Title:Nature* **1979**, 282, 680.
- [4] D. Voet, Voet, J.G., and Prat,C.W., *Fundamentals of Biochemistry*, **1999**.
- [5] B. P. Belotserkovskii, E. De Silva, S. Tornaletti, G. Wang, K. M. Vasquez, P. C. Hanawalt, *J Biol Chem* **2007**, 282, 32433.
- [6] M. J. van Dongen, J. F. Doreleijers, G. A. van der Marel, J. H. van Boom, C. W. Hilbers, S. S. Wijmenga, *Nat Struct Biol* **1999**, 6, 854.
- [7] A. T. Phan, J.-L. Mergny, *Nucl. Acids Res.* **2002**, 30, 4618.
- [8] K. Gehring, J. L. Leroy, M. Gueron, *Nature FIELD Full Journal Title:Nature* **1993**, 363, 561.
- [9] S. Nonin, J.-L. Leroy, *Journal of Molecular Biology* **1996**, 261, 399.
- [10] A. T. Phan, M. Gueron, J. L. Leroy, *J Mol Biol* **2000**, 299, 123.
- [11] S. Burge, G. N. Parkinson, P. Hazel, A. K. Todd, S. Neidle, *Nucleic Acids Res* **2006**, 34, 5402.
- [12] H. Han, L. H. Hurley, *Trends in Pharmacological Sciences* **2000**, 21, 136.
- [13] J. D. Griffith, L. Comeau, S. Rosenfield, R. M. Stansel, A. Bianchi, H. Moss, T. de Lange, *Cell* **1999**, 97, 503.
- [14] E. M. Rezler, D. J. Bearss, L. H. Hurley, *Annual Review of Pharmacology and Toxicology* **2003**, 43, 359.
- [15] A. Ambrus, D. Chen, J. Dai, R. A. Jones, D. Yang, *Biochemistry* **2005**, 44, 2048.
- [16] Y. Qin, E. M. Rezler, V. Gokhale, D. Sun, L. H. Hurley, *Nucl. Acids Res.* **2007**, 35, 7698.
- [17] T. Simonsson, *Biological Chemistry* **2001**, 382, 621.
- [18] J. Eddy, N. Maizels, *Nucl. Acids Res.* **2006**, 34, 3887.
- [19] A. Siddiqui-Jain, C. L. Grand, D. J. Bearss, L. H. Hurley, *Proc Natl Acad Sci U S A* **2002**, 99, 11593.
- [20] F. Han, *JACS* **1999**, 121, 3561.
- [21] M. P. Teulade-Fichou, C. Carrasco, L. Guittat, C. Bailly, P. Alberti, J. L. Mergny, A. David, J. M. Lehn, W. D. Wilson, *J Am Chem Soc* **2003**, 125, 4732.
- [22] M. Bejugam, S. Sewitz, P. S. Shirude, R. Rodriguez, R. Shahid, S. Balasubramanian, *J Am Chem Soc* **2007**, 129, 12926.
- [23] E. Gavathiotis, R. A. Heald, M. F. Stevens, M. S. Searle, *J Mol Biol* **2003**, 334, 25.
- [24] D. P. Goncalves, R. Rodriguez, S. Balasubramanian, J. K. Sanders, *Chem Commun (Camb)* **2006**, 4685.
- [25] L. Ren, A. Zhang, J. Huang, P. Wang, X. Weng, L. Zhang, F. Liang, Z. Tan, X. Zhou, *Chembiochem* **2007**, 8, 775.
- [26] D. Miyoshi, A. Nakao, N. Sugimoto, *Biochemistry* **2002**, 41, 15017.
- [27] P. A. Wender, W. C. Galliher, E. A. Goun, L. R. Jones, T. H. Pillow, *Advanced Drug Delivery Reviews* **2008**, 60, 452.
- [28] N. W. Luedtke, P. Carmichael, Y. Tor, *J Am Chem Soc* **2003**, 125, 12374.
- [29] N. W. Luedtke, T. J. Baker, M. Goodman, Y. Tor, *Journal of the American Chemical Society* **2000**, 122, 12035.
- [30] F.-D. N. Cong, Bo; Du, Xi-Guang; Ma, Chun-Yu; Yu, Hai-Feng; Chen, Bin, *Dyes and Pigments* **2005**, 66, 149.

References

- [31] S.-H. Jung, J.-H. Choi, S.-M. Yang, W.-J. Cho, C.-S. Ha, *Materials Science and Engineering B* **2001**, *85*, 160.
- [32] P. Gregory, *Journal of Porphyrins and Phthalocyanines* **2000**, *4*, 432
- [33] H. Zollinger, *Color Chemistry: Syntheses, Properties, and Applications of Organic Dyes*, third ed., Helvetica Chimica Acta, **2003**.
- [34] S. W. Zhou, Shaowu; Yang, Gaosheng; Li, Qinghai; Zhang, Lijun; Yao, Zijian; Zhou, Zhangkai; Song, Hai-bin, *Organometallics* **2007**, *26*, 3755.
- [35] A. B. P. L. Phthalocyanines. Edited by C.C. Leznoff, VCH, New York, NY.
- [36] I. Okura, *Photosensitization of Porphyrins and Phthalocyanines*, Gordon and Breach Science, Tokyo, **2001**.
- [37] K. Msayib, S. Makhseed, N. B. McKeown, *Journal of Materials Chemistry* **2001**, *11*, 2784.
- [38] F. Mitzel, S. FitzGerald, A. Beeby, R. Faust, *Chemical Communications (Cambridge, United Kingdom)* **2001**, 2596.
- [39] K. M. S. Karl M. Kadish, Roger Guilard, **2003**, *Volume 15*.
- [40] S.-i. Hachiya, A. S. Cook, D. B. G. Williams, A. G. Montalban, A. G. M. Barrett, B. M. Hoffman, *Tetrahedron* **2000**, *56*, 6565.
- [41] Á. Zsigmond, F. Notheisz, M. Bartók, J. E. Bäckvall, in *Heterogeneous Catalysis and Fine Chemicals III, Proceedings of the 3rd International Symposium*, Volume 78 ed. (Ed.: J. B. M. Guisnet, J. Barrault, C. Bouchoule, D. Duprez, G. Pérot and C. Montassier), Elsevier, **1993**, pp. 417.
- [42] B. N. Achar, K. S. Lokesh, *Journal of Organometallic Chemistry* **2004**, *689*, 3357.
- [43] L. Zhang, J. Huang, L. Ren, M. Bai, L. Wu, B. Zhai, X. Zhou, *Bioorganic & Medicinal Chemistry* *Nucleic Acid Modification for Fluorescence-Based Technologies* **2008**, *16*, 303.
- [44] M. Durmus, S. Yesilot, V. Ahsen, *New Journal of Chemistry* **2006**, *30*, 675.
- [45] B. P. Orner, A. D. Hamilton, *Journal of Inclusion Phenomena and Macrocyclic Chemistry* **2001**, *41*, 141.
- [46] T. Suhs, B. Konig, *Mini-Reviews in Organic Chemistry* **2006**, *3*, 315.
- [47] N. M. K. Alan R. Katritzky, Sergey Bobrov., *Helvetica Chimica Acta* **2005**, *88*, 1664.
- [48] Q. W. Li, Shaowu; Zhou, Shuangliu; Yang, Gaosheng; Zhu, Xiancui; Liu, Yuyu, *Journal of Organic Chemistry* **2007**, *72*, 6763.
- [49] W. Weith, *Chem. Ber.* **1873**, *6*, 1389.
- [50] L. Edwards, M. Gouterman, *Journal of Molecular Spectroscopy* **1970**, *33*, 292.
- [51] V. N. Nemykin, R. G. Hadt, R. V. Belosludov, H. Mizuseki, Y. Kawazoe, *J. Phys. Chem. A* **2007**, *111*, 12901.
- [52] T. M. Lohman, D. P. Mascotti, in *DNA Structures Part B: Chemical and Electrophoretic Analysis of DNA*, Volume 212 ed. (Ed.: D. M. J. L. a. J. E. Dahlberg), Academic Press, **1992**, pp. 400.

10. Acknowledgements

I would like to show my appreciation to *Prof. Dr. Nathan W. Luedtke* for giving me the chance to work on this interesting project and for sharing his broad knowledge with me.

I would also like to thank *Dr. Jawad Alzeer* for his kind support throughout the project and for sharing his experience in the organic chemistry.

Many thanks to the rest of the members of the Luedtke's group for their helpfulness and pleasant atmosphere in the lab.

Further thanks go to the analytical departments of the University of Zurich (MS-service) for recording spectra of some of my compounds.

I would like to thank the Kanton Thurgau for their scholarship during my studies.

Finally, I would like to thank my family and friends for their support throughout my studies.